Geotechnical Seismic Design Code Calibration

A probabilistic study of seismic design code safety

by

R.G.M. de Munck

to obtain the degree of Master of Science
at the Delft University of Technology,
to be defended publicly on Wednesday January 22, 2020 at 15:00

Student number:	4348001	
Project duration:	January 23, 2019 – January 22, 2020	
Thesis Chairman:	Prof. dr. M. A. Hicks	TU Delft
Thesis committee:	Prof. dr. G. A. Fenton,	Dalhousie University, supervisor
	Dr. ir. A. P. van den Eijnden,	TU Delft
	Dr. F. Pisanò,	TU Delft

An electronic version of this thesis is available at http://repository.tudelft.nl/.

TU Delft

Preface

It has taken a little while, but this is the final version of my thesis. The last requirement in achieving a Masters Degree in Geotechnical Engineering at Delft University of Technology, and the final hurdle in completing my education at said university. I should give a little background about how this project came to be. Professor Gordon Fenton had a sabbatical year in Delft and was looking for a student to do a project with. Because I enjoyed the course ”Risk and Variability” the most of all my courses, that student ended up being me. Professor Fenton and I have spent a number of weeks together working on this project during the summer.

I would like to thank Professor Fenton for his invaluable advice during this thesis, for the access to his systems and for the endless number of corrections that he has given me. Without his help I would not have been able to finish this thesis. Secondly, I would like to thank my committee for their efforts in trying to improve my research and my writeup. Bram van den Eijnden has spent a lot of time converting the FEM code used in this thesis, for which I am thankful. Finally, I would like to thank my family for their continued support. My parents had to put up with my stress, and it was great to have my nieces to tell my troubles to, especially the youngest one who wasn't able to talk back yet.

R.G.M. de Munck
Maasdijk, January 2020

Abstract

Seismic design codes are currently moving from a force-based design approach to a performance-based design approach. For example, in a performance-based design approach it could be specified how many lanes must be available during the lifetime of a bridge given a certain earthquake intensity. The problem with this approach is that it is not specified what the probability must be that the performance criterion is satisfied. This raises the question whether the design codes are acceptably safe or not.

Resistance factors are a way to take into account uncertainty in the design resistance of a (geotechnical) system. Different types of resistance factors exist, but in this thesis focus is laid on the Canadian Highway Bridge Design Code (CHBDC), in which a total resistance factor approach is used. In a total resistance factor approach, the total design resistance is calculated with unfactored strength parameters, after which the total design resistance is multiplied with the total resistance factor φ_{gu}. Because the total resistance factor in the CHBDC is a multiplicative factor, lower resistance factors lead to stronger foundation designs.

The goal of this thesis is to calibrate the design procedure in the CHBDC for geotechnical systems under seismic loading, by finding a relationship between resistance factors and the lifetime probabilities of failure of said systems. The resistance factor can then be fine-tuned to a lifetime probability of failure that is consistent with the lifetime probability of failure targeted in static design. As an example problem, the bearing capacity of a shallow foundation on a clay with a pseudo-dynamic earthquake load is tested. The research question that is answered in this thesis is: "What should the resistance factors for geotechnical seismic design be in order to achieve a target lifetime probability of failure that is consistent with static design targets?"

Not every possible combination of soil strengths and forces on the superstructure can be taken into account, and therefore the random finite element method (RFEM) is used in a Monte Carlo simulation. In RFEM, each realization of a Monte Carlo FEM simulation has a random soil field and random forces acting on the structure. Thousands of realizations are performed for each resistance factor, design return period, and "actual" return period that the designed foundations are tested against. By seeing how many realizations of the Monte Carlo simulation fail given a certain earthquake intensity, the conditional probability of failure given that earthquake intensity can be estimated. The total lifetime probability of failure can then be estimated from the conditional probabilities of failure with the "total probability theorem". As part of a parametric study, the lifetime probabilities of failure are estimated for six different scenarios, each of which has different sources of uncertainty.

The resulting lifetime probabilities of failure for specific resistance factors are interpolated in order to find a resistance factor that targets a lifetime probability of failure of 10^{-3}, which is consistent with static design targets. Given that a design return period of 475 years is the lowest design return period possible in the design code, a resistance factor of 0.53 is recommended.

Currently, the resistance factor that the CHBDC recommends for geotechnical systems under seismic loading are defined as the static resistance factor for that geotechnical system incremented with 0.20, meaning that compared to static design, weaker foundations are designed for seismic load cases. For the problem in this thesis, the CHBDC recommends that a static resistance factor of 0.50 is used, and thus the resistance factor for seismic loading is $0.50 + 0.20 = 0.70$. It can be noticed that the resistance factor found in this thesis is closer to the resistance factor for static design than to the resistance factor for seismic design. In order to achieve a lifetime reliability for geotechnical systems under seismic loading that is consistent with static design targets, it should be considered to lower the seismic resistance factor to the value of the static resistance factor, and thus to remove the $+0.20$ clause.

In order to save computational time, simplified models are used. These simplifications could lead to inaccuracies compared to coupled FEM models or/and a fully dynamic approach. As a recommendation for future research, a more complex model should be considered without lowering the number of realizations. It should also be considered to assess failure of a foundation completely on the performance-criterion for a certain design return period, and thus to target different lifetime probabilities of failure for different design return periods.

Contents

List of Figures

List of Tables

1

Introduction

Soil is a highly variable material. Since it is infeasible to test the soil strength parameters at every single location on a site, the soil parameters need to be estimated based on the results of a limited number of locations, making the exact strength of the soil uncertain. The uncertainty in the soil parameter field carries over to the design equations of geotechnical systems, and thus to the lifetime reliability of these systems. In order to target a certain lifetime reliability of a geotechnical system, a Load and Resistance Factor Approach is often used.

Resistance factors are a way to take into account uncertainty in a during the design phase estimated resistance to loads. First the bearing capacity of a geotechnical structure is estimated using the sampled soil strength parameters, after which this bearing capacity is weakened with the resistance factor. The weakened bearing capacity has to be larger than the factored design load in order for the design not to fail.

Currently in the Canadian Highway Bridge Design Code (CHBDC), the seismic resistance factors allow for weaker foundation design than the static resistance factors. The question now is, are the levels of safety that design codes give for seismic design the same as those targeted for static design? The resistance factor required for seismic design is calibrated in this thesis so that the same lifetime reliability as targeted in static design can be achieved, using an example problem of a shallow foundation with a pseudo-dynamic earthquake load.

In this chapter, the topic of this thesis is motivated, the importance of the research is underlined, and an outline of the thesis structure is given.

1.1. Topic Motivation

Seismic design codes are moving from a force-based design approach to a performance-based design approach. Performance-based design means that structures are designed to allow (or not allow) a certain level of damage for a certain hazard level (CSA, 2019a). An example of performance based design in the Canadian Highway Bridge Design Code is the following:

> "Major-route geotechnical systems shall have 100% of the traveled lanes available for use following ground motions with a return period of at least 475 years."

The problem with performance-based approaches is that the performance requirements are not accompanied by any target reliability level. For example, the above performance specification should include a statement such as "with probability 0.90 over the design lifetime". It is not known how conservative the current design procedure for geotechnical systems under seismic loading really is. If the building codes are too conservative, this could lead to a structural waste of (public) resources. However, if the code is unconservative, the potential for human harm would be unacceptable. Calibration of design codes therefore is an important matter.

Because not much research has been done on the calibration of resistance factors for seismic shallow foundation design, this research is much needed. There are some relevant papers written about similar topics in related fields. An outline of how design calibration in general should be conducted is given in a circular by Allen et al. (2005). A source of inspiration may be taken from past work on static

pile foundation design calibration (e.g. Fenton & Naghibi, 2011; Oudah et al., 2019; Rahman et al., 2002; Park et al., 2013) or static shallow foundation design calibration (e.g. Fenton et al., 2005; Foye et al., 2006; Honjo & Amatya, 2004). Finally there are assessments of static resistance factor safety (e.g. Fenton et al., 2016; Scott et al., 2003).

1.2. Research Strategy

The goal of this thesis is to estimate the resistance factor needed to achieve a certain target lifetime probability of failure for geotechnical systems under seismic loading. It is important to know whether or not current resistance factor practice in seismic design needs to be changed. If this design does need to be changed, it is important to know what it should be changed to.

The way this is planned to be achieved is by first studying relevant theory, consisting of probabilistic theory and seismic theory used in modeling geotechnical systems. Most importantly, the total probability theorem is explained, which is basis with which the lifetime probability of failure is estimated for a geotechnical system under seismic loading.

When the theory has been studied, it can be implemented in a simulation program. The random finite element method (RFEM) is used because it accurately describes the failure mechanisms through spatially variable soil, which is especially important in this research for the additional complexity of seismic loading.

The total lifetime probability of failure given a set of design parameters will be determined for an example case, namely the bearing capacity of a shallow foundation under seismic loading. A parametric study will be undertaken to consider multiple possible scenarios with different sources of uncertainty. The different scenarios include strength degradation effects on the soil, different values for live loads and different parameters in the design procedure.

Results for each set of simulations based on the various scenarios will be presented in the form of conditional probabilities of failure given an earthquake return period, design return period earthquake, and resistance factor. These conditional probabilities of failure need to be combined into unconditional probabilities of failure by using the total probability theorem for each possible seismic resistance factor. The resistance factor required to achieve a target failure probability can then be estimated by interpolating the estimated lifetime probability of failure to a specific target lifetime probability of failure.

Summarizing, the main research question becomes: “What should the resistance factors for geotechnical seismic design be in order to achieve a target lifetime probability of failure that is consistent with static design targets?”

1.3. Document Structure

First the relevant literature and theory are discussed in Chapter 2. This includes the design procedures currently implemented in the Eurocode and the CHBDC. In Chapter 3 details are given on the numerical modeling theory that was used to estimate the conditional probabilities of failure. In Chapter 4 the reasoning behind the chosen values of variables is explained, and an overview is given of the scenarios that have been considered in this thesis. It is also explained how the results are processed in order to find the total lifetime probability of failure given a resistance factor. The results of the tested scenarios are then presented in Chapter 5. Relevant figures that have been produced for each scenario are shown and discussed. The conclusions derived from the research conducted in this thesis work are given in Chapter 6. Finally, recommended steps for further research are given in Chapter 7.

2

Theoretical Background

In Section 2.1 key details are explained of the philosophy of the Eurocode and Canadian Highway Bridge Design Code (CHBDC). To give more insight into the structure of the theory sections, a flowchart of the algorithm used is given in Figure 2.5, which can be seen as a summary of Section 3.2.1. In Section 2.2 it is described how the effects of earthquakes are modelled, including the acceleration forces induced by earthquakes and the effects on soil properties. The described theory comes together in Section 2.3, where the foundation design equation that is used in the Monte Carlo simulation is described. Finally, in Section 2.4 the probabilistic theory used in this thesis is described.

2.1. Design Codes

Design codes are often based on the principle that the resistance of a structure to actions has to be larger than the effect of actions on the structure, or so called *limit states*. The two groups of limit states are the ultimate limit state (ULS), which concerns itself with failure of the structure and potential loss of life, and the serviceability limit state (SLS), which concerns itself with the functionality of the structure and how comfortable people are using the structure (Bond & Harris, 2008). Only ULS is taken into account in this study. The principle of limit state design is shown in the following equation,

$$E_d \leq R_d \tag{2.1}$$

where E_d is the design effect of the actions on the structure, and R_d is the design resistance of the structure to actions.

It used to be common for building codes to use a so called allowable or working stress design (ASD or WSD) up until the final quarter of the 20th century (Bond & Harris, 2008). Design codes started using a load and resistance factor design approach (LRFD) in the second half of the 20th century, which is now standard in most modern design codes (Bond & Harris, 2008; Fenton et al., 2016). The difference between the WSD and LRFD approaches is that WSD concentrates the uncertainty in one single factor (the factor of safety F_s), whereas in LRFD different factors are used for different sources of uncertainty (Bond & Harris, 2008), such as for live load and dead load.

There are generally two approaches to LRFD: the total resistance factor approach, and the partial resistance factor approach (Fenton et al., 2016). The total resistance factor approach is often used in North-America, whereas the partial resistance factor is used in other parts of the world (Bond & Harris, 2008). In short, with the partial resistance factor approach it is assumed that different sources of strength (i.e. cohesion and friction angle) bring with them different uncertainties. With the total resistance factor approach it is assumed that the resistance can be calculated with so called characteristic values, and then one single resistance factor can be used to weaken the calculated resistance.

A characteristic value of a parameter is a single representative value of an uncertain design parameter (Fenton, 2013). How this representative value is defined is different for different design codes. In the Canadian Highway Bridge Design Code a “cautious estimate of the mean value” is used (CSA, 2019, section 6.2). In Eurocode, space is left for incorporation of spatial variability in the determination of the characteristic values (Hicks, 2013).

Although the different design codes have different approaches to designing a geotechnical system, many static design approaches have a similar target lifetime probability of failure (Fenton et al., 2016). In the following sections some aspects of the Canadian Highway Bridge Design Code and the Eurocode are explained. For each section the respective design code is a source, although they will not be cited every time. It is advised to go through the design codes if more information is required: Sections 4 and 6 of the CHBDC (CSA, 2019c; CSA, 2019), and the relevant Eurocode parts and national annexes.

2.1.1. Canadian Highway Bridge Design Code

The Canadian Highway Bridge Design Code (CHBDC) uses the total resistance factor approach. An expansion of Equation 2.1 that is given in the CHBDC can be seen in the following equation,

$$E_d = \sum_i \left(I_E \eta_i \alpha_i \hat{F}_i\right) \leq \psi \varphi_g \hat{R} = R_d \tag{2.2}$$

where I_E is the importance factor (1.0 for all non-major-route bridges, (CSA, 2019c)), subscript i is a set of different load types acting on the structure, η_i is the load combination factor of the i^{th} load (see CSA, 2019b, Table 3.1), α_i is the load factor of the i^{th} load (e.g. see CSA, 2019b, Table 3.2), $\hat{F}_i$ is the i^{th} characteristic load, ψ is the consequence factor, φ_g is the resistance factor for the relevant failure mechanism, and $\hat{R}$ is the characteristic resistance to actions.

Some factors are specified differently for SLS and ULS. When ULS is regarded, the parameters gain the subscript "u", such as φ_{gu}, α_{ui} and $\hat{F}_{ui}$.

For earthquake cases the CHBDC prescribes ULS Combination 5, in which only permanent loads and earthquake loads are taken into account. Transitory loads (or live loads) such as traffic and wind load are assumed to not be present during an earthquake. Transitory loads thus get $\eta_{ui} = 0$ in Equation 2.2. Load factors α_{ui} also have different values in this load combination than they have in static design.

Whereas the resistance factors for static design can be found in Table 6.2 of the CHBDC, the resistance factors for seismic design, φ_{gu}, are equal to the static resistance factors incremented with +0.2 (CSA, 2019, Table 6.5). Because the resistance factor in the CHBDC is multiplicative, a higher resistance factor leads to weaker designed foundations than lower resistance factors do. Consequence factor ψ is always equal to 1.0 for seismic design.

In the CHBDC it is given that "the reduction in the factored geotechnical resistance due to liquefaction or cyclic mobility shall be considered" (CSA, 2019, 6.14.5.3). How this should be done is not specified quantitatively, which is therefore worked out in Section 2.2.3 of this thesis.

2.1.2. Eurocode

Eurocode is a standardized building code for multiple countries. Each country has its own preferences, which are specified in national annexes. Three different design approaches may be used (CEN, 2005a, Section 2.4.7.3.4). In each approach a characteristic action F_k is transformed into a representative action F_{rep} by multiplying the actions with a load combination factor ψ_i (note, the symbol is η_i in the CHBDC), after which different factors are used for transitory and permanent loads to go from F_{rep} to F_d. A short explanation for all three approaches is given:

1. Design Approach 1 (has to satisfy two different combinations):

   (a) Design Approach 1, Combination 1:
   In Combination 1 it is assumed that the characteristic material strength X_k is equal to the design material strength X_d. In other words, the partial material factors γ_ϕ and γ_{c_u} are assumed to be equal to 1. However, the partial factors γ_Q and γ_G for the actions are more conservative than in Approach 1, Combination 2. Figure 2.1 shows a diagram of this load combination (Bond & Harris, 2008).

   (b) Design Approach 1, Combination 2:
   In Combination 2 it is assumed that the partial material factors γ_ϕ and γ_{c_u} are not equal to one. The partial factors γ_Q and γ_G for the actions are more lenient in Combination 2 than in Combination 1. Figure 2.2 shows a diagram of this load combination (Bond & Harris, 2008).

2. Design Approach 2:
   Design Approach 2 is a total resistance factor approach. This means that the partial factors for soil γ_ϕ and γ_{c_u} are equal to 1.0. Instead of using partial factors to go to the design resistance R_d, the characteristic resistance R_k is divided by a total resistance factor γ_R. This is comparable to the method used in the CHBDC (see Section 2.1.1), although the total resistance factor is a multiplicative factor in the CHBDC. Figure 2.3 shows a diagram of this load combination (Bond & Harris, 2008).

3. Design Approach 3:
   Design Approach 3 is a partial resistance factor approach. Characteristic soil strength parameters X_k are taken to their design value X_d by applying partial material factors γ_ϕ and γ_{c_u}. Although this approach is similar to Design Approach 1, Combination 2, in Design Approach 3 different factors for structural and geotechnical actions are used. Figure 2.4 shows a diagram of this load combination (Bond & Harris, 2008).

In seismic design, the quasi-permanent load factor $\psi_{2,i}$ is used for transitory loads. Just like how different countries can choose different design approaches, they can also specify their own quasi-permanent load combination factors. For the Dutch national annex this load combination factor is specified to be equal to zero for traffic bridges, which is the same as in the CHBDC (see Section 2.1.1).

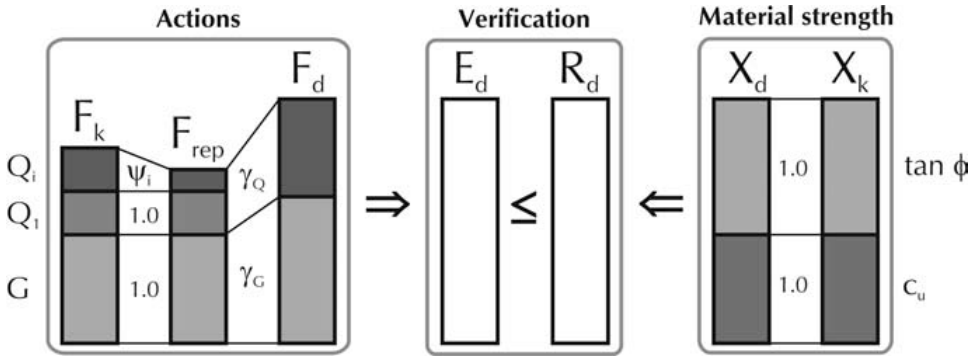

Figure 2.1: "Hierarchy of parameters for Design Approach 1, Combination 1." (Bond & Harris, 2008)

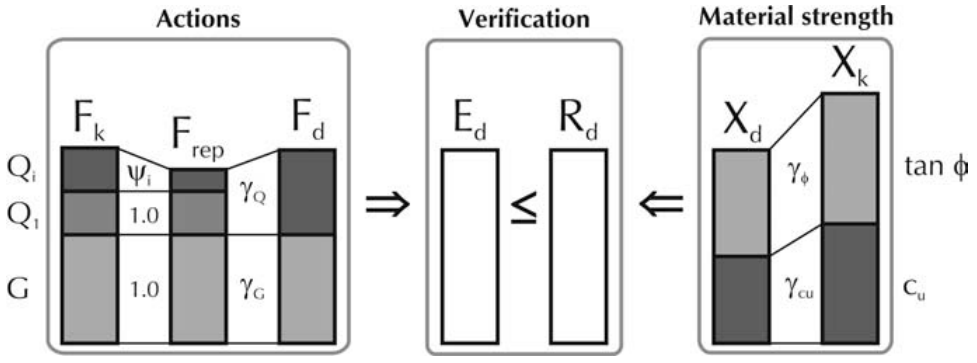

Figure 2.2: "Hierarchy of parameters for Design Approach 1, Combination 2." (Bond & Harris, 2008)

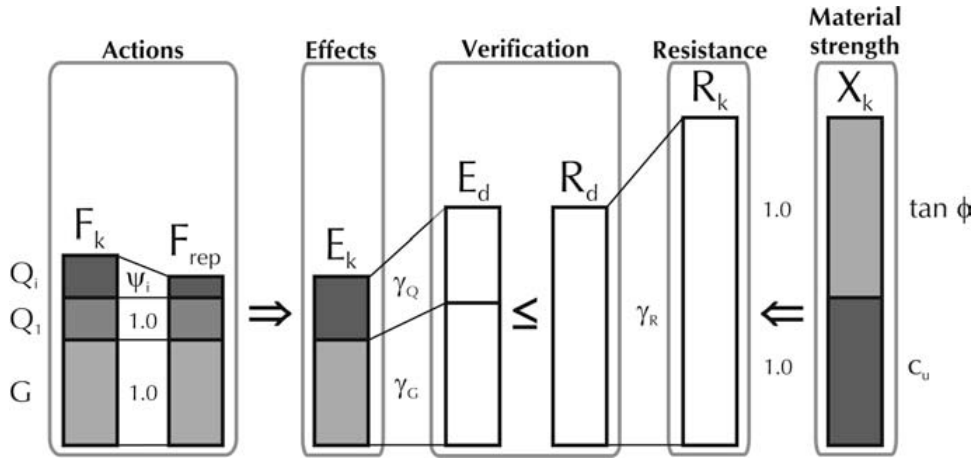

Figure 2.3: “Hierarchy of parameters for Design Approach 2.” (Bond & Harris, 2008)

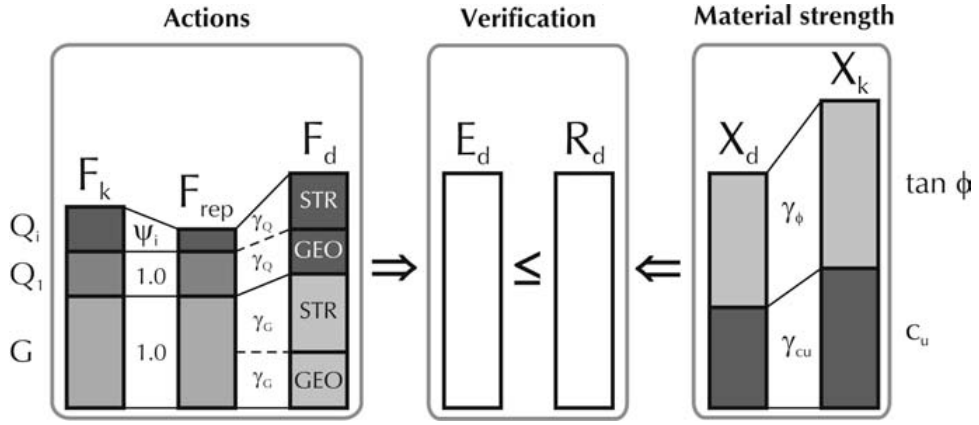

Figure 2.4: “Hierarchy of parameters for Design Approach 3.” (Bond & Harris, 2008)

2.2. Seismic Modelling

Instead of using one of many available advanced seismic models, the seismic theory in this section will be kept as simple as possible. Simplicity is important because each set of Monte Carlo simulations, used to estimate failure probability, will have a very large number of realizations, going as high as $100\ 000$. A realization is a set of variables x that have been sampled from their respective probability distributions X and are tested together as as a step in a Monte Carlo simulation. Every second of run time on $100\ 000$ individual realizations would add 27.8 hours to the total run time, making it unfeasible to have complex models given the time frame of this thesis.

Simple models are acceptable, because resistance factor calibration is not so much about the mean of actions and design, but more about the deviation from that mean. As long as both the design procedure and the procedure used to determine the bearing capacity of the designed footing are similar, the results are accurate enough. This is the case for the seismic loading theory, where both the design forces and the forces used in the FEM testing are generated with the same seismic model. The following sections describe the procedure used to model the effects of earthquakes on geotechnical systems.

2.2.1. Peak Ground Acceleration vs Return Period

The main parameter used in this thesis to indicate earthquake intensity is peak ground acceleration (PGA). PGA is the largest ground acceleration during an earthquake at a location. It is often represented in units of gravitational acceleration g, meaning it has units of m/s^2. Besides PGA there are also other parameters that are needed to describe an earthquake. These parameters are the frequency and time

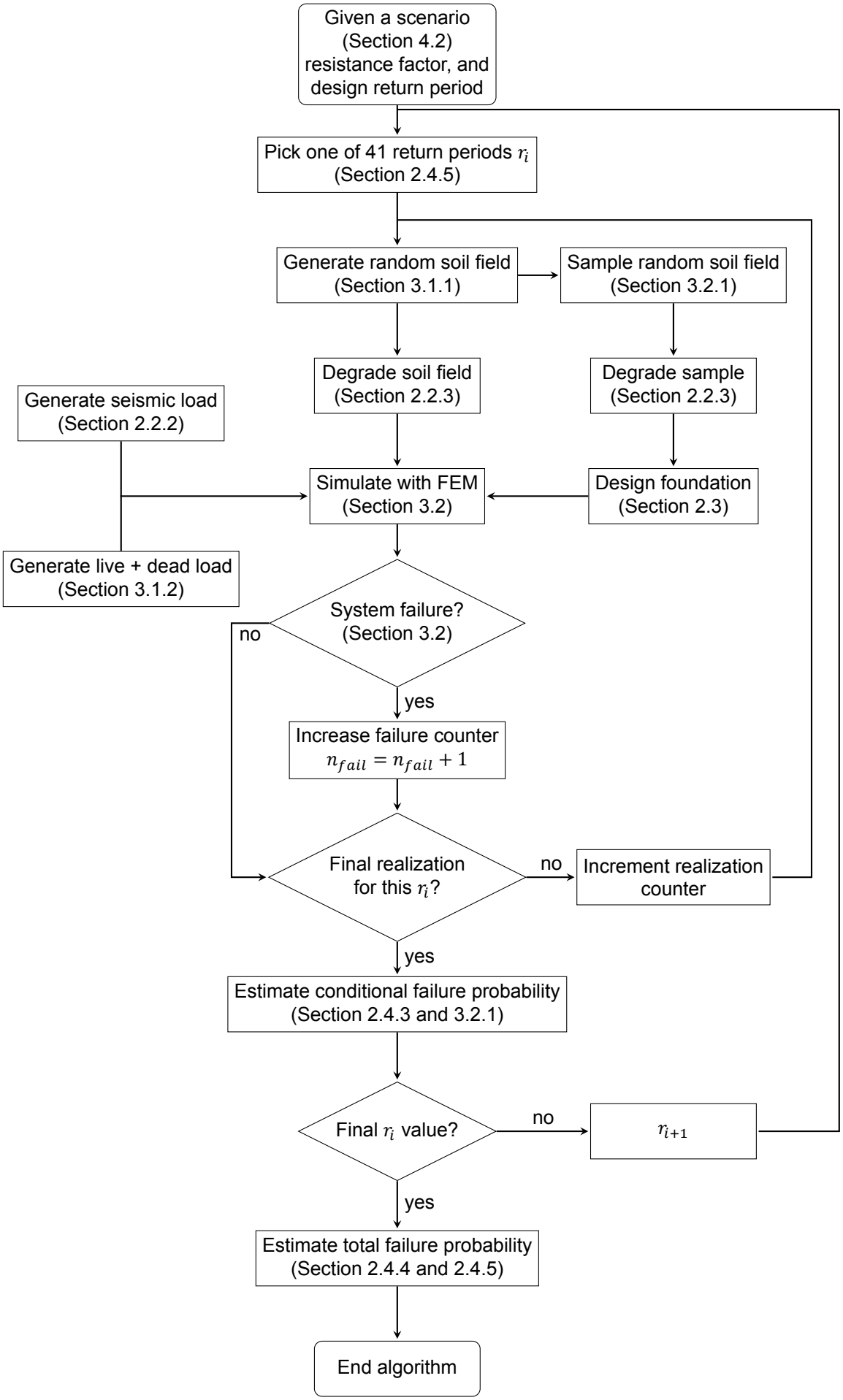

Figure 2.5: Flowchart of algorithm with corresponding theory sections

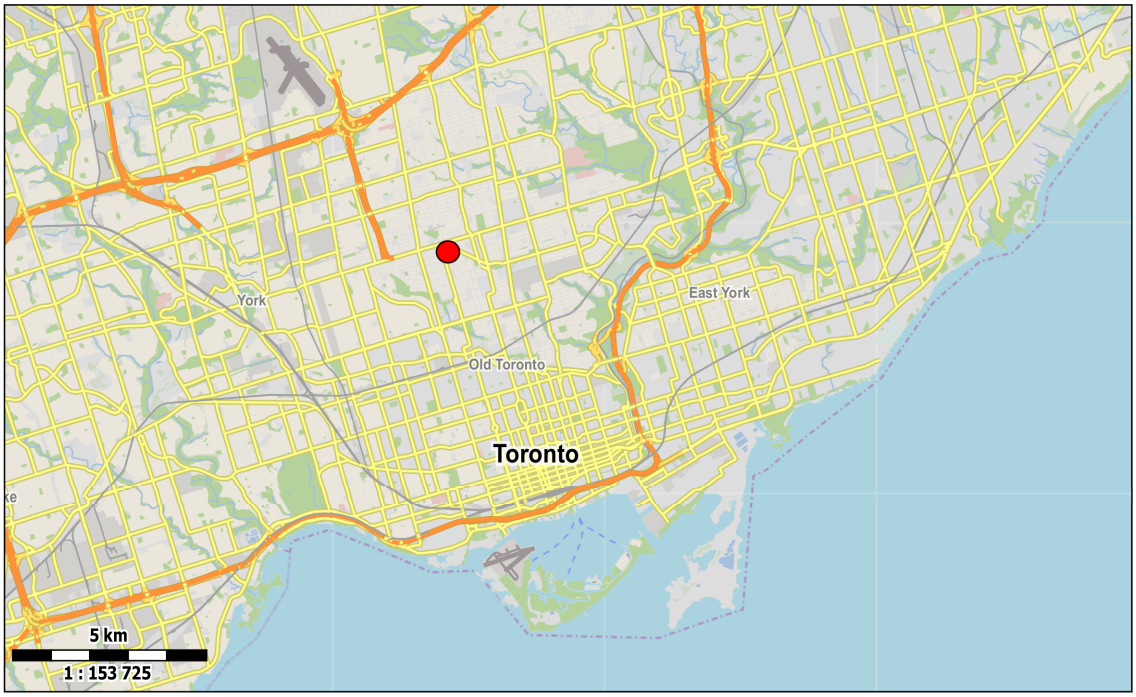

Figure 2.6: Indication of where NRCAN data was taken, 43°42'00.4"N 79°24'58.7"W (OpenStreetMap contributors, 2019)

parameters (Cimellaro & Marasco, 2018). PGA alone was deemed sufficient for the purpose of this thesis, since only a pseudo-dynamic force and resistance model is considered (Section 2.2.2).

One of the reasons why PGA is so convenient, is that there are plenty of data available through use of the NRCAN seismic hazard value calculator (nrcan, 2015). The NRCAN calculator gives a number of different seismic parameters for the 100, 475, 975 and 2475 year return period earthquakes. For this section, only the return period and the PGA are considered, although other values from NRCAN are used in Sections 2.2.2 and 2.2.3.

An example location was taken in Toronto at the coordinates 43°42'00.4"N 79°24'58.7"W. The location of this site can be seen in Figure 2.6, where the red dot is the example location. Different locations give different values for the PGA, but it is assumed that the selected location is roughly representative for the general region.

Not only the 100, 475, 975 and 2475 year return periods are of interest, but also all return periods in between. The data points from NRCAN therefore are interpolated with a power regression, for which the general expression is given in the following equation,

$$PGA = a \cdot r_i^b \tag{2.3}$$

where r_i is the return period of an earthquake, and the regression coefficients a and b have the values $a = 2.3102 \cdot 10^{-4}$ and $b = 0.82839$. A plot of the regression can be found in Figure 2.7. This approach for the PGA regression is similar to the approach of Esposito et al. (2019). Although they performed a regression for a slightly different location in Toronto, the fit of the regression is roughly the same.

2.2.2. Pseudo-Dynamic Forces

Pseudo-dynamic forces are forces or motions that are dynamic in real life, but are modelled with a single representative static force as a simplified model. The established term for these forces is "pseudo-static forces". However, since the forces are completely static and model dynamic forces, pseudo-dynamic is a more accurate term.

The method used in the CHBDC to determine the intensity of the pseudo-dynamic forces utilizes spectral acceleration (CSA, 2019c). A spectral acceleration S is multiplied with an importance factor I_E and the weight of the structure W to get the pseudo-dynamic horizontal force $F_{seis,h}$ created by an earthquake on the structure,

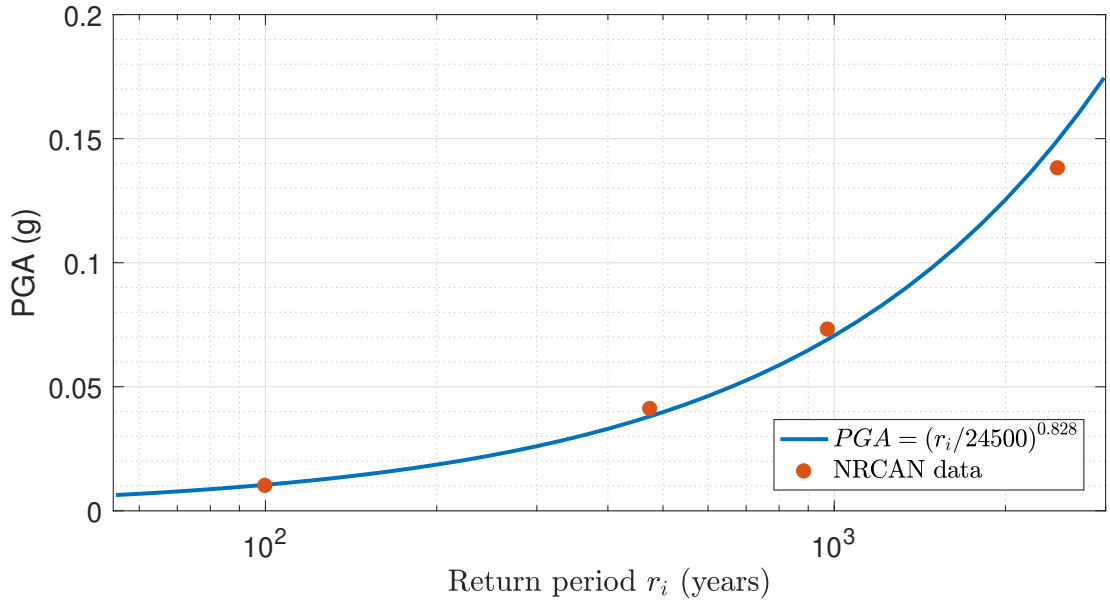

Figure 2.7: A regression of the peak ground acceleration vs the return period using data from nrcan (2015)

$$F_{seis,h} = S(T, PGA) I_E W \tag{2.4}$$

The importance factor I_E is equal to 1.0 for bridges that are not part of major-routes. As also can be seen in Equation 2.4, the spectral acceleration is a function of fundamental (natural) period T and peak ground acceleration of the earthquake in question (more about PGA in Section 2.2.1). Every bridge has a different fundamental period for which seismic forces on the structure are at a maximum. Spectral acceleration S is calculated through the following equation,

$$S(T, PGA) = F(T, PGA) S_a(T, PGA) \tag{2.5}$$

where F is the site coefficient and S_a is the 5% damped spectral acceleration, of which the values depend on T and PGA. F has a different value per soil type, as is specified in tables in Section 4 of the CHBDC. If the PGA value for which a seismic force is needed is in between the PGA values for which F is specified in the tables, linear interpolation must be used to determine F at that PGA. Similarly, a linear regression between the 5% damped spectral acceleration S_a and PGA can be established using the data of NRCAN, for the location seen in Figure 2.6, as shown in Figure 2.8.

Using Equation 2.5 and substituting it into Equation 2.4 leads to the following equation for $F_{seis,h}$,

$$F_{seis,h} = F(T, PGA) S_a(T, PGA) I_E W \tag{2.6}$$

In this thesis it is assumed that the fundamental period T is equal to 1 second. The theory described above then leads to the spectral acceleration points shown in Figure 2.9, to which another power regression has been fitted. This regression can be used to estimate the horizontal seismic force $F_{seis,h}$ at any PGA value, and therefore for any earthquake return period.

Now that the horizontal seismic force $F_{seis,h}$ is known, the vertical seismic force $F_{seis,v}$ can be estimated. A popular approach to estimating the vertical seismic force $F_{seis,v}$ is by assuming that it is a percentage of the horizontal seismic force $F_{seis,h}$. The ratio of $F_{seis,v}/F_{seis,h}$ will from now on be referred to as λ.

What value λ should be is not clear cut. The Eurocode prescribes a λ of either 0.33 or 0.5, depending on the value of the design acceleration (CEN, 2005c). Other design codes, such as the Algerian and the Indian design codes prescribe λ values of 0.3 and 0.67 respectively (Hamrouni et al., 2018; Latha & Garaga, 2010). There are papers in favor of a λ value of 0.25 (Melo & Sharma, 2004), 0.5 (Nouri et al., 2008), and 0.67 (Sun & Ruan, 2013). In real life, the ratio between the horizontal and vertical seismic forces depends on the characteristics of each earthquake. Huang (2005) gave a range of λ values accurate for most major pulses of earthquakes. Major pulses are assumed to be within $-0.322 \leq \lambda \leq$

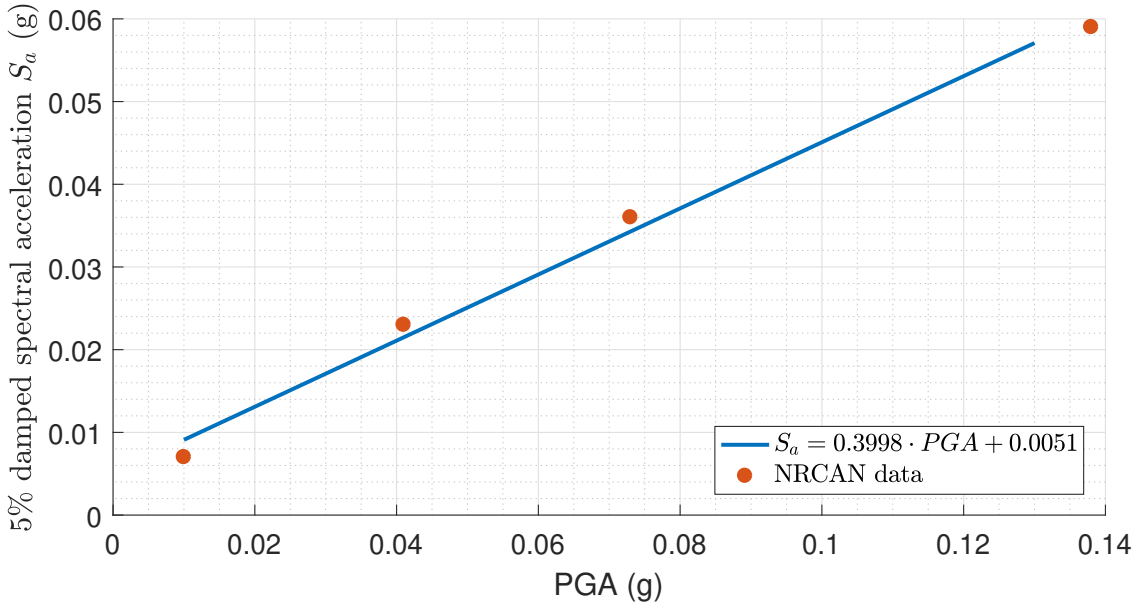

Figure 2.8: A regression of the 5% damped spectral acceleration vs peak ground acceleration using data from nrcan (2015)

0.293 and $-0.544 \leq \lambda \leq 0.379$. Since an upwards seismic force is beneficial for the bearing capacity, λ is assumed to only be positive and thus in the downward direction. For this thesis it is decided that $\lambda = +0.3$ is an acceptable value.

2.2.3. Cyclic Degradation Factor

The repeated straining of soils during earthquakes can lead to a degradation of shear strength. This cyclic softening leads to a reduction of the bearing capacity of a shallow foundation. If the Canadian Highway Bridge Design Code is followed for the design of a shallow foundation, cyclic degradation of the shear strength should be taken into account (see CSA, 2019, section 6.14.5.3). How the reduction should be calculated is left open in the CHBDC and in most other literature (e.g. Puri & Prakash, 2013; Jakka, 2013).

A review of the literature suggests that reducing the soil shear strength can be done by multiplying the maximum shear strength τ with a factor which depends on the earthquake magnitude, its duration, the number of cycles, etc. The factor with which the soil shear strength is reduced will be called the cyclic degradation factor, δ_τ, in the rest of this document.

In order to calculate δ_τ, this thesis follows the strain-based procedure described by Tsai et al. (2014). Two variables are of importance in computing the cyclic degradation factor: the number of equivalent earthquake cycles N_c, which is defined as the number of uniform stress cycles that is representative for a certain non-uniform stress cycle (Srbulov, 2008), and the cyclic shear strain γ.

To calculate both variables, the moment magnitude M_w has to be known, with preferably a relationship to peak ground acceleration, which can then be related to the earthquake return period. A relationship between moment magnitude and PGA is found in the work of Campbell (1997),

$$\begin{aligned}\ln(PGA) = &-3.512 + 0.904M_w - \frac{1.328}{2}\ln\left(R_{seis}^2 + \left(0.149\exp(0.647M_w)\right)^2\right) \\ &+ 0.5 \cdot \left(1.125 - 0.112\ln\left(R_{seis}\right) - 0.0957M_w\right) + \left(0.440 - 0.171\ln\left(R_{seis}\right)\right) \end{aligned} \tag{2.7}$$

where R_{seis} is the distance from the epicenter of the earthquake to the site in kilometers. Campbell's equation can't easily be inverted so that M_w can be determined from PGA. Therefore a relationship to calculate M_w from PGA is established by fitting a curve to a range of points derived from Equation 2.7, as seen in Figure 2.10. The rest of this section will focus on how to calculate the cyclic shear strain γ, the number of equivalent cycles N_c, and finally the cyclic degradation factor δ_τ.

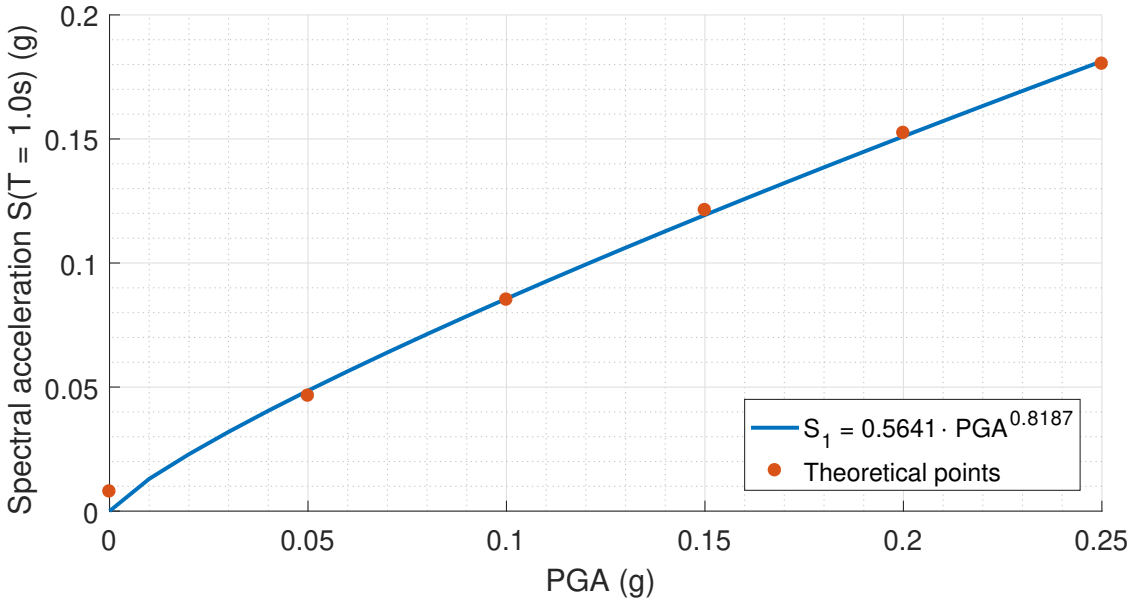

Figure 2.9: A regression of the spectral acceleration vs peak ground acceleration using data from nrcan (2015)

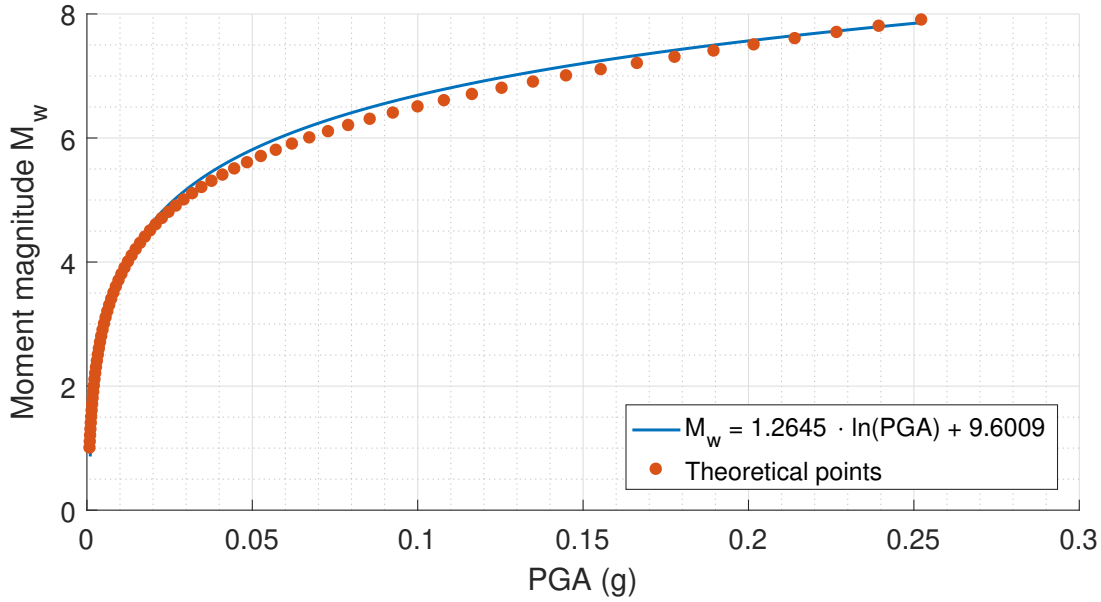

Figure 2.10: A regression of the moment magnitude vs peak ground acceleration

Cyclic Shear Strain

The first component that is needed to calculate the cyclic shear strain γ is the stress reduction coefficient r_d. r_d is a way to capture the dynamic response of the soil, and is defined as "the ratio of cyclic stresses for a flexible soil column to the cyclic stresses for a rigid column" (Idriss & Boulanger, 2006). Idriss and Boulanger (2006), have calibrated the relationship for the calculation of r_d as a function of moment magnitude M_w and depth z, as follows,

$$\begin{aligned} \alpha(z) &= -1.012 - 1.126\sin(\frac{z}{11.73} + 5.133) \\ \beta(z) &= 0.106 + 0.118\sin(\frac{z}{11.28} + 5.124) \\ \ln(r_d) &= \alpha(z) + \beta(z) \cdot M_w \end{aligned} \tag{2.8}$$

Another parameter needed in order to estimate the cyclic shear strain is the small strain shear modulus G_{max}. Tsai et al. (2014) propose to use the following equation,

$$G_{max} = \rho \cdot V_s^2 \tag{2.9}$$

where ρ is the mass density of the soil in kg/m^3 and V_s is the shear wave velocity in m/s.

Although Srbulov (2008) states that Equation 2.9 is only valid for shear strains that are small enough for the soil to behave linear-elastically, it is assumed that it is a good enough approximation for the current goals. Plausible V_s values were determined with tables in the CHBDC.

The output of Equation 2.8 and Equation 2.9 are now used in the following equation (Idriss & Boulanger, 2006; Tsai et al., 2014),

$$\gamma \frac{G}{G_{max}} = 0.65 \frac{PGA}{G_{max}} \sigma_0 r_d \tag{2.10}$$

where G/G_{max} is the normalized modulus reduction curve and σ_0 is the in-situ vertical stress. Darendeli (2001) gives an equation to calculate the normalized modulus reduction curve ${}^{G}/_{G_{max}}$ as a function of γ, which has the following form,

$$\frac{G}{G_{max}} = \frac{1}{1 + \frac{\gamma}{\gamma_r}} \tag{2.11}$$

where γ_r is the cyclic reference strain.

Both sides of Equation 2.11 are multiplied by γ, and the equation is inverted to output γ as a function of $\gamma \frac{G}{G_{max}}$,

$$\begin{aligned} \gamma \frac{G}{G_{max}} &= \frac{\gamma}{1 + ({}^{\gamma}/_{\gamma_r})} \\ \rightarrow \gamma &= \frac{\gamma \frac{G}{G_{max}}}{1 - \frac{\gamma \frac{G}{G_{max}}}{\gamma_r}} \end{aligned} \tag{2.12}$$

Substituting Equation 2.10 into Equation 2.12, an equation for γ as a function of PGA is found,

$$\gamma = \frac{0.65 \frac{PGA}{G_{max}} \sigma_0 r_d}{1 - 0.65 \frac{PGA}{\gamma_r G_{max}} \sigma_0 r_d} \tag{2.13}$$

Equivalent Number of Cycles

The equivalent number of cycles N_c for a saturated clay during an earthquake are assumed in this thesis to be as given by Kishida and Tsai (2014),

$$N_c = \frac{\exp(c_0 + c_1 \ln(PGA) + c_2 \ln(S_1) + c_3 M_w) + 0.5}{0.65} \tag{2.14}$$

where variables c_0, c_1, c_2, and c_3 are regression parameters, and S_1 is the ratio between the spectral acceleration at $T = 0.2s$ and $T = 1.0s$ (See Section 2.2.2).

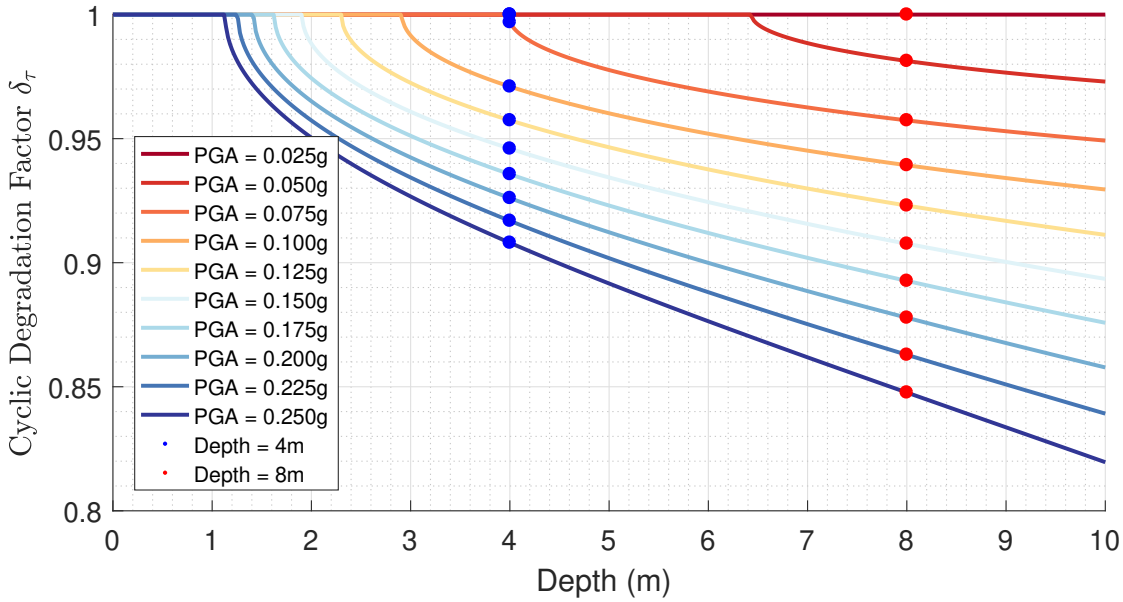

Figure 2.11: A plot of the cyclic degradation factor vs depth. Depths of 4 and 8 meters have been marked

Cyclic Degradation Factor

Matasovic (1993) gives an equation for the cyclic degradation as follows,

$$\delta_\tau = N_c^{-s(\gamma-\gamma_t)^r} \tag{2.15}$$

where variables s and r are regression variables and γ_t is the shear strain below which there is no strength degradation. It must be noted here that the cyclic degradation factor δ_τ in Equation 2.15 is assumed to be equal to the degradation of the small strain shear modulus.

The outcomes of Equation 2.13, γ, and the outcome of Equation 2.14, N_c, are used to determine δ_τ throughout the soil profile for different earthquake intensities. The results of the cyclic degradation factor calculation can be found in Figure 2.11, where δ_τ is plotted against the depth for various PGA values.

A number of simplifying assumptions have been made. Firstly it is assumed that δ_τ increases linearly throughout the soil. Secondly it is assumed that the linear trend is defined by two values: one value at a depth of 8 meters, and a value at the surface just below the foundation. The reason why a cyclic degradation is assumed at ground level, is to incorporate effects the mass of the structure has on the soil when the structure is in motion. The cyclic degradation factor at 8 meters depth is determined through Equation 2.15. A simplified relationship for these values can be seen in Figure 2.12. Figure 2.12 also shows δ_τ at a depth of 4 meters, which shall be used (as a deterministic value) in the design, if this is part of the scenario. The cyclic degradation factor at ground level is assumed to be equal to a percentage of the degradation at 8 meters depth.

A reduced soil strength τ_1 at a certain depth can now be estimated by multiplying the in situ soil strength τ_0 with the cyclic degradation factor at that depth,

$$\tau_1 = \delta_\tau \tau_0 \tag{2.16}$$

2.3. Foundation Design

Because for each realization random soil parameters are generated, a different footing width is required for each realization in order to resist the factored design load E_d. In the finite element model, the design is changed by changing the number of surface nodes that represent the footing.

To estimate the required footing width, a modified version of the classic Prandtl equation is used. Prandtl's design equation has had many additions over the years, such as by Meyerhoff, Terzaghi and Brinch Hansen. Earthquake design has also been added to Prandtl's equation, making for a pseudo-dynamic approach (Sarma & Iossifelis, 1990; Budhu & Al-Karni, 1993; Paolucci & Pecker, 1997; Cas-

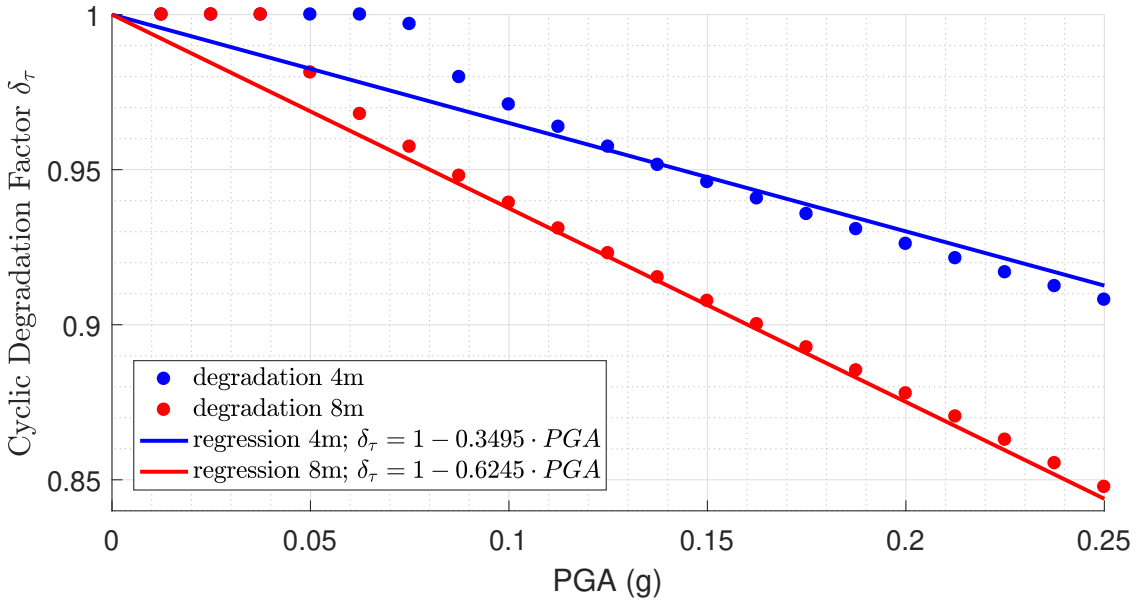

Figure 2.12: A regression of the cyclic degradation factor vs peak ground acceleration at depths 4 and 8 meters

cone & Casablanca, 2016). In this research, the version of Prandtl's equation that is recommended in the CHBDC is chosen, in order to keep the design as close to the code as possible. Although the equation is only applicable on homogeneous soil bodies, it is assumed that the equation targets the mean bearing capacity reasonably accurately given input soil parameters that are also estimates of the mean. The CHBDC version of Prandtl's equation is the following,

$$\hat{q_u} = \hat{c} N_c i_c + q N_q i_q + 0.5 \gamma \hat{B} N_\gamma i_\gamma \tag{2.17}$$

where $\hat{q_u}$ is the bearing capacity, the N factors are factors that depend on the soil strength parameters, the i factors are load inclination factors, $\hat{c}$ is the cohesion, q is the surcharge, and γ is the specific weight of the soil and $\hat{B}$ is the width of the foundation. The hat signs on the bearing capacity $\hat{q}_u$, the cohesion $\hat{c}$ and the foundation width $\hat{B}$ mean that they are the *characteristic* values. Characteristic soil properties are defined in CHBDC as "cautious estimates of the mean". What is not shown in Equation 2.17 is the characteristic value of the friction angle $\hat{\phi}$, which is used in the N factors,

$$\begin{aligned} N_q &= e^{\pi \tan(\hat{\phi})} \tan^2\left(\frac{\pi}{4} + \frac{\hat{\phi}}{2}\right) \\ N_\gamma &= 0.1054 \cdot \exp(0.1675 \hat{\phi}) \\ N_c &= \left(N_q - 1\right) \cot(\hat{\phi}) \end{aligned} \tag{2.18}$$

This definition of the N factors is only valid for $\hat{\phi} > 0$. If $\hat{\phi}$ is equal to zero, i.e. the soil is purely cohesive, then all factors except N_c are equal to zero. N_c then becomes equal to $2 + \pi$ (Das, 2011).

The definition of the inclination factors i are given as follows,

$$\begin{aligned} \theta &= \tan^{-1}\left(\frac{F_h}{F_v}\right) \\ i_c = i_q &= \left(1 - \frac{\theta}{\pi/_2}\right)^2 \\ i_\gamma &= \left(1 - \frac{\theta}{\hat{\phi}}\right)^2 \end{aligned} \tag{2.19}$$

where θ is the angle that the combination of all forces makes with the vertical, F_h is the horizontal factored design load on the foundation and F_v is the vertical factored design load on the foundation. Angles are measured in radians. If there is no horizontal force, the i factors become equal to 1.

Every designed foundation has to withstand at least the factored design load E_d. On the resistance side, the withstandable force is calculated by multiplying the characteristic bearing capacity $\hat{q}_u$ with the characteristic footing width $\hat{B}$, which consists of a multiplication of the design width and the resistance factor $\varphi_{gu}B_d$,

$$E_d \leq \varphi_{gu}B_d\hat{q_u} \tag{2.20}$$

Now Equation 2.17 is substituted into the inequality of Equation 2.20 and everything is written to one side,

$$0.5\gamma B_d^2 N_\gamma i_\gamma + \hat{c}N_c i_c B_d + qN_q i_q B_d - \frac{E_d}{\varphi_{gu}} \geq 0 \tag{2.21}$$

where it must be noted that the total resistance factor φ_{gu} is put together in a fraction with E_d to shorten the equation. A solution for B_d in the above quadratic equation can be found by using the quadratic formula,

$$B_d \geq \frac{-b + \sqrt{b^2 - 4ac}}{2a} \tag{2.22}$$

where a, b and c have the following definitions, taken directly from Equation 2.21,

$$\begin{aligned} a &= 0.5\gamma N_\gamma i_\gamma \\ b &= \hat{c}N_c i_c + qN_q i_q \\ c &= -\frac{E_d}{\varphi_{gu}} \end{aligned} \tag{2.23}$$

Usually the quadratic formula would give two solutions, with both an addition and a subtraction in the numerator. Since the width of a foundation cannot be negative, only the addition is valid, and therefore there is only one solution to Equation 2.21.

When either the soil weight or the friction angle is zero, Equation 2.22 becomes invalid. For that special case, a different solution is found using simple algebra,

$$B_d \geq \frac{E_d}{\left(\hat{c}N_c i_c + qN_q i_q\right)\varphi_{gu}} \tag{2.24}$$

Equations 2.22 and 2.24 result in a design foundation width B_d that is larger than a certain value. In the simulations, the smallest value possible is used, and therefore the “greater than” sign in the equations is replaced with an “equal to” sign.

2.4. Probabilistic Theory

In order to estimate the failure probability of a shallow foundation under seismic loading sometime during the design lifetime of the structure, first the conditional failure probability given that an earthquake with return period r_i acts upon the foundation must be estimated. The total lifetime probability of failure is then estimated by using the total probability theorem, in which each conditional probability of failure given an earthquake return period r_i is multiplied with the probability of an earthquake with return period r_i occurring, and then summed together. The details of this procedure and other relevant probabilistic theory are discussed in the following sections. More in depth information can be found in Fenton and Griffiths (2008).

2.4.1. Log-normal Distribution

The log-normal distribution is a non-negative, continuous probability distribution. It is constructed by generating a normal probability distribution and taking the natural exponent of that value.

The parameters of the log-normal distribution can be obtained from the parameters of the underlying normal distribution as follows (Fenton & Griffiths, 2008),

$$\sigma^2_{\ln X} = \ln\left(1 + \frac{\sigma_X^2}{\mu_X^2}\right) \tag{2.25}$$

$$\mu_{\ln X}^2 = \ln(\mu_X) - \frac{1}{2}\sigma_{\ln X}^2 \tag{2.26}$$

2.4.2. Correlation Length

The correlation length, θ, can be roughly defined as the separation distance between two points in a random field beyond which the correlation coefficient between them becomes negligible (Fenton & Griffiths, 2008). In this research, the correlation coefficient between any two points in the soil is assumed to be described by a Markov correlation function (Fenton & Griffiths, 2008),

$$\rho(\tau) = \exp\left(-\frac{2|\tau|}{\theta}\right) \tag{2.27}$$

where τ is the distance between two points. The correlation exponentially decays towards zero with distance τ.

2.4.3. Conditional Probability

Conditional probability is the probability of an event given that another event has already occurred (Fenton & Griffiths, 2008). The conditional probability of an event F given that an event R happens will be denoted as $P[F|R]$. This conditional probability can be calculated as the probability of the intersection of events F and R, divided by the probability of event R occurring. This is shown symbolically, as follows,

$$P[F|R] = \frac{P[F \cap R]}{P[R]} \tag{2.28}$$

2.4.4. Total Probability Theorem

The total probability theorem, also known as the law of total probability, is a way to find the unconditional probability of an event by combining the conditional probabilities of a number of sub events that together make up the event of interest, multiplied by their probabilities of occurrence (Fenton & Griffiths, 2008), as shown in the following equation,

$$P[F] = \sum_{i=1}^{n} P[F|X_i]\,P[X_i] = \sum_{i=1}^{n} P[F \cap X_i] \tag{2.29}$$

where $P[F]$ is the probability of event F, $P[F|X_i]$ is the probability of event F given that subevent X_i occurs, and $P[X_i]$ is the probability that subevent X_i occurs. There are n different subevents X_i in Equation 2.29. By multiplying the conditional probability of event F given X_i by the probability that X_i occurs, the intersection between events F and X_i is calculated. In fact, the essence of the total probability theorem is that all possible intersections between events F and X_i are summed.

A requirement for the usage of the total probability theorem is that there is no intersection between the sub events (i.e. they are disjoint), and that all sub events together make up for the complete event (i.e. they are collectively exhaustive). The equation for the continuous total probability theorem is given as follows,

$$P[F] = \int P[F|X = x]\,f(x)\,dx \tag{2.30}$$

where the probability density function $f(x)$ is the continuous probability density function of a continuous set of subevents.

Because the maximum intensity of an earthquake during the lifetime of a structure is random, the total probability theorem must be used to determine the total lifetime probability of failure of the geotechnical system. Since return periods are a continuous variable, the continuous total probability theorem in Equation 2.30 should ideally be used. For the lifetime probability of failure given seismic events in Equation 2.30, X would be stochastic return period R, and x the realization of an i number of actual return periods r_i.

Equation 2.30 is only useful when an analytical solution exists for both the integral and the conditional probability of failure. In the case of this thesis, there appears to be no such solution. Therefore

an approximation has to be used which makes use of simulated estimations of the conditional probability of failure. Since simulations cannot be done on an infinite scale, a range of return periods is discretized, which means that the previously continuous set of sub events r_i is no longer collectively exhaustive. The estimation now makes use of the discrete Equation 2.29 instead of the continuous Equation 2.30, and the total probability theorem becomes only an approximation for the total lifetime probability of failure. It is, however, a good estimation if enough return periods are used and those return period earthquakes that are omitted do not contribute much to the overall lifetime probability of failure.

An example to demonstrate what the problem is with a not collectively exhaustive group of events is the following: Consider a failure event F in which n return period seismic events are possible. Although n is infinite in reality, let's consider what happens if only the first $n = 10$ years of return periods are included, i.e., only r_1 to r_{10} are considered, where r_i is the seismic event having a return period of i years. If the total probability theorem is applied to this case, the probability intersection $P[F \cap r_1 \leq R \leq r_{10}]$ will be found instead of the unconditional probability of failure $P[F]$. Because the sum of the probability of failure for all larger return periods is cut off at $P[F \cap R > r_{10}]$, a large number of subevents is not taken into account, therefore giving a faulty approximation of the total lifetime probability of failure.

Assuming that seismic events lower than some return period, r_m, can be considered to be static load cases, and that the design lifetime probabilities of occurrence of seismic events having return periods in excess of r_n are negligible, the total lifetime probability of failure can be approximated as a purely seismic case as follows,

$$P[F] \approx P[F|r_m \leq R \leq r_n] = \frac{P\Big[F \cap (r_m \leq R \leq r_n)\Big]}{P[r_m \leq R \leq r_n]}$$

$$= \frac{\sum_{i=m}^{n} \Big(P[F|R = r_i]\, P[R = r_i]\Big)}{P[r_m \leq R \leq r_n]} \tag{2.31}$$

2.4.5. Earthquake Event Probability

Assuming that an earthquake can occur at any instant in time, the probability of an earthquake occurring can be characterized using a Poisson distribution (see e.g. Fenton & Naghibi, 2017). Simply said, with the Poisson distribution it is assumed that whether or not a seismic event occurs can be described by an infinite set of (binomial) trials, one at each instant in time. The probability of a certain number of events occurring according to the Poisson distribution has the following equation,

$$P[N_t = k] = \frac{(\lambda t)^k}{k!} e^{-\lambda t} \tag{2.32}$$

where t is the time during which the binomial trials take place (the design lifetime of a structure), N_t and k are the number of earthquake events in t years, and λ is the mean rate of earthquake events.

If the return period of a specific earthquake intensity is r_i years, then the mean rate is equal to 1 over that return period: $\lambda_i = 1/r_i$. Equation 2.32 gives the probability that a certain number of earthquakes occurs during the lifetime of the structure t. However, it is not of interest if 2, 3,or 25 earthquakes of a certain return period occur. Instead, the probability of at least one earthquake with a certain return period $R > r_i$ occurring during the lifetime of the structure is of interest. This probability can be determined by taking the complement of the probability that no earthquake of that strength occurs,

$$P[N_t > 0] = P[R > r_i] = 1 - P[N_t = 0] \tag{2.33}$$

which, using Equation 2.32, leads to,

$$P[N_t > 0] = 1 - e^{-\frac{t}{r_i}} \tag{2.34}$$

$P[N_t > 0]$ is also the probability that a random return period R is larger than r_i. To now calculate the probability of an earthquake with a specific return period r_i occurring, an infinitesimally small interval should be considered, as follows,

$$P\left[R = r_i\right] = \lim_{\Delta r \to 0} \left(e^{-\frac{t}{r_i + \Delta r}} - e^{-\frac{t}{r_i - \Delta r}} \right) \tag{2.35}$$

Of course an infinitesimally small interval is impossible to realize when doing simulations. A decent approximation is found by using larger intervals.

In this research, the same number of return period intervals are assumed as done by Naghibi and Fenton (2018). The return period range goes from $\ln(r_m) = 4.0$ to $\ln(r_n) = 8.0$, with 40 steps of $ln(r_i) = ln(r_{i-1}) + 0.1$ in total. The lower boundary r_m and the upper boundary r_n correspond to earthquake return periods of 52 years and 3134 years. The approximate probability that a specific return period earthquake occurs over the design lifetime t is then,

$$P\left[R = r_i\right] \approx e^{-\frac{t}{r_{i+0.5}}} - e^{-\frac{t}{r_{i-0.5}}} \tag{2.36}$$

2.4.6. Probability of Failure Standard Deviation

Each conditional probability of failure is estimated through a number of simulations n_{sim}. Because there is a limited number of simulations that can realistically be performed, there is also a limit to how precise the answers can be. The standard deviation, $\sigma_{\hat{p}_f}$, of the estimated conditional probability of failure $\hat{p}_f$ can be used to specify the confidence interval of the answers, which is shown in Section 5.3.1.

$\sigma_{\hat{p}_f}$ can be estimated as follows (Fenton & Griffiths, 2008, eq. 6.101),

$$\sigma_{\hat{p}_f} \simeq \sqrt{\frac{\hat{p}_f \left(1 - \hat{p}_f\right)}{n_{sim}}} \tag{2.37}$$

2.4.7. Reliability Index

For assessment of the failure of a structure, there are two main variables, namely the design resistance R_d and the design actions E_d. The resistance has to be larger than the loads, otherwise a structure fails. Both variables can be combined into a single variable with a single probability distribution, called the *limit state* Z ($Z = R_d - E_d$). As long as Z is larger than zero, the resistance will be larger than the loads, and the structure does not fail.

The *reliability index* β is the number of standard deviations that the mean of Z is away from zero, and thus is a way to express the likelihood of a structure failing,

$$\beta = \frac{\mu_Z}{\sigma_Z} \tag{2.38}$$

where μ_Z is the mean value of Z, and σ_Z is the standard deviation of Z.

The reliability index is used as a different way to define the lifetime reliability of a geotechnical system under seismic loading. It is used specifically in Section 5.1.3.

3

Numerical Modelling

3.1. Modelling Theory

Modelling is the procedure of representing reality by using mathematics. Simplified mathematics are often accurate enough for engineering purposes.

3.1.1. Soil Property Modelling

Not every single particle at a building site can be tested and evaluated. Representative soil parameters need to be determined from a limited number of samples, which brings uncertainty into calculations of the bearing capacity. Are there weak soil zones in between tested locations, and do these weak zones affect the bearing capacity of the foundation? In order to imitate spatial variability of soil parameters in the simulations, an algorithm called local average subdivision (LAS) is used.

LAS is based on the principle that engineering measurements are not continuous up to the individual soil grains, but are discrete, local averages of a group of soil grains (Fenton & Griffiths, 2008). Four of a possibly infinite number of stages of a one dimensional LAS process are presented in Figure 3.1 (Fenton & Griffiths, 2008). Starting from Stage 0, the generated random field becomes more refined with each subsequent stage. The value of the generated soil parameter in each cell is Z_j^i, where i is the stage number, and j is the cell number. Every cell in Figure 3.1 has a certain color, which is an example of the random value Z_j^i that a cell could have. The darker the color is, the larger the value of Z_j^i is compared to the mean of the random field. This one dimensional random field could for example be the results of a cone penetration test, although Figure 3.1 would need to be turned by 90 degrees.

A written description of the stages of one dimensional LAS corresponding to Figure 3.1 is given as follows, as specified by Fenton and Griffiths (2008),

Stage 0: Generate the global average of the random field, Z_1^0. The global average is drawn from a normal distribution if the the modelled soil parameter is normally or lognormally distributed (see Section 2.4.1 for the normal distribution corresponding to a specific lognormal distribution);

Stage 1: Divide the initial cell Z_1^0 into two new cells, Z_1^1 and Z_2^1. The generation of Z_1^1 and Z_2^1 has to satisfy three conditions:

(a) The average of Z_1^1 and Z_2^1 has to be equal to parent value Z_1^0. This can be done by generating Z_2^1, and then deriving Z_1^1 from the fact that $Z_1^0 = \left(Z_1^1 + Z_2^1\right)/2$;

(b) The values of Z_1^1 and Z_2^1 have to be properly correlated (e.g. with a Markov Correlation, Section 2.4.2);

(c) Both Z_1^1 and Z_2^1 have to have the correct variance that is related to the generated field.

Stage 2: All cells from the previous stage are divided into two new cells. The same three conditions as in the previous stage apply. Additionally, the correlation with cells further away must be correct. For example, if Z_1^2 and Z_2^2 are being generated, these values can have a correlation with Z_3^2 and Z_4^2, depending on the correlation length.

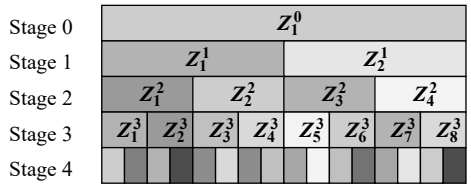

Figure 3.1: "Top-down approach to LAS construction of local average random process." (Fenton & Griffiths, 2008)

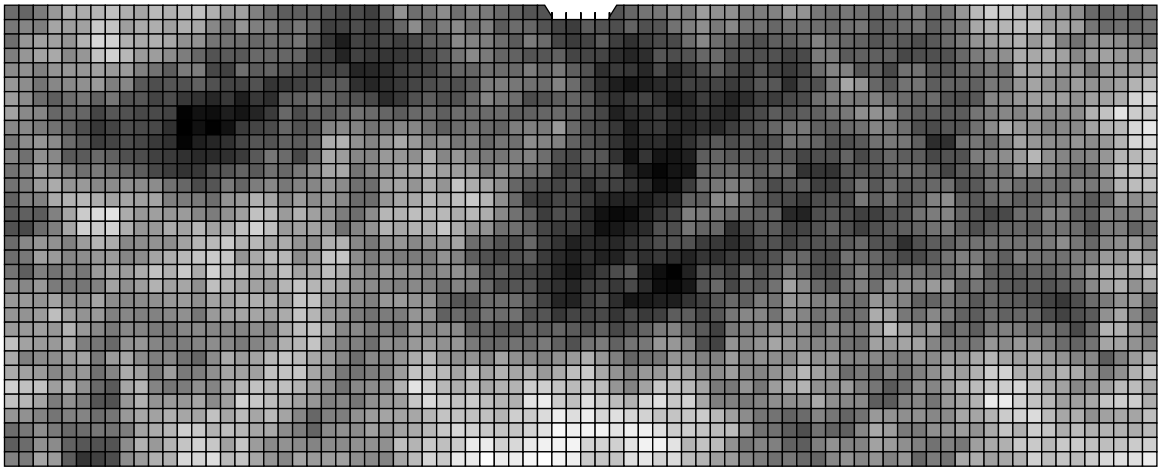

Figure 3.2: Example of a lognormally distributed random cohesion field as produced by the LAS algorithm

Stage 3: Repeat the procedure in Stage 2 until the desired resolution of the soil parameter field is reached. If the required field is lognormally distributed, the values should be converted from the corresponding normal distribution (Section 2.4.1) at the end of the final stage.

Similarly to the one dimensional process described above, LAS can be used to generate two dimensional random parameter fields. Instead of dividing cells into two new cells, cells are quartered. Of these four cells, three cells are randomly generated, after which the value of the fourth cell is calculated in such a way that the mean of the four new cells is equal to the mean of the parent cell.

After the desired resolution has been reached, the randomly generated parameter field can be allocated to different elements in a finite element mesh, resulting in something similar to what can be seen in Figure 3.2, in which the cohesion has been mapped to the finite element mesh. As with the one dimensional example in Figure 3.1, the darker the cell is, the higher the value is relatively to the mean of the random field. The generated field is isotropic, which can be noticed from the similar dimensions of the color patches in both the horizontal and vertical directions.

3.1.2. Load Modelling

Earthquake accelerations introduce horizontal and vertical forces on the foundation. Seismic forces for different return periods r_i are modelled through the theory given in Section 2.2.2.

Besides seismic forces, the weight of the foundation and superstructure must be modelled, which is called the dead load. At the moment of designing, the dead load is not known exactly, nor is the exact force transfer from the bridge to the different parts of the foundation known.

Finally, the live load must be modelled, which is the load due to traffic, weather, and other transitory effects. Since earthquakes are random in time, it is unknown what the traffic load is during an earthquake, as can be seen from a traffic load over time diagram plotted in Figure 3.3.

The seismic loads, dead loads and live loads are all chosen to be lognormally distributed. The non-negative property of the lognormal distribution is desirable, because gravity does not work upwards, therefore the sign of the modelled load is preferred to be always positive (and thus downwards). Every property of the used distributions is given in Section 4.1.3, where the variables are justified. This includes the values of the deterministic parameters used in the design of the simulations, which are based on the means of the random parameters.

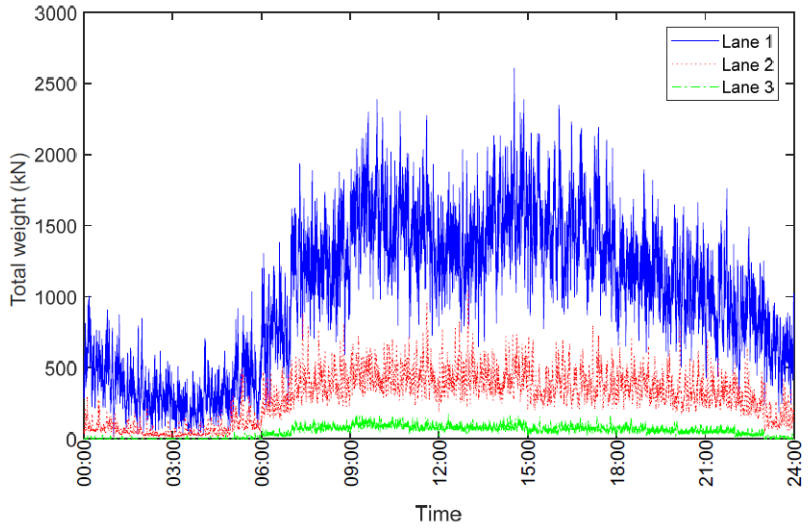

Figure 3.3: "Time history of the total weights of vehicles on the bridge from 2005" (Wang & Xu, 2019)

3.2. Program Description

3.2.1. Simulation Algorithm

In order to estimate the total lifetime probability of failure, n_{sim} realizations are performed for each of the 41 earthquake return periods r_i. The discretization of r_i is given in Section 2.4.5.

Each total lifetime probability of failure is estimated with a different resistance factor φ_{gu} and design return period. The resistance factors considered are 0.4, 0.5, 0.6, 0.7, 0.8, 0.9 and 1.0. The design return periods considered are earthquakes of a return period of 0 years, 475 years, 975 years, and 2475 years. Given an "actual" earthquake return period r_i, design return period earthquake, and resistance factor φ_{gu}, n_{sim} realizations are performed of the following algorithm, as presented by Naghibi and Fenton (2018) in Figure 3.4:

1. Generate the random soil parameter fields using local average subdivision (LAS):
   LAS is described in Section 3.1.1. Not every soil parameter has an impact on the design procedure, for which reason random fields are generated on only those parameters that do. Which variables are random and which variables are deterministic are given in Chapter 4.

2. Sample the characteristic strength values from the random soil parameter fields:
   This step is comparable to a real life cone penetration test. A virtual sample is taken by calculating the average of a set of nodes in each of the random soil parameter fields. Since in real life it is not often known exactly where a foundation has to be, the samples are taken at a specified distance r from the center of the random field.

   The characteristic value $\hat{X}$ of a normally distributed random variable is found with the arithmetic average, which has the following equation (Fenton & Griffiths, 2008),

$$\hat{X} = \frac{1}{n}\sum_{i=1}^{n}\hat{X}_i \tag{3.1}$$

   The characteristic value $\hat{X}$ of a lognormally distributed random variable is found with the geometric average, which has to following equation (Fenton & Griffiths, 2008),

$$\hat{X} = \left(\hat{X}_1\hat{X}_2\ldots\hat{X}_n\right)^{\frac{1}{n}} = \exp\left(\frac{1}{n}\sum_{i=1}^{n}\ln\hat{X}_i\right) \tag{3.2}$$

   in which $\hat{X}_i$ are the parameter values of the random field at sampled elements i. The values of i are taken from ground level $i = 1$ to a specified depth of $i = n$.

3. Design the foundation for this realization:
   A footing is designed for the random soil field that is generated in Step 1, by using the design procedure described in Section 2.3 and using the characteristic soil parameters $\hat{X}$ found in Step 2. In the design, the intensity of the seismic effects are estimated with a design return period earthquake. It is this step where the resistance factor φ_{gu} is used to get the design foundation width B_d.

   Finally, the designed footing is modelled on the finite element mesh by converting the design width to a number of surface nodes, which is then rounded upwards. For example, if the finite elements are 0.25 by 0.25 meters and the foundation has to be 1.05 meters wide, the footing is given 5 different elements, because $1.05/0.25 = 4.2$, which is rounded up to 5.

4. Optional: Reduce the soil strength:
   If part of the scenario, the random soil parameter field is multiplied with a random cyclic degradation factor field δ_τ after the characteristic soil parameters are sampled in step 2. A with depth increasing random parameter field is generated for δ_τ (see Section 2.2.3). In case that cyclic degradation is part of the scenario, the characteristic soil parameters that are used in the design are also degraded with a deterministic value in the previous step.

5. Generate loads:
   In real life there will be a certain unknown load on the footing when an earthquake hits. This unknown load consist of seismic loads, dead load and live load. In order to be able to test the designed foundation against these loads, they need to be randomly generated. The intensity of the generated seismic load depends on for which return period r_i the conditional probability of failure is being estimated in this set of n_{sim} realizations. More is explained in Section 2.2.2 and in Section 3.1.2.

6. Test the designed footing for failure:
   The randomly generated load from Step 5 is spread out over the number of surface nodes corresponding to the foundation design width found in Step 3. A FEM analysis is then conducted over a mesh with the properties of the random soil fields that have been generated in Step 1. If the simulated foundation fails, a counter n_{fails} is incremented.

After n_{sim} realizations of steps 1 to 6 have finished, the conditional probability of failure given an earthquake return period r_i can be estimated. This conditional probability of failure is for the specific design return period and resistance factor that have been used in the algorithm. The following formula is used to estimate the conditional probability of failure given an earthquake return period r_i,

$$P\left[F|R = r_i\right] \approx \frac{n_{fails}}{n_{sim}} \tag{3.3}$$

after which the procedure is repeated for return period r_{i+1}, with the same resistance factor and design return period. When the conditional probability of failure for each of the 41 return periods has been estimated, the unconditional probability of failure can be estimated using the total probability theorem (Section 2.4.4).

3.2.2. RFEM Specifications

In this thesis, soil is modelled with the random finite element method (RFEM). RFEM is a finite element method (FEM) that is used in a Monte Carlo simulation. Each realization of the Monte Carlo simulation has random properties, such as a random soil parameter field, or forces acting on the structure. In FEM, reality is modelled by discretizing differential equations that are representative for a physical process over space into “finite elements” (Smith et al., 2014).

RFEM also has more advanced approaches, such as the random material point method (e.g. Wang et al., 2016), importance sampling (e.g. Soubra et al., 2019), or coupled approaches (e.g. Karamitros et al., 2013; Elia & Rouainia, 2014). None of these are used in this thesis due to time constraints. More in depth information on the (random) finite element method can be found in Smith et al. (2014) and in Fenton and Griffiths (2008).

The used RFEM program is a modified version of a program called “RBEAR2D” (Fenton & Griffiths, 2000). The new program is called “RBEAR2S”, because it is the pseudo-dynamic seismic load version

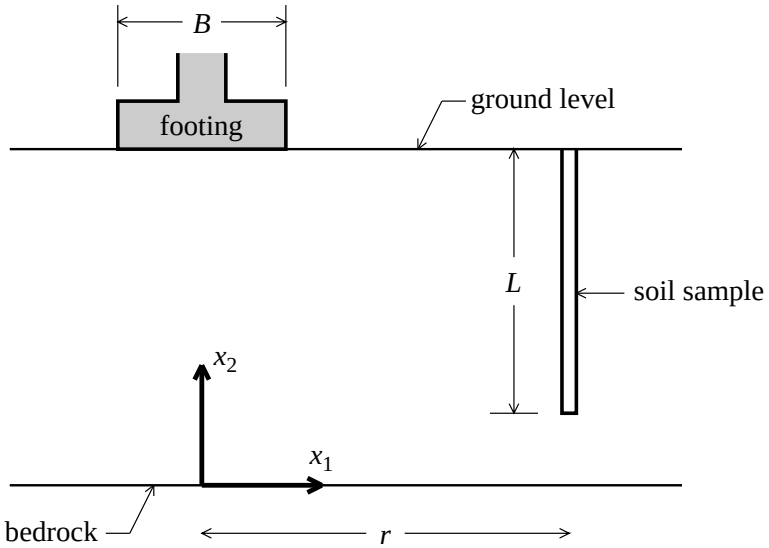

Figure 3.4: "[Schematic of procedure] used to predict probability of bearing capacity failure." (Naghibi & Fenton, 2018)

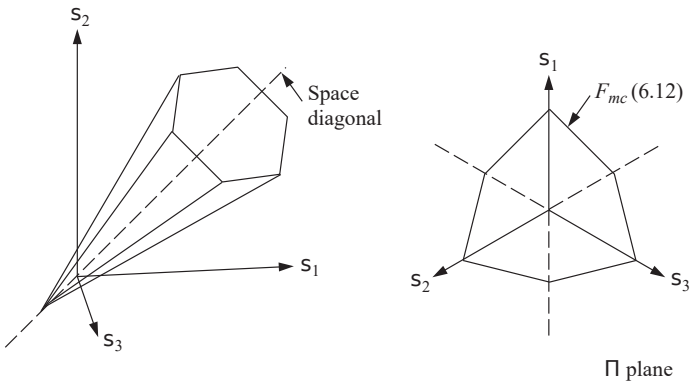

Figure 3.5: "Mohr–Coulomb failure criterion." (Smith et al., 2014)

of RBEAR2D. Whereas in RBEAR2D displacement steps are made until the footing fails, in RBEAR2S a load based approach is used. This load-based addition was programmed by Dr. ir. Bram van den Eijnden. Instead of cycling through displacement steps until failure, it is now tested whether or not the solution converges given that a certain load is present on the virtual foundation.

The FEM program goes through a number of iterations in which displacements are calculated. If the difference in displacements compared to the previous iteration is below a certain threshold, the solution has converged. If a larger number of iterations is needed without convergence occurring, the footing has failed.

All elements are 8-node quadrilaterals.

All variables are of single precision floating point format in order to save time.

3.2.3. Yield Criterion

In RBEAR2D, the von Mises yield criterion is used. Because both frictional and cohesive soil parameters can be input into RBEAR2S, a so called "conical" model is preferred over von Mises (Smith et al., 2014). Therefore the Mohr-Coulomb model was chosen as a yield criterion. If the soil is assumed to be frictionless, the Mohr-Coulomb model reduces to the Tresca model (Yu, 2006), which is an acceptable model for the behavior of clay in undrained conditions(Smith et al., 2014).

A graphic representation of the Mohr-Coulomb failure criterion by Smith et al. (2014) can be found in Figure 3.5. For the Tresca failure space, the graphic is similar, but instead of a cone, the failure space is an infinite hexagonal prism.

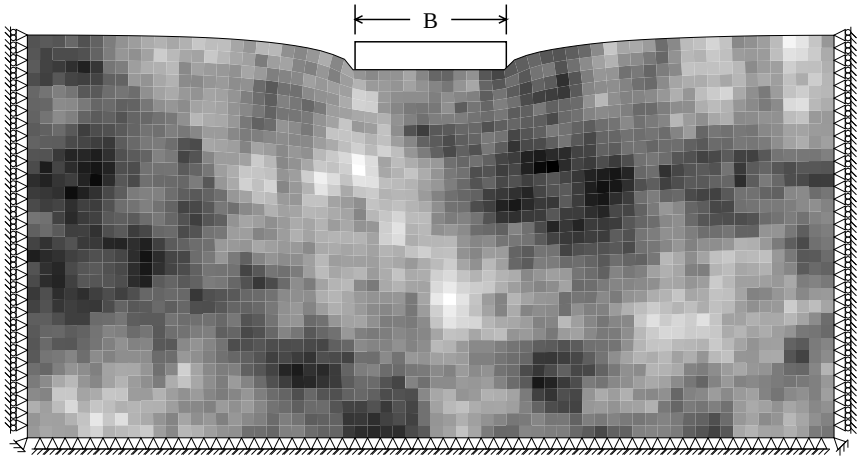

Figure 3.6: Schematic of the FEM boundary conditions. “Cross-section through a realization of the random soil underlying the footing.” (Fenton et al., 2005)

3.2.4. Boundary Conditions

The outer nodes of the mesh are restricted in their movements. Preferably, the failure zone is not influenced by these boundary conditions.

A schematic of the degrees of freedom of the mesh can be seen in Figure 3.6. The dimensions of the mesh in Figure 3.6 are different than the dimensions of the mesh in this thesis, but the boundary conditions are the same.

The bottom nodes of the mesh are fixed in both the horizontal and vertical directions. It can be assumed that this is a solid rock layer.

The nodes at the sides of the mesh are fixed in the horizontal direction, but can move vertically. In real life, there is soil beyond these nodes, which mostly holds back the soil from moving in the horizontal direction.

At the top of the mesh, all nodes are free to move, except the nodes at which the foundation is modelled to be. The footing nodes are tied together in the both the horizontal and vertical direction. It is assumed that the footing is rough, rigid and does not rotate. The vertical and horizontal load are spread out over the footing nodes, forcing the footing nodes to move in a way that corresponds to the loads on them.

4

Simulations

4.1. Justification of Variables

How many of the n_{sim} realizations fail is partly dictated by the standard deviation of the randomly generated variables. In order for the results of this study to be trustworthy, the parameters of both the deterministic and random variables need to be plausible.

In Section 4.1.1 the soil parameters are justified. Secondly, in Section 4.1.2 the mesh dimensions are justified. Finally, in Section 4.1.3 the design loads and simulated loads are justified.

4.1.1. Soil Parameter Justification

1. Cohesion (c):
   The modelled soil is a high strength clay in undrained conditions. According to the Dutch annex of Eurocode 1997-1 (Nen-En, 2018), a value of 40 kPa is reasonable for the cohesion of clay. The coefficient of variation for the cohesion is chosen to be 0.3 (Phoon & Kulhawy, 1999).

2. Friction angle (ϕ):
   It is generally accepted that clay may be purely cohesive in undrained conditions. Therefore the friction angle is chosen to be $\phi = 0°$.

3. Dilation angle (ψ):
   The value of the dilation angle has a negligible effect on the results of the simulations. $\psi = 0°$ has been chosen.

4. Poisson's ratio (ν):
   Poisson's ratio is limited to a range of 0.0 to $+0.5$. Generally, the Poisson's ratio in medium strength clay ranges from 0.2 to 0.5 (Das, 2008, Table 12.6). A Poisson's ratio of 0.3 is a conservative estimate that falls within this range.

5. Young's modulus (E):
   The value of the Young's modulus has a negligible effect on the results of the simulations. Young's modulus influences the deformation of the mesh, but does not change the bearing capacity. A reasonable order of magnitude for clay is 10^4 kPa (Das, 2008, Table 12.6), which will be the value used in the simulations.

6. Specific weight (γ):
   The specific weight of the saturated clay is chosen to be 17 kN/m^3, supported by Eurocode 1997-1 Dutch annex (Nen-En, 2018).

7. Sampling distance:
   The sampling distance is 5 meters from the center of the footing, to 5 meters deep. This is rather arbitrarily selected. However, in practice it is unlikely that a borehole will be taken directly under every foundation, and so the sample is likely to be some distance from the foundation. A value of 5 meters was selected as a reasonable average distance to the closest borehole at a typical site.

8. Scale of fluctuation (θ):
   The scale of fluctuation, θ, has been assumed to be 5 meters in both the horizontal and vertical directions; the field is isotropic. If soil is modelled as being isotropic over a large mesh depth, soil layers are assumed to not be present. However, this is acceptable since the problem described in this thesis is more about the variability between sampling, design and actual bearing capacity than about how close to a realistically layered soil the model comes. The choice of taking the same length for the scale of fluctuation and the sampling distance is reasonably conservative.

9. Cyclic degradation factor (δ_τ):
   In Section 2.2.3 the cyclic degradation factor (δ_τ) theory has been described. Since in the cyclic degradation factor theory it is assumed that the soil has nothing built on it, the (potentially negative) impact of a foundation on δ_τ is not taken into account. For that reason, it is assumed that at ground level, the cyclic degradation factor is 25% of what it is at 8 meters depth. The coefficient of variation is taken to be 0.2 (Pecker, 2004).

4.1.2. Mesh Justification

Mesh dimensions are determined through a careful assessment of three criteria.

The first criterion is that the width of the largest designed footing should be within a certain threshold. If a designed footing is too large, the simulated bearing capacity will be in error due to the finite element boundary conditions affecting the results. In the program, designed footings should be rejected if they are too large for the mesh dimensions, which is the case when the foundation width exceeds one-third of the total mesh width.

The second criterion is the other extreme: if a designed footing is too small, the program should reject it, because using too few elements makes the solution inaccurate.

The third criterion is that the mesh resolution should be feasible for use in a simulation. A mesh with a high resolution is preferable over a mesh with a low resolution, because a high resolution leads to a better approximation of the underlying differential equations. However, with a high resolution the stiffness matrix also becomes larger. Because of the use of the Cholesky decomposition to transform the stiffness matrix into a set of triangular matrices, all roundoff errors are multiplied and added up many times. If too many elements are used, that will eventually lead to numerical instability.

Based on the three criteria, a choice needs to be made on what the mesh size and resolution should be. Assuming a factored design load that gives a 1 meter wide foundation at the mean cohesion and a resistance factor $\varphi_{gu} = 1.0$, most outliers of the footing width are under 6.5 meters wide when designed with the lowest resistance factor that is considered in this study. Considering the mesh width criterion, the minimum mesh width is 19.5 meters wide, which is rounded up to 20 meters. The mesh height would be acceptable at 8 meters high, which is a bit less than half of the mesh width. The mesh element dimensions are chosen to be 0.25 by 0.25 meter, which does not lead to instabilities. By using these determined dimensions for the element size and mesh width, the total mesh is 80 by 25 elements.

4.1.3. Load Justification

The factored design load E_d is calculated with the following equation,

$$E_d = \alpha_L \frac{\mu_L}{K_L} + \alpha_D \frac{\mu_D}{k_D} \tag{4.1}$$

where α_i is the load factor, k_i is the bias factor that transforms the mean load μ_i into a characteristic load, subscript L stands for live load, and subscript D stands for dead load. The value of the live load factor α_L depends on what the current scenario is that is being simulated (see Section 4.2).

E_d is kept constant for all scenarios, which has the result that the mean footing width does not change between scenarios. The mesh dimensions can therefore be kept the same for all scenarios. In order for the design width to be 1 meter at a resistance factor $\varphi_{gu} = 1$ (as stated in Section 4.1.2), the factored design load is calculated to be 204 kN when assuming that the characteristic strength parameters are equal to the mean value.

The mean live and dead loads μ_L and μ_D have to be chosen in such a way that they fit Equation 4.1 for the (constant) factored design load E_d. Using the assumption that the mean live load is a certain percentage of the mean dead load, the live and dead load can be determined. In general, a live load

that is one-third of the dead load is assumed (Fenton et al., 2016), although this fraction is lowered for Scenario 6.

The coefficient of variation for the dead load is taken at 0.15 (Bartlett et al., 2003). Live load, which is expected to be more variable, is given a coefficient of variation of 0.30 (Becker, 1996a, 1996b). Lastly, the seismic loads are assumed to have a coefficient of variation of 0.85. The intensity of the seismic loads depends on the value of the dead load, although they have not been correlated within the program, for which reason the coefficient of variation for this load is rather large.

4.2. Scenarios

4.2.1. Scenario 1 - Vertical Load Only

In Scenario 1 a footing is simulated on which only a dead load and a vertical seismic load are present. Live load and horizontal seismic load are assumed to be absent in both the design and in testing. Cyclic degradation, however, is taken into account. An overview of the in Scenario 1 incorporated effects can be found in Table 4.1.

The purpose of this simple scenario is to find the baseline recommended resistance factors. If only the vertical seismic load is tested, the effect of the incorporation of horizontal seismic loads can be investigated when this scenario is compared against a scenario that is the same, but that does incorporate a horizontal seismic load.

The expected results from this scenario are a first indication of the order of magnitude of the resistance factors that target a reliability that is similar to static design targets. Although not every source of uncertainty is taken into account yet in this scenario, it is expected that the total lifetime probability of failure found in this scenario will be higher than what the CHBDC should be targeting.

Table 4.1: Scenario 1 - Vertical load only

Variables	Used in	
	Design	Simulations
Live load	No	No
Dead load	Yes	Yes
Seismic vertical load	Yes	Yes
Seismic horizontal load	No	No
Soil degradation	Yes	Yes

4.2.2. Scenario 2 - Horizontal Load (Degradation)

The only difference between Scenario 1 and Scenario 2 is the assumption of a horizontal seismic load acting on the geotechnical system. An overview of all incorporated effects in Scenario 2 can be found in Table 4.2.

The purpose of this scenario is to find out what the influence is of horizontal seismic loads on the required value of the resistance factor, which can be seen when the results of this scenario are compared to the results of Scenario 1.

It is expected that the influence of the by the horizontal seismic forces added uncertainty leads to lower resistance factors than are found in Scenario 1, and also to larger differences between the results for the different design return period earthquakes.

4.2.3. Scenario 3 - Horizontal Load (No Degradation)

Scenario 3 is the same as Scenario 2, with the only difference being that cyclic degradation is neglected in Scenario 3. An overview of all incorporated effects in Scenario 3 can be found in Table 4.3.

The purpose of this scenario is to find out what influence the cyclic degradation factor theory has on the recommended resistance factor. Because the lowest cyclic degradation factors are not much lower than 0.9 at the largest return period earthquake, it is expected that the results of Scenario 3 won't deviate from the results of Scenario 2 by a large margin. However, the spread of resistance factors for the different design return periods may become smaller, because the cyclic degradation theory appears to be on the conservative side.

Table 4.2: Scenario 2 - Horizontal load (degradation)

Variables	Used in	
	Design	Simulations
Live load	No	No
Dead load	Yes	Yes
Seismic vertical load	Yes	Yes
Seismic horizontal load	Yes	Yes
Soil degradation	Yes	Yes

Table 4.3: Scenario 3 - Horizontal load (no degradation)

Variables	Used in	
	Design	Simulations
Live load	No	No
Dead load	Yes	Yes
Seismic vertical load	Yes	Yes
Seismic horizontal load	Yes	Yes
Soil degradation	No	No

4.2.4. Scenario 4 - Live Load (factor 1.0)

In Scenario 4 a live load is assumed to be present during the earthquake. Live load was not designed for, nor simulated for, in previous scenarios, which is in agreement with the CHBDC. With a live load factor of 1.0, the live load assumed in the design is the same as the mean of the simulated live load in testing. An important note here is that to incorporate the live load in the design, the dead load had to be scaled down. This scaling is done so that the constant E_d requirement in Equation 4.1 would be satisfied, which means that the mesh does not need to be adjusted (See Section 4.1.3). Because of this change in mean dead load, the seismic forces on the footing change in intensity slightly. This change is not expected to make a significant impact on the recommended resistance factors. An overview of the incorporated effects in Scenario 4 can be found in Table 4.4.

The purpose of this scenario is to see what happens to the recommended resistance factor once a live load is being taken into account. This is an interesting scenario, because in the CHBDC live load is neglected for seismic load cases.

If a bridge has a constant flow of traffic over time, there is a probability that a live load is acting on the structure during an earthquake, and in that case it is expected that Scenario 4 more accurately models the conditions on the geotechnical system than the previous scenarios do. It is expected that the resulting resistance factors for Scenario 4 are lower than those in previous scenarios, since more uncertainty has been added to the system with the live loads.

Table 4.4: Scenario 4 - Live load (factor 1.0)

Variables	Used in	
	Design	Simulations
Live load	1.0	$F_{dead}/3$
Dead load	Yes	Yes
Seismic vertical load	Yes	Yes
Seismic horizontal load	Yes	Yes
Soil degradation	Yes	Yes

4.2.5. Scenario 5 - Live Load (factor 1.7)

Scenario 5 is the same as Scenario 4, but with a larger live load factor of 1.7. As was the case in Scenario 4, the addition of a live load in the design changes the seismic forces slightly, though not significantly. An overview of all incorporated effects in Scenario 5 can be found in Table 4.5.

The purpose of this scenario is to find out what happens to the recommended resistance factor when the live load factor in seismic design becomes more like the live load factor in static design. In static design, extreme (live) load cases are assumed, which means that the design in this scenario is expected to be conservative. However, Scenario 5 should be seen more as an experiment to see if the resistance factors go up towards the resistance factors the CHBDC recommends currently for seismic design of geotechnical systems.

Since the design in Scenario 5 is more conservative than the design in Scenario 4, the estimated lifetime probabilities of failure will be lower, which results in higher recommended resistance factors for Scenario 5. In general, the characteristics of the conditional failure probability figures are expected to be similar to those produced from the results of Scenarios 2 and 4, but shifted upwards.

Table 4.5: Scenario 5 - Live load (factor 1.7)

Variables	Used in	
	Design	Simulations
Live load	1.7	$F_{dead}/3$
Dead load	Yes	Yes
Seismic vertical load	Yes	Yes
Seismic horizontal load	Yes	Yes
Soil degradation	Yes	Yes

4.2.6. Scenario 6 - Live Load (factor 0.0)

Scenario 6 is the same as the previous two scenarios, except for the fact that the live load factor is assumed to be 0.0 in Scenario 6, and thus no live load is taken into account in the design step of the algorithm. A lower value is used for the simulated live load than is used in the other scenarios: the mean of the live load μ_L has been reduced from $1/3rd$ of the dead load to $1/15th$ of the dead load. The dead load has remained unchanged from the dead load in Scenario 2. An overview of all incorporated effects in Scenario 6 can be found in Table 4.6.

In current CHBDC practice it is assumed that no live load is present on a structure during an earthquake. Of course, it is always possible to have some sort of live load on a structure. The question is if such a load is certain enough to justify a live load factor.

The purpose of this scenario is to see what happens to the recommended resistance factors when there is a live load on the footing that has not been taken into account in the design. A comparison to Scenario 2 can then be made to see what the difference is with the idealized scenario where there is no live load on the structure.

Compared to Scenario 2, it is expected that the recommended resistance factors are a lot lower in Scenario 6. It is difficult to say what the difference will be compared to the results of Scenario 4. Although a live load is taken into account in Scenario 4, the larger variance in the live load of Scenario 4 might be more dominant than the change to the live load factor.

Table 4.6: Scenario 6 - Live load (factor 0.0)

Variables	Used in	
	Design	Simulations
Live load	No	$F_{dead}/15$
Dead load	Yes	Yes
Seismic vertical load	Yes	Yes
Seismic horizontal load	Yes	Yes
Soil degradation	Yes	Yes

4.3. Number of Realizations

All scenarios have the same number of realizations n_{sim}. As shown in Table 4.7, the number of realizations gets smaller with an increasing resistance factor. Because higher resistance factors make for weaker foundation designs, the conditional probability of failure becomes higher as the resistance factor becomes higher. With higher probabilities of failure, the sampling errors will become less dominant, as will be explained in Section 5.3.1.

Table 4.7: Number of realizations per run for different resistance factors for all scenarios

	n_{sim} at φ_{gu} for each actual return period r_i						
	0.4	0.5	0.6	0.7	0.8	0.9	1.0
Scenario 1	10,000	10,000	6,000	6,000	3,000	3,000	3,000
Scenario 2	10,000	10,000	6,000	6,000	3,000	3,000	3,000
Scenario 3	10,000	10,000	6,000	6,000	3,000	3,000	3,000
Scenario 4	10,000	10,000	6,000	6,000	3,000	3,000	3,000
Scenario 5	10,000	10,000	6,000	6,000	3,000	3,000	3,000
Scenario 6	10,000	10,000	6,000	6,000	3,000	3,000	3,000

In each scenario, four different return period earthquakes are used in the design, and those design parameters are tested gainst 41 different "actual" return period eathquakes. The number of realizations per lifetime probability of failure for each resistance factor is given in Table 4.8.

Table 4.8: Total number of realizations per design return period for different resistance factors for all scenarios

	n_{sim} at φ_{gu} for each design return period						
	0.4	0.5	0.6	0.7	0.8	0.9	1.0
Scenario 1	410,000	410,000	246,000	246,000	123,000	123,000	123,000
Scenario 2	410,000	410,000	246,000	246,000	123,000	123,000	123,000
Scenario 3	410,000	410,000	246,000	246,000	123,000	123,000	123,000
Scenario 4	410,000	410,000	246,000	246,000	123,000	123,000	123,000
Scenario 5	410,000	410,000	246,000	246,000	123,000	123,000	123,000
Scenario 6	410,000	410,000	246,000	246,000	123,000	123,000	123,000

4.4. Results Processing

As an example of how the lifetime probability of failure is estimated for a resistance factor, the results of Scenario 2 at resistance factor $\varphi_{gu} = 0.8$ are used.

Each simulation has an output that consists of 41 data points of estimated conditional probabilities of failure given a return period earthquake, $P[F|R = r_i]$. The conditional probabilities of failure are also specific for a resistance factor φ_{gu} and a design return period. In Figure 4.1, raw output from the simulation is plotted.

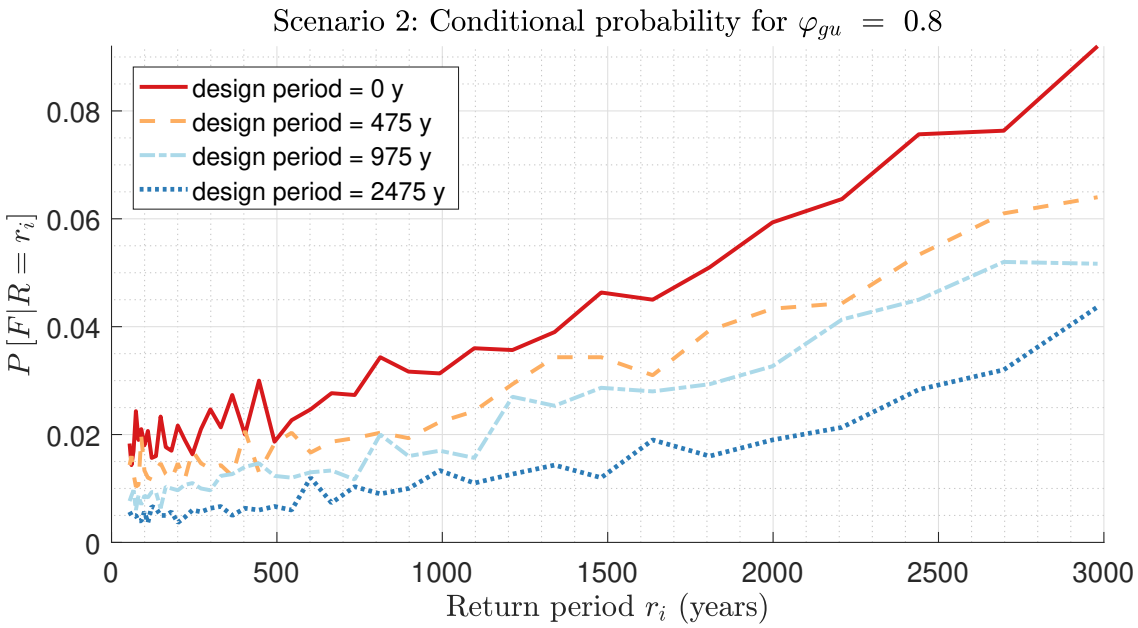

Figure 4.1: Example output of simulation - conditional probability of failure vs return period r_i

The total probability theorem utilizes each of the 41 data points (as described in Section 2.4.4). In Figure 4.2 the interim results of the total probability theorem are plotted: all estimated conditional probabilities of failure have been multiplied with their probability of occurrence, and are then cumulatively summed up over the horizontal axis. At the largest return period, which is 3000 years, the value of the unconditional lifetime probability of failure can be found.

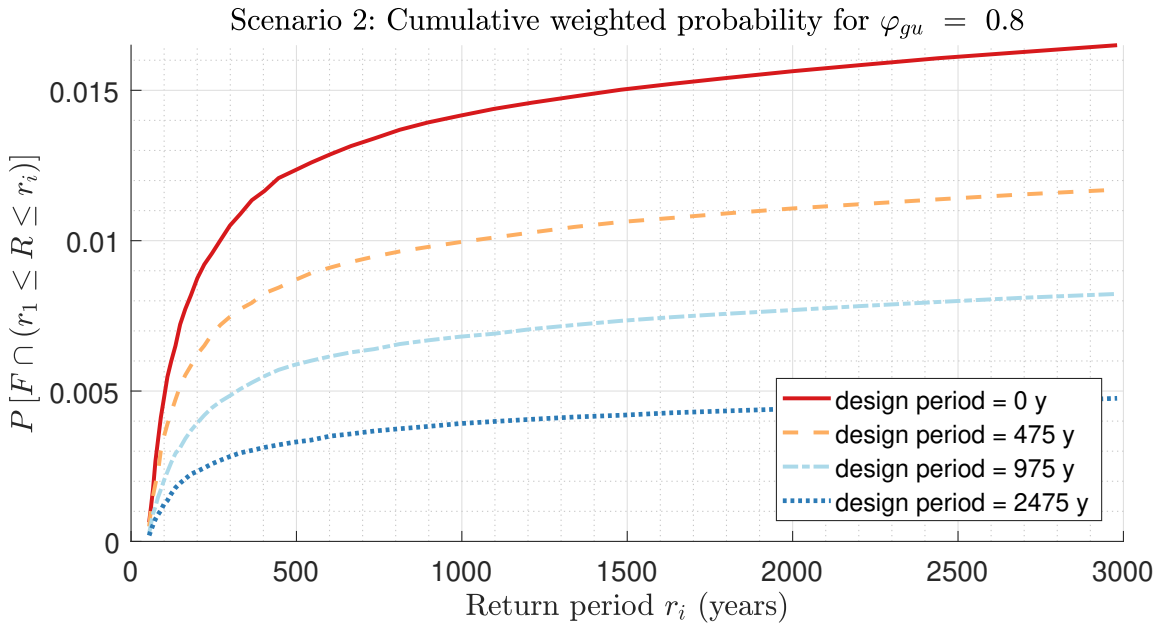

Figure 4.2: Example output of simulation - Cumulative weighted conditional probability of failure vs return period r_i

After all of the total lifetime probabilities of failure have been estimated, they can be conditionalized to the probability of the range of return periods occurring (Equation 2.31). Now the conditional probability of failure given a range of return periods can be plotted against the resistance factor, as seen in Figure 4.3.

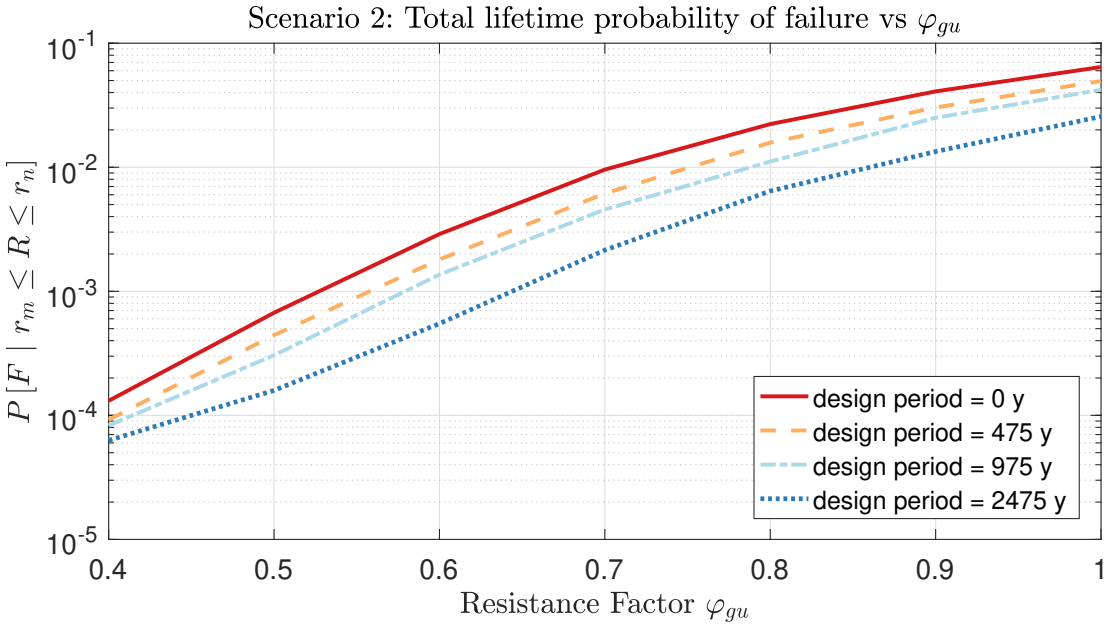

Figure 4.3: Example output of simulation - Normalized total probability of failure vs resistance factor

A presentation of all relevant results is given in Chapter 5.

5

Results

The results of the RFEM investigation are presented in Section 5.1, in the form of graphs of the estimated conditional probability of failure and graphs of the estimated lifetime probability of failure. Section 5.1.3 contains an explanation on how to find a resistance factor that successfully targets a lifetime probability of failure. An interpretation of the results is given in Section 5.2. What are the resistance factors that can successfully target a lifetime probability of failure similar to static design targets for a geotechnical system under seismic loading? How do the results compare to the resistance factors recommended by the CHBDC and how do they compare to other research? Finally, the quality of the results is discussed in Section 5.3.

A summary of the different scenarios considered is shown in Table 5.1.

Table 5.1: Scenario summary

	Description	Live load	Live load factor	Cyclic degradation
Scenario 1	Seismic vertical load only	no	-	yes
Scenario 2	Horizontal and vertical seismic load	no	-	yes
Scenario 3	Horizontal and vertical seismic load	no	-	no
Scenario 4	Horizontal and vertical seismic load	yes	1.0	yes
Scenario 5	Horizontal and vertical seismic load	yes	1.7	yes
Scenario 6	Horizontal and vertical seismic load	yes	0.0	yes

5.1. Results Presentation

All figures in Section 5.1 are grouped by graph type. For example, all graphs of the estimated conditional probability of failure for resistance factor $\varphi_{gu} = 0.5$ are presented in the same section. Grouping by graph type makes comparisons between scenarios easier.

5.1.1. Conditional Probabilities of Failure

The design step in the algorithm in Section 3.2.1 is run for four different design return period earthquakes. In other words, a design is produced using four different assumed earthquake loads. For each resistance factor φ_{gu} the analysis results in 4 sets of 41 estimated conditional probabilities of failure given a return period r_i; one set for each design return period.

Figures 5.1 to 5.6 present the estimated conditional probability of failure given a return period $R = r_i$ plotted against r_i for resistance factor $\varphi_{gu} = 0.5$ for each scenario. i ranges from 1 to 41. In Figures 5.7 to 5.12 the same data is presented for resistance factor $\varphi_{gu} = 1.0$. One line is plotted for each of the four design return periods.

Among other examples, Figure 5.1 and Figure 5.7 appear to have oscillations. Because the conditional failure probability is estimated by using random variables in a Monte Carlo simulation, the probabilities contain so called sampling errors, which is the source of the noise that is seen in the fig-

ures. Section 5.3.1 contains more discussion on sampling errors and their influence on the quality of the estimated lifetime probability of failure for a geotechnical system under seismic loading.

Using a higher design return period results in lower conditional probabilities of failure, because a foundation designed for a high return period earthquake will be stronger than a foundation designed for a low return period earthquake. This explains why the design return period of 2475 years has a lower probability of failure than the design return period of zero years.

A high return period on the horizontal axis implies that a more intense earthquake is acted on the geotechnical system. If earthquakes of higher intensity occur, the conditional probability of failure given that return period increases compared to lower return periods. Therefore the estimated conditional failure probability generally increases with the return period.

The estimated conditional probability of failure is different for each resistance factor φ_{gu}. Only the conditional probability of failure graphs for resistance factors $\varphi_{gu} = 0.5$ and $\varphi_{gu} = 1.0$ are presented in this section, although the results for the other resistance factors have also been verified. Results for other resistance factors are presented in the Appendix of this document.

The reason for presenting $\varphi_{gu} = 0.5$ is that the lifetime probabilities of failure tied to this resistance factor are generally just below or very close to the lifetime probability of failure targeted in static design.

The reason for presenting $\varphi_{gu} = 1.0$ is that this is the largest resistance factor that has been simulated.

Results for $\varphi_{gu} = 0.5$

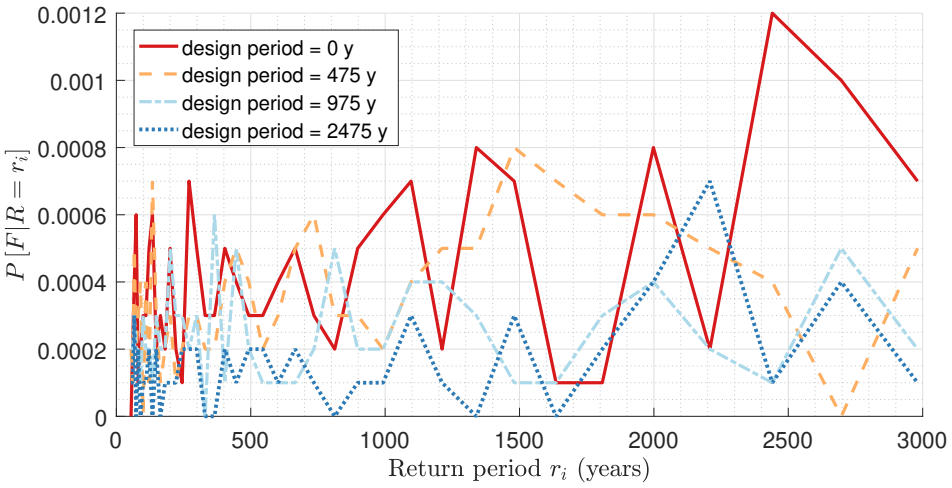

Figure 5.1: Scenario 1 - A plot of the conditional probability of failure against the return period ($\varphi_{gu} = 0.5$)

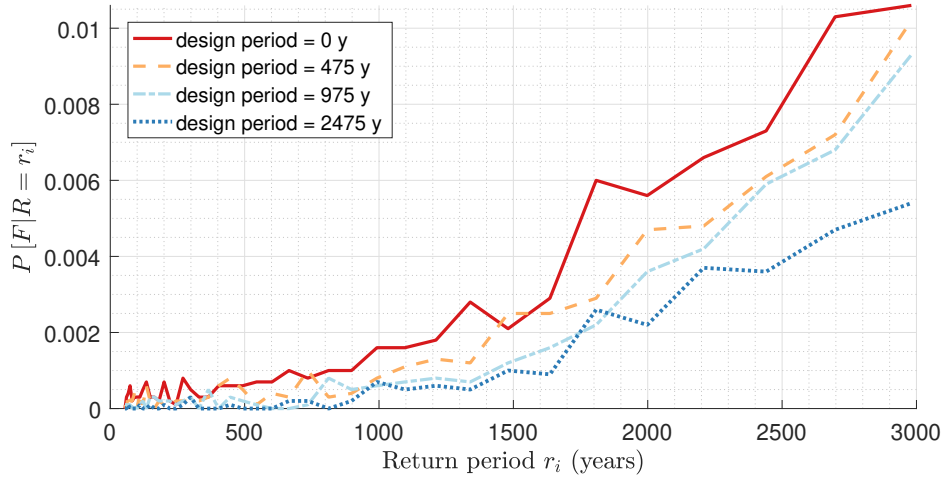

Figure 5.2: Scenario 2 - A plot of the conditional probability of failure against the return period ($\varphi_{gu} = 0.5$)

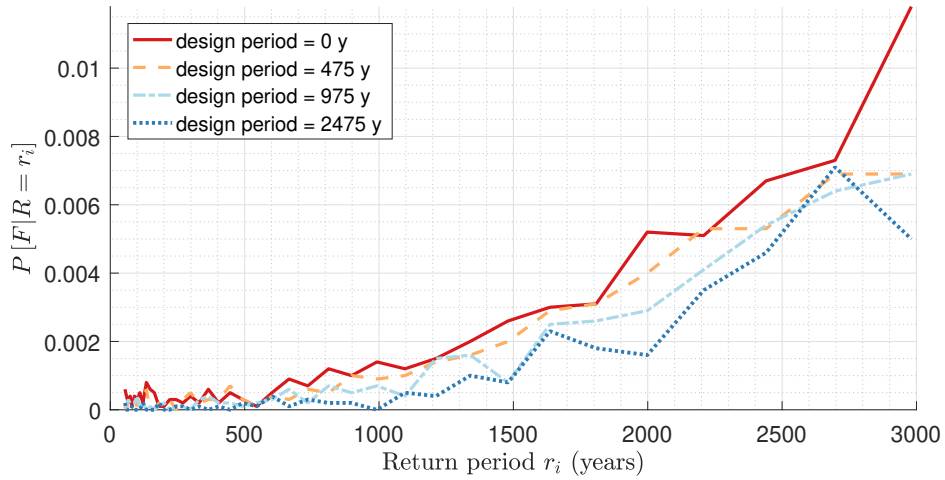

Figure 5.3: Scenario 3 - A plot of the conditional probability of failure against the return period ($\varphi_{gu} = 0.5$)

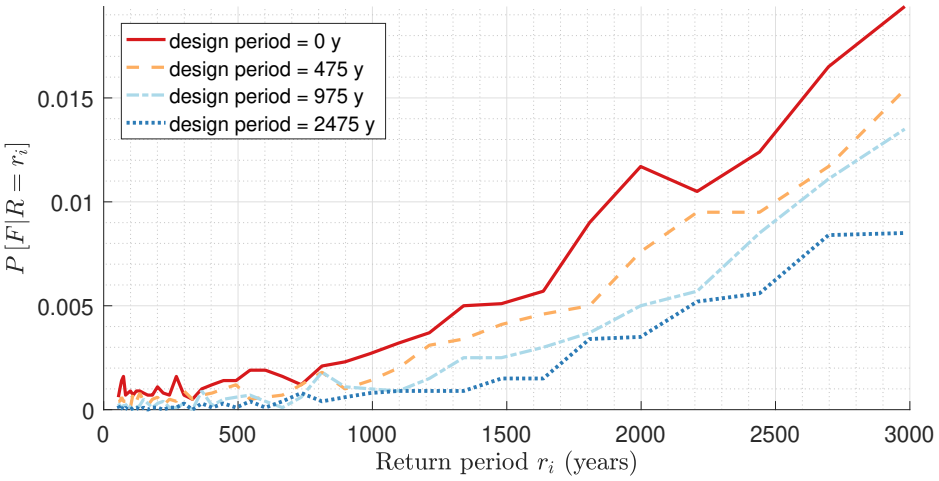

Figure 5.4: Scenario 4 - A plot of the conditional probability of failure against the return period (φ_{gu} = 0.5)

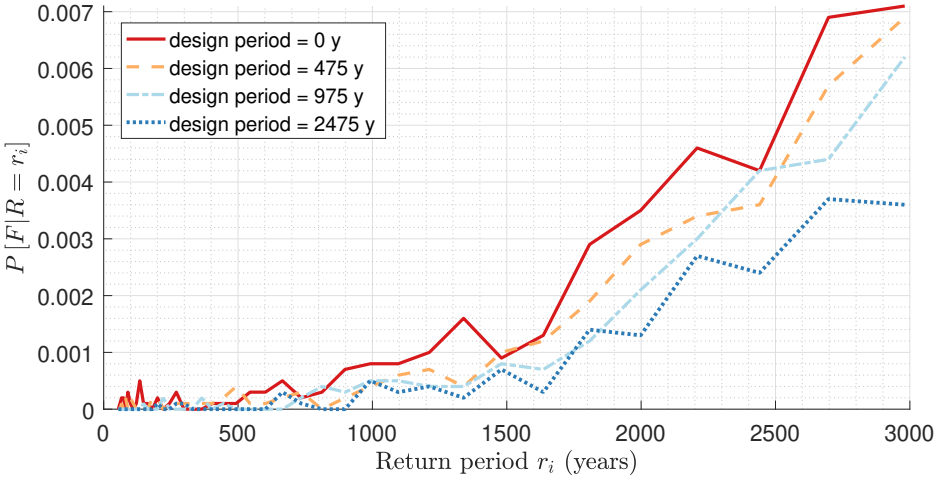

Figure 5.5: Scenario 5 - A plot of the conditional probability of failure against the return period (φ_{gu} = 0.5)

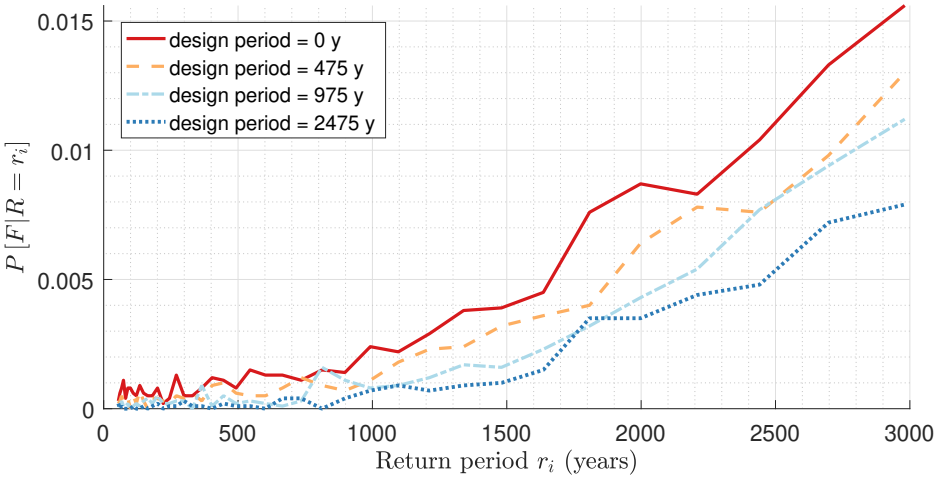

Figure 5.6: Scenario 6 - A plot of the conditional probability of failure against the return period (φ_{gu} = 0.5)

Results for $\varphi_{gu} = 1.0$

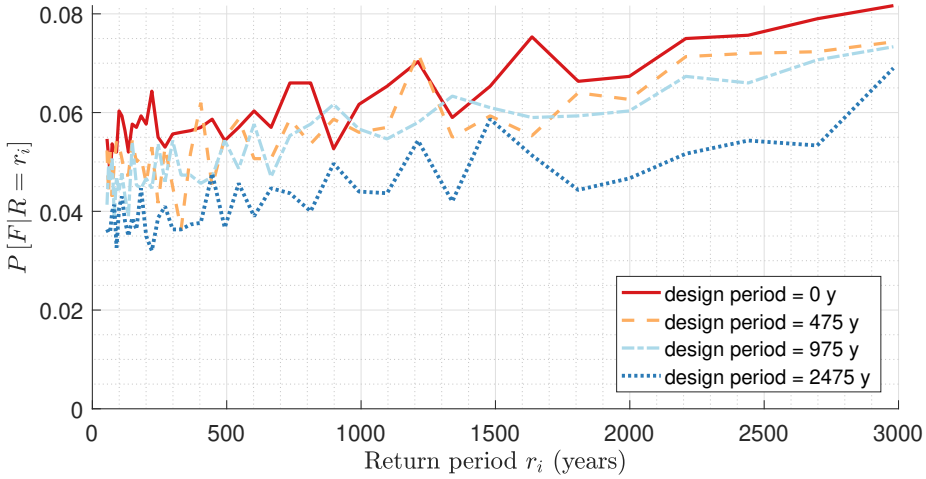

Figure 5.7: Scenario 1 - A plot of the conditional probability of failure against the return period ($\varphi_{gu} = 1.0$)

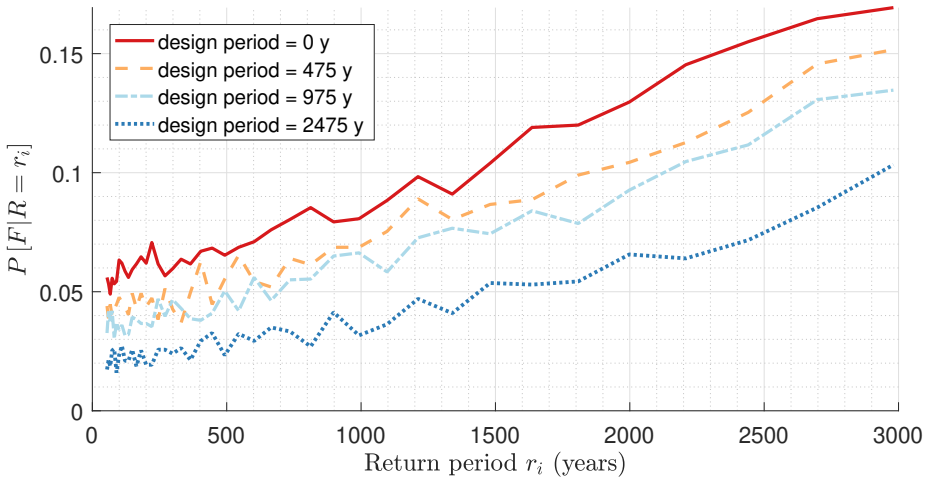

Figure 5.8: Scenario 2 - A plot of the conditional probability of failure against the return period ($\varphi_{gu} = 1.0$)

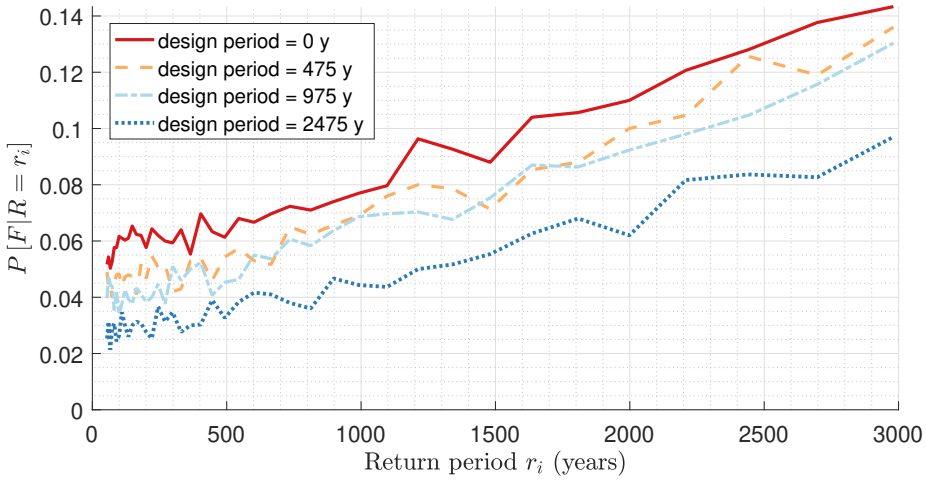

Figure 5.9: Scenario 3 - A plot of the conditional probability of failure against the return period ($\varphi_{gu} = 1.0$)

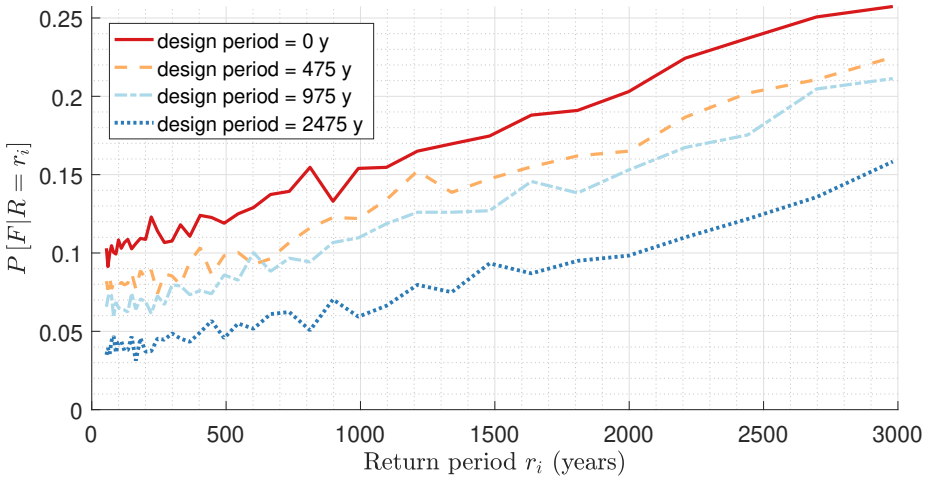

Figure 5.10: Scenario 4 - A plot of the conditional probability of failure against the return period (φ_{gu} = 1.0)

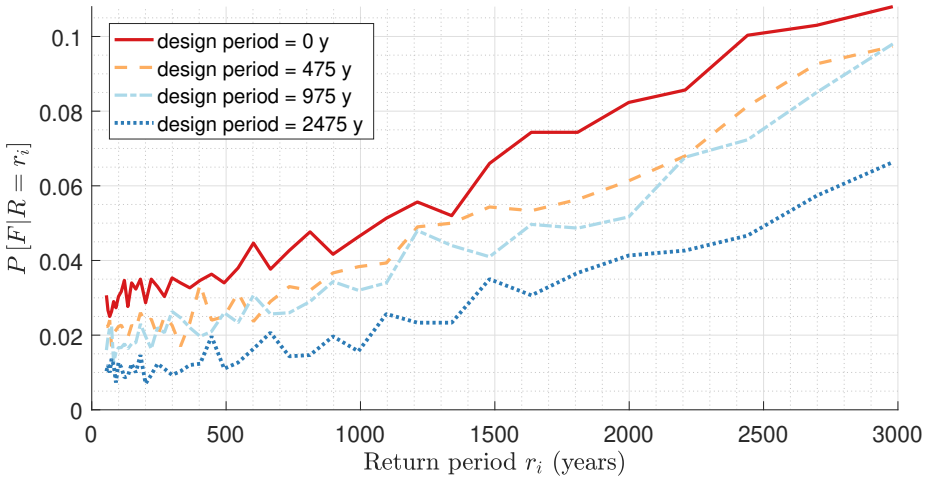

Figure 5.11: Scenario 5 - A plot of the conditional probability of failure against the return period (φ_{gu} = 1.0)

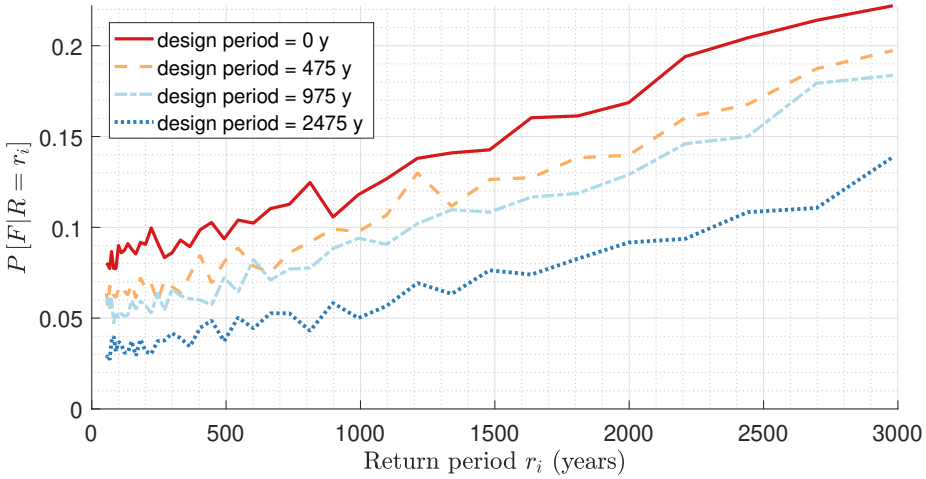

Figure 5.12: Scenario 6 - A plot of the conditional probability of failure against the return period (φ_{gu} = 1.0)

5.1.2. Total Probability of Failure

Figures 5.13 to 5.18 present the lifetime probability of failure plotted against the resistance factor φ_{gu}.

Similarly to the conditional failure probability graphs, the lifetime probability of failure graphs contain a line for each of the four design return periods. The vertical axis contains the total lifetime probability of failure given a range of earthquake return periods r_m to r_n, obtained by using the total probability theorem.

Because a high resistance factor leads to weaker foundations than a low resistance factor does, the lifetime probability of failure for a geotechnical system is expected to increase with the resistance factor, which is a trend that can be seen in the figures. As is the case with the estimated conditional probability of failure graphs in Section 5.1.1, a larger design return period results in lower probabilities of failure, which explains the order of the design return period lines.

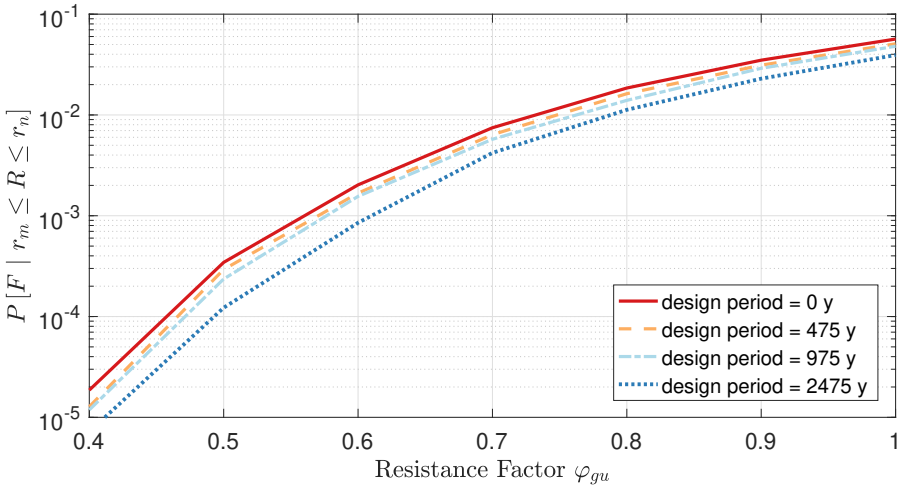

Figure 5.13: Scenario 1 - A plot of the total probability of failure against the resistance factor

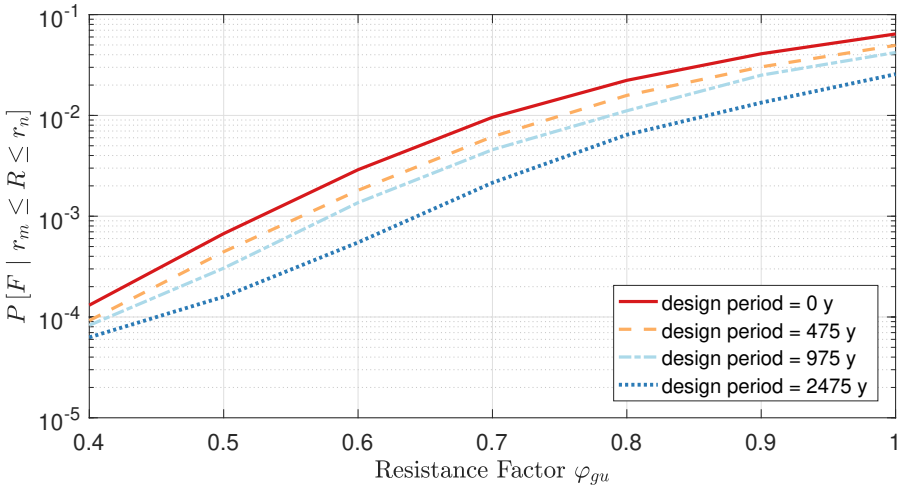

Figure 5.14: Scenario 2 - A plot of the total probability of failure against the resistance factor

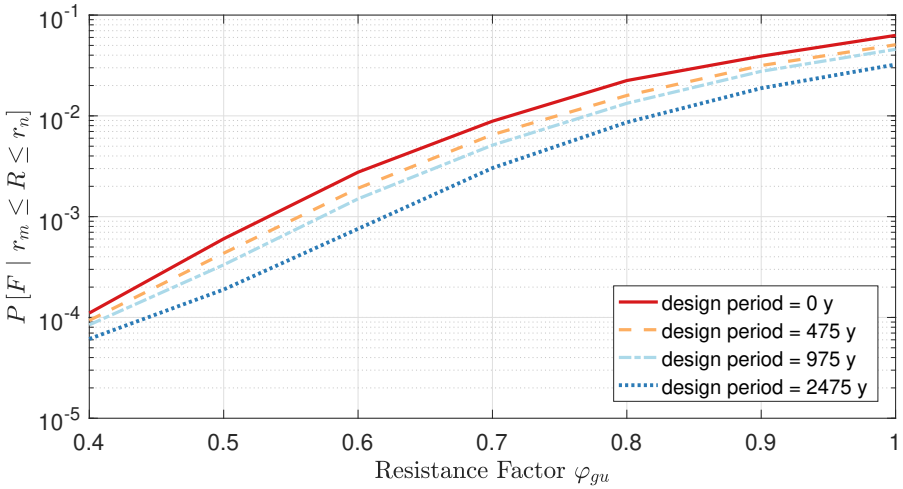

Figure 5.15: Scenario 3 - A plot of the total probability of failure against the resistance factor

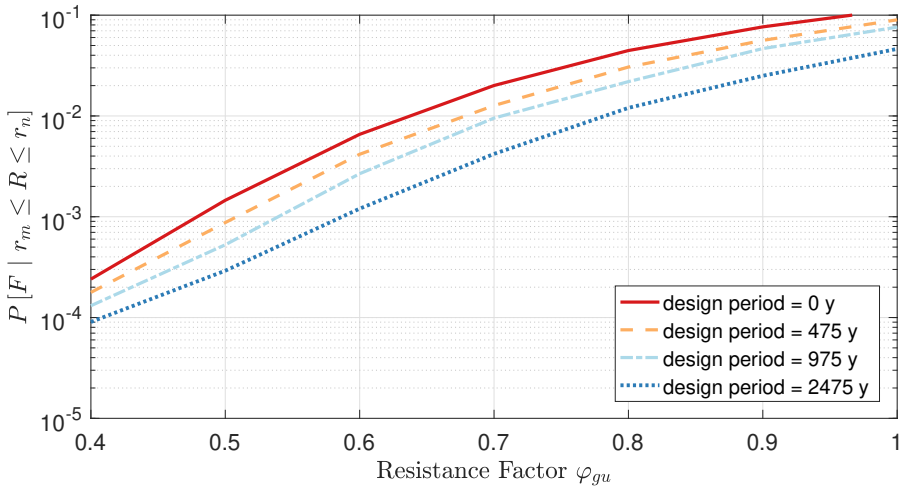

Figure 5.16: Scenario 4 - A plot of the total probability of failure against the resistance factor

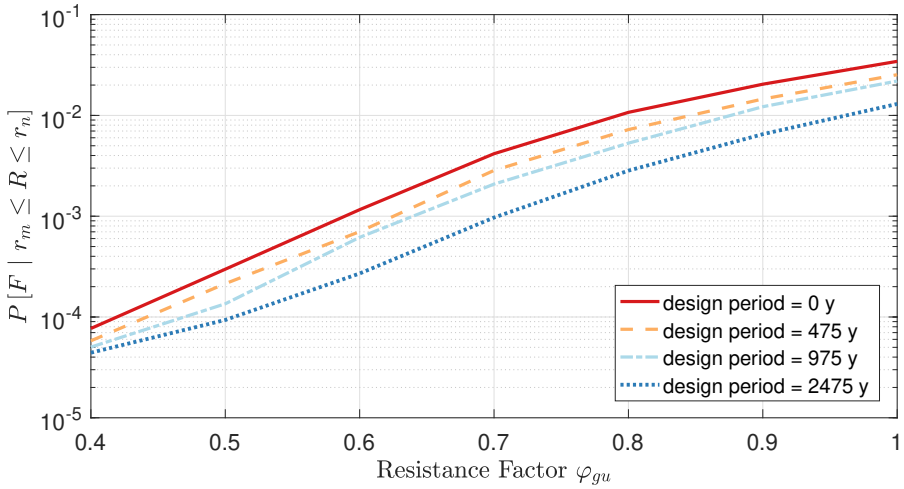

Figure 5.17: Scenario 5 - A plot of the total probability of failure against the resistance factor

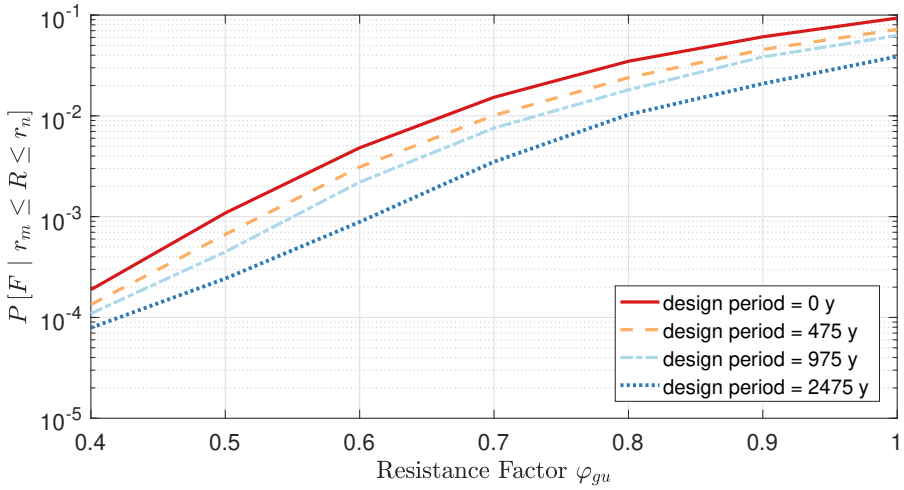

Figure 5.18: Scenario 6 - A plot of the total probability of failure against the resistance factor

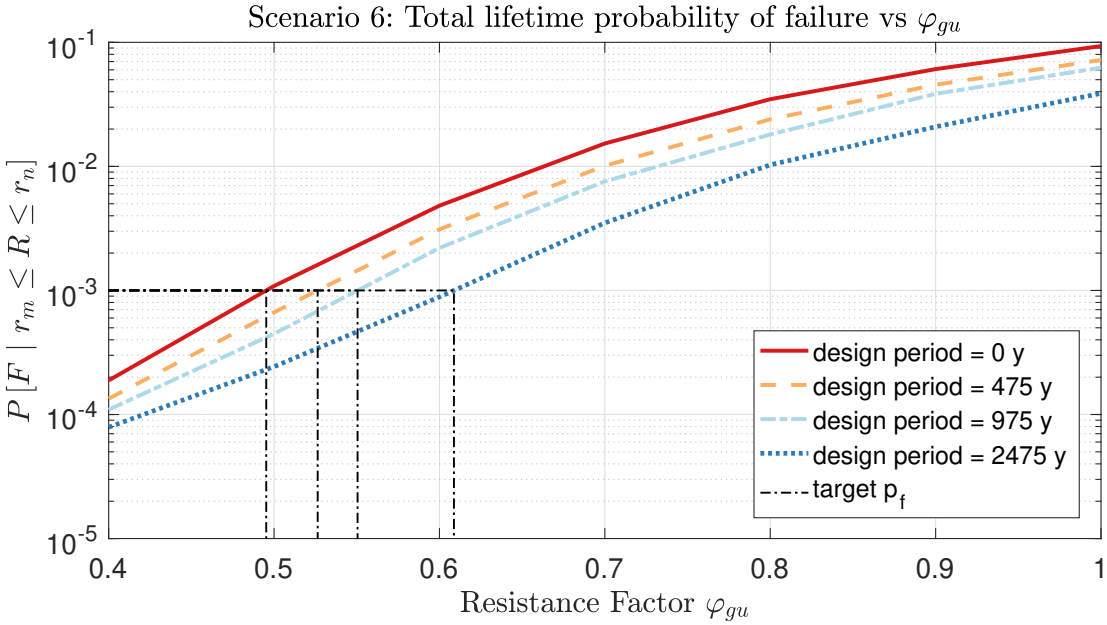

Figure 5.19: Example of resistance factor determination - Scenario 6

5.1.3. Resistance Factor Determination

By interpolating the lifetime probability of failure graphs in Section 5.1.2, the resistance factors can be determined that correspond with a similar lifetime reliability index (β, Section 2.4.7) as is being targeted in static design.

Fenton et al. (2016) state that in the static design of the 2014 edition of the CHBDC, an annual reliability index of $\beta = 3.7$ is targeted. With an annual β value of 3.7, a geotechnical system with a lifetime of 75 years has a lifetime reliability index estimated to be between $\beta = 3.0$ and $\beta = 3.5$. What the value of β is, depends on resistance degradation over the lifetime of the geotechnical system, because of things such as weather, (super)structure usage and how well the system is maintained. A target lifetime probability of failure of 10^{-3} corresponds with a lifetime reliability index $\beta = 3.1$, and therefore is chosen to be adequate in this thesis.

A graphical example of the interpolation procedure for Scenario 6 can be seen in Figure 5.19. Figure 5.19 is the same as Figure 5.18, except for the line that indicates the target lifetime probability of failure, 10^{-3}. The resistance factor where the target lifetime probability of failure intersects with the failure lines, is the resistance factor that successfully targets the lifetime probability of failure.

The results of the interpolations for each scenario are plotted in Figure 5.20. The vertical axis in Figure 5.20 contains the resistance factor that achieves a target lifetime probability of failure of 10^{-3}. Each scenario has its own coordinate on the horizontal axis. It should not be attempted to find a trend in this data, since the scenarios are independent of each other.

5.2. Interpretation

5.2.1. Results vs CHBDC

To make an assessment of the reliability that is currently being targeted in the CHBDC for geotechnical systems under seismic loading, it must first be known what the resistance factor in the CHBDC is. This value of the resistance factor depends on how extensive the performed site investigation is. For the static bearing capacity of a shallow foundation, the resistance factors are 0.45, 0.50 and 0.60 for low, typical and high site understanding respectively. The reason for this difference is that if the site is investigated thoroughly, there is less uncertainty in the design, meaning that the resistance factor does not have to be as conservative as for a limited site investigation. To find the seismic resistance factors, the static resistance factors are incremented by $+0.20$, which makes them 0.65, 0.70 and 0.80 for low, typical and high site understanding respectively.

If site understanding is low, the site investigation consists mostly of an extrapolation of previous experiences. If site understanding is high, an extensive analysis of both the soils and risks has been

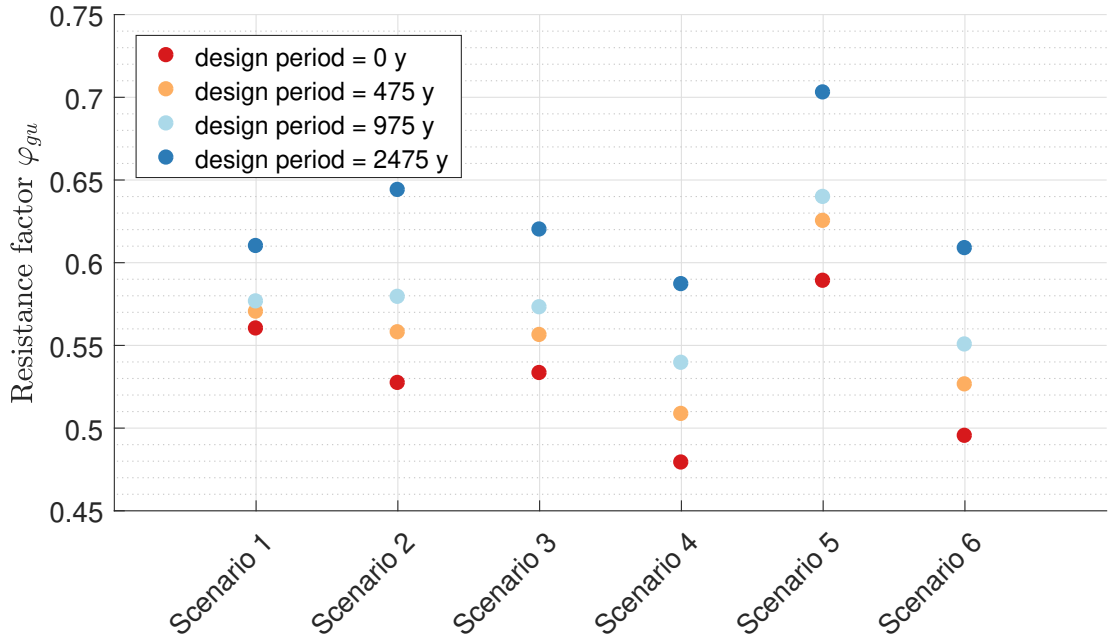

Figure 5.20: Interpolated required resistance factors for a target probability of 10^{-3}

performed. Typical site understanding is somewhere in between low and high site understanding. In this thesis, a virtual sample is taken for each realization. The site investigation consists of more than an extrapolation of similar sites, and therefore the site understanding can't be categorized as low. However, one sample is not enough for the investigation to be called extensive. Therefore the CHBDC would classify the in this thesis performed virtual investigation as "typical", making the resistance factor for static design 0.50, and the resistance factor for seismic design 0.70.

All of the recommended resistance factors in Figure 5.20 are below $\varphi_{gu} = 0.70$, except for the design period of 2475 years in Scenario 5. The results indicate that the CHBDC is not targeting a lifetime probability of failure of 10^{-3}, but targets an increased lifetime probability of failure, such as 10^{-2}, instead. Scenarios 2 and 3 are the scenarios that come closest to the idealized situation that the CHBDC assumes, since there is no live load taken into account in those scenarios. Even without live loads, which means that one source of uncertainty is taken away from the problem, the required resistance factors are around 0.56. Live load Scenarios 4 and 6 indicate even lower resistance factors are needed than those found in Scenarios 2 and 3. In general, the recommended seismic resistance factors are closer to the CHBDC's static resistance factor ($\varphi_{gu} = 0.50$) than to its seismic resistance factor.

5.2.2. Recommended Resistance Factor

Each scenario has a different level of conservatism in the design because of different effects and different design parameters that are taken into account. For example, Scenario 5 is more conservative than Scenario 4, where a smaller live load factor is used.

If a design in a scenario is conservative, that means that foundations are overdesigned in the simulation. An overdesigned foundation is less likely to fail, lowering the lifetime probability of failure for that design, which in turn means that the target lifetime probability of failure can be achieved with a higher resistance factor. Thus, conservative designs in the simulations lead to unconservative target resistance factors.

The resistance factor must be on the conservative side, because the potential loss of human life with an unconservative resistance factor is unacceptable. One choice could be to recommend the lowest resistance factor found in all simulations, which would be the most conservative resistance factor. The worst-case situation has a very small probability of occurrence, and although designs would be safest with the worst case resistance factor, they would also be overdesigned. Another choice could be to take the average resistance factor of all results. However, results of conservative and unconservative scenarios should not be given the same weight. An assessment must be made on which scenario gives

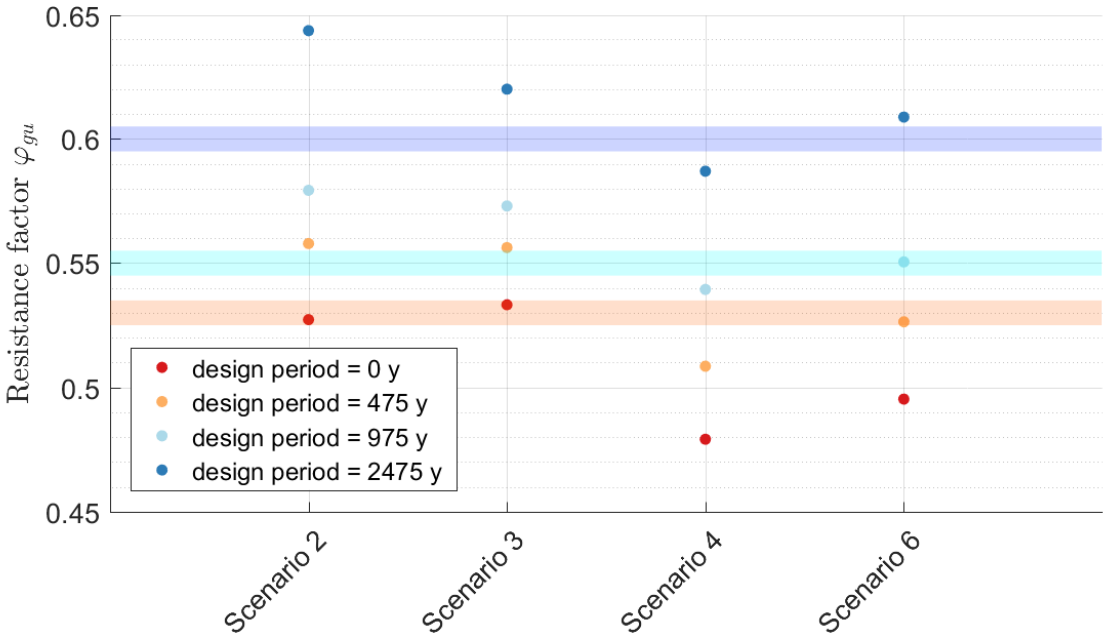

Figure 5.21: Determination of required resistance factors for a target probability of 10^{-3}

the results that are wished for.

In Scenario 1, only a vertical seismic force is taken into account. Not having horizontal components in the seismic forces is an optimistic assumption. By neglecting the horizontal seismic forces, uncertainty is left out of the problem, which can be seen from the low estimated conditional probabilities of failure in Figure 5.1. Scenario 1 is therefore not used to estimate the resistance factor.

A question that must be asked is: “should live load be taken into account in the design?” If a live load factor is used, it should be a quasi-permanent live load factor. If a static live load factor is used instead, the live load is assumed to be an extreme load in the design. An earthquake can happen at any point in time, so the probability of an extreme live load being present during an earthquake is low. Only Scenarios 4, 5, and 6 have live load in either the design or testing. However, it can be stated that the live load factor of 1.7 in Scenario 5 is too pessimistic, for which reason Scenario 5 is disregarded in targeting the resistance factor.

Since Scenarios 1 and 5 are disregarded, only Scenarios 2, 3, 4 and 6 are assumed to be accurate enough to base the target resistance factor on.

In Scenario 2, the live load is modelled exactly as specified in the CHBDC; no live load is modelled in either the design or testing of this scenario.

In Scenario 3, cyclic degradation is not taken into account. The design procedure for cyclic degradation is an assumption based on theory. An assumption can be accurate or inaccurate, but it can be seen that incorporating the cyclic degradation factor in the simulations does not have a large impact on the targeted resistance factor by comparing Scenario 2 to Scenario 3. For this reason, no errors are expected to be present in the results of scenarios that use the cyclic degradation factor in the design.

In Scenario 4, a live load is taken into account in which the load factor is equal to 1.0. This load factor is on the conservative side for a quasi-permanent load factor.

In Scenario 6, a live load is modelled to be on the foundation, although the live load factor is equal to 0.0. Compared to Scenario 2, the results for Scenario 6 show (logically) that the lifetime probability of failure goes up if a live load is present that has not been taken into account in the design. This difference between the targeted resistance factors in Scenario 2 and Scenario 6 is only 0.03.

Figure 5.21 is the same as Figure 5.20 with Scenarios 1 and 5 left out. Included in Figure 5.21 are

colored areas that indicate the final estimates of the resistance factor for the design return periods of the same color. The ranges on the recommended resistance factors between scenarios for the different design periods are all within 0.05.

The results for a design return period of zero years are disregarded, since a 0 year design return period means that there is no seismic design. Not having a seismic design defeats the purpose of calibrating the seismic design code. This leaves the results for design return periods 475, 975 and 2475 years.

For a design return period earthquake of 475 years, the recommended resistance factors range from 0.51 to 0.56, for which the chosen resistance factor is 0.53. For a design return period earthquake of 975 years, the recommended resistance factors range from 0.54 to 0.58, for which the chosen resistance factor is 0.55. For a design return period earthquake of 2475 years, the recommended resistance factors range from 0.59 to 0.64, for which the chosen resistance factor is 0.60. Each of the chosen resistance factors is conservative for Scenarios 2 and 3, slightly unconservative for Scenario 4, and relatively close to the results of Scenario 6.

In the CHBDC, the resistance factor is not defined differently for different design return period earthquakes. For a design return period of 475 years, the lifetime probability of failure is higher than it is for higher design return periods. Since the target lifetime probability of failure for the geotechnical system needs to be satisfied, no matter what the design return period is, the results for a design return period earthquake of 475 years are the governing values. Therefore the recommended resistance factor is chosen to be 0.53.

A resistance factor of 0.53 for geotechnical systems under seismic loading is close to the resistance factor for systems under static loading for a typical site understanding case, which is 0.50. For simplicity in the design code, it might be recommendable to use the static resistance factor as a seismic resistance factor, and thus to omit the $+0.20$ with which the seismic resistance factor is determined now. Taking into account the results of Scenario 6, it can be said with reasonable certainty that a live load factor is not needed if the resistance factor for design under seismic loading is equal to the static resistance factor, since the target lifetime reliability is easily satisfied with a resistance factor of 0.50, even if an unexpected live load is present on the foundation during an earthquake event.

5.2.3. Recommended Resistance Factor vs Other Research

A similar study has been performed by Naghibi and Fenton (2018). Between their work and this thesis, a number of differences can be noted.

One of the largest differences is that Naghibi and Fenton used an averaging domain to simulate the modelled foundations, whereas the finite element method is used in this thesis. An averaging domain results in a much lighter algorithm than FEM is, and therefore they were able to perform more realizations per run. Their results therefore have a higher failure probability resolution and smaller sampling errors. This local average representation was found to be reasonably accurate (Fenton & Griffiths, 2003; Fenton et al., 2008).

A different design equation was used in this thesis compared to the study by Naghibi and Fenton, who used the equations provided by Budhu and Al-Karni (1993), which makes use of earthquake accelerations coefficients. They tested the design against the same equations, but with parameters based on ”actual” strength parameters taken from the averaging domain. In this thesis, the design equation in the CHBDC was used in combination with pseudo-dynamic forces to test the bearing capacity of the designed foundations.

The ratio between the vertical and horizontal seismic accelerations λ is taken to be 0.25 in Naghibi and Fenton's work, whereas a value of $\lambda = 0.3$ is used in this thesis.

Another difference is that Naghibi and Fenton simulated a soil that was both frictional and cohesive, whereas in this thesis a frictionless soil was assumed.

Finally, Naghibi and Fenton studied cases for multiple cities, none of which were Toronto (as is used in this thesis).

For a target lifetime probability of failure of 10^{-3}, the results of Naghibi and Fenton (2018) suggest a seismic resistance factor of about 0.35. Most cities have similar total failure probability curves, so it can be said that $\varphi_{gu} = 0.35$ is universal for those results. This resulting resistance factor is significantly lower than the resistance factor found in this thesis. One thing that both studies agree on is that the resistance factors in the CHBDC for a geotechnical system under seismic loading are unconservative.

It is expected that the results found in this thesis more accurately target a lifetime reliability than

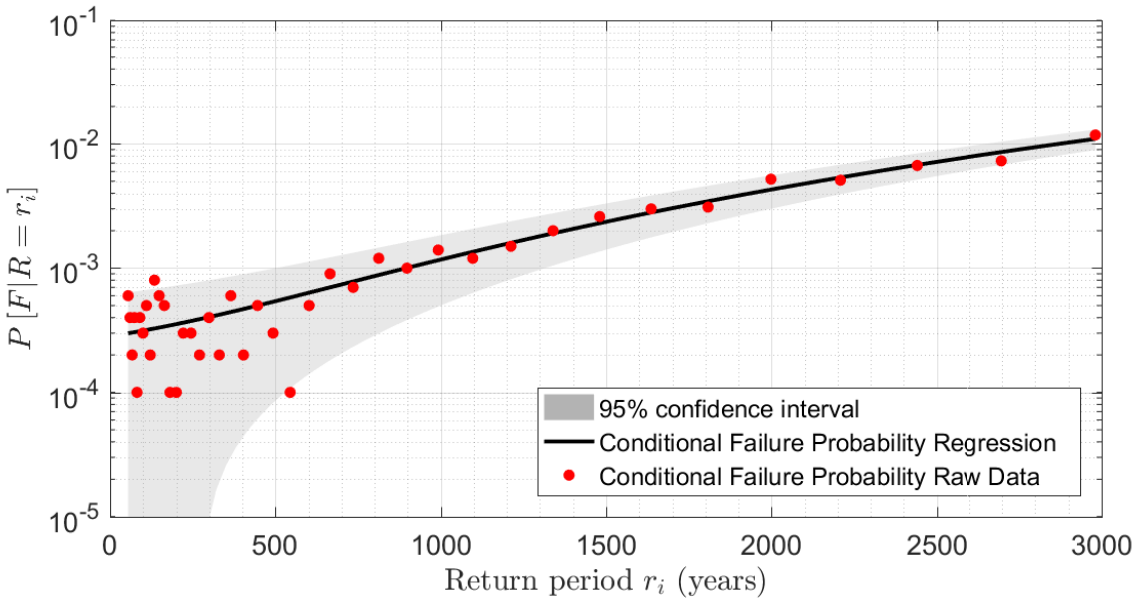

Figure 5.22: Example of the 95% confidence interval for the conditional probabilities of failure of Scenario 3

the research by Naghibi and Fenton did. The main difference between the two studies is the extensive use of the Budhu and Al-Karni equation by Naghibi and Fenton. Although this method seems accurate enough, it is not exactly known what data the Budhu and Al-Karni equations are calibrated to. For this reason it is expected that the use of the finite element method in this thesis has lead to more accurate results.

5.3. Discussion

5.3.1. Quality of the Results

All of the estimated conditional probabilities of failure are polluted with random noise from so called sampling errors. “The sampling error is the error caused by observing a sample instead of the whole population.” (Särndal et al., 2003). This means that a random sample from an infinite range of possibilities can contain worse cases, but also better cases than is representative for the population that the sample is approximating. Because of the difference in quality between each of the estimated conditional probabilities of failure, the figures in Section 5.1 are not completely smooth, but appear to be oscillating.

Sampling errors can be considered to be a normally distributed random variable with a mean of zero. The standard deviation of the sampling error can be estimated through Equation 2.37 and depends on the size of the estimated conditional failure probability and the number of realizations used for this estimation. The more realizations used in the estimation, the more precise the estimate of the conditional probability of failure is.

A 95% confidence interval can be determined for the estimated conditional probabilities of failure by making a regression through those data points and estimating the standard deviation for every single point. Since sampling errors are assumed to be normally distributed, the 95% confidence interval can be found at $\pm 1.96 \cdot \sigma$ around the regression. As a demonstration, a third degree polynomial regression has been fitted to the estimated conditional probabilities of failure of Scenario 3, $\varphi_g = 0.5$ in Figure 5.22. In Figure 5.22 the 95% confidence interval is drawn as a gray area.

One thing that can be noticed is that most outlying data points are near the 95% confidence line. This

means that all values have sampling errors of expected proportions, and thus the regression appears to be accurate. Secondly, the confidence interval is relatively larger at lower return periods, where the failure probability is lower, than at the higher return periods. The logic behind this can be seen when the coefficient of variation CV of the estimated conditional probability of failure $\hat{p}_f$ is calculated,

$$CV_{\hat{p}_f} = \frac{\sigma_{\hat{p}_f}}{\mu_{\hat{p}_f}} \simeq \frac{\sqrt{\hat{p}_f\left(1-\hat{p}_f\right)/n_{sim}}}{\hat{p}_f} = \frac{1}{\sqrt{n_{sim}}}\sqrt{\frac{1}{\hat{p}_f}-1} \tag{5.1}$$

in which the standard deviation of $\hat{p}_f$, found through Equation 2.37, is divided by the mean of $\hat{p}_f$, which is assumed to be similar or equal to $\hat{p}_f$. In the final expression, the denominator $\hat{p}_f$ is incorporated into the square root of the numerator.

Equation 5.1 has a vertical asymptote at $\hat{p}_f = 0$ and decreases monotonically towards $\hat{p}_f = 1.0$. So, the closer to zero $\hat{p}_f$ is, the larger the coefficient of variation of $\hat{p}_f$ is, and the relatively more dominant the sampling errors are. Of course, $\hat{p}_f$ is limited by the number of realizations n_{sim}; the lowest $\hat{p}_f$ that can be estimated is $\hat{p}_f = 1/n_{sim}$. By assuming $\hat{p}_f = 1/n_{sim}$, the square root in the final expression of Equation 5.1, $\sqrt{1/\hat{p}_f - 1}$, becomes $\sqrt{n_{sim} - 1}$. If n_{sim} is large enough, $\sqrt{n_{sim} - 1}$ approximately becomes $\sqrt{n_{sim}}$, which means that $CV_{\hat{p}_f}$ tends to 1 as the estimated failure probability decreases. In other words, when the conditional probability of failure comes close to the lowest value that can be estimated, the standard deviation become just as large as the conditional probability of failure itself.

The relatively large sampling errors for low return period earthquakes can have an impact on the total lifetime probability of failure. Lower return period earthquakes have a larger probability of occurrence, and therefore potentially contribute more to the total lifetime probability of failure than the higher return period earthquakes do. Of course, there are many data points in the lower return periods, and in each of those points sampling errors are present in either the positive or the negative direction. All these small errors mostly cancel each other out. On the other hand, the conditional failure probability at these low return periods is much smaller than at higher return periods. This, combined with the canceling of errors, means that the overall effect of the sampling errors is small. This is demonstrated when the total lifetime probability of failure is estimated with both the regression and the simulation results. In the example given in Figure 5.22, the simulated data results in an estimated lifetime probability of failure of $4.46 \cdot 10^{-4}$, whereas the regression results in a lifetime probability of failure of $4.37 \cdot 10^{-4}$. This difference between the total lifetime probability of failure found through the simulations and the one found through the regression is negligible for the determination of the required resistance factor.

As long as most data points are within the 95% confidence interval from a regression, the quality of the resulting total lifetime probability of failure is good enough for the goal in this thesis. Even results as poor as Scenario 1 in Figure 5.1 fall within $\pm 1.96 \cdot \sigma$ of a regression, and thus the sampling errors are not out of the ordinary. Most outliers are within the 95% confidence interval for every scenario and resistance factor, and therefore the quality of the results is trustworthy.

5.3.2. Research Shortcomings

Shortcomings in the research mostly come from a limitation of time and a limitation of computational power. Simplifications have been made to seismic processes, because a coupled FEM model was not feasible with the large number of realizations needed. If more computational power had been available, the seismic forces could have been modelled dynamically instead of pseudo-dynamically, for example. Simplifying assumptions such as the vertical seismic force being a percentage of the horizontal seismic force, or certain regressions that have been assumed, could have all lead to inaccuracies.

Another simplification is the way cyclic degradation is taken into account. Little quantitative information was available in the literature, though it was qualitatively suggested that cyclic degradation should be incorporated.

The simplifications in the theory have cut the simulation run time drastically, but it was still not feasible to do hundreds of thousands of realizations for every run. Although the results seem reasonable, it is believed that the precision of the results has still suffered because of the limited number of realizations.

6

Conclusion

In this document a study has been conducted to find the resistance factor φ_{gu} that successfully targets a lifetime reliability for geotechnical systems under seismic loads similar to static design targets. As an example, the design procedure described by the Canadian Highway Bridge Design Code (CHBDC) has been used.

The total resistance factors for a target lifetime probability of failure of 10^{-3} resulting from simulations are lower than the resistance factors that are recommended in the CHBDC. Lower resistance factors are more conservative, and thus the CHBDC is unconservative. Whereas the CHBDC recommends a total resistance factor of 0.70 for what is called a "typical soil investigation", the results of the study point towards a seismic resistance factor of 0.53. This value of 0.53 comes closer to the static resistance factor in the CHBDC, which is 0.50. This confirms the answers found by Naghibi and Fenton (2018), albeit a bit less drastically.

Before a big change is made to the CHBDC, more research should be conducted. However, recommendations on changes can still be made.

Firstly, it should be considered to use a quasi-permanent live load factor that is larger than zero. It is presently assumed that no live load is acting on the foundation during an earthquake. Although this could be true, it is always possible to have some live load on a bridge, since earthquakes can happen at any point in time.

Secondly, the most important consideration is to lower the resistance factor for geotechnical systems under seismic loading. The results of this thesis indicate that the resistance factor for seismic design that is recommended in the CHBDC is too high. A better choice would be to use the same resistance factors for both static and seismic design. This avoids confusion, and if future research agrees, might be conservative enough so that no quasi-permanent live load factor is needed at all. Therefore, it should be considered for the $static + 0.20$ clause to be left out.

The calibration of building codes is an important activity. If the resistance factors are too conservative, more money might be spent on structures than is needed. However, if the resistance factors aren't conservative enough, the safety of people cannot be guaranteed. Earthquakes of large magnitudes are rare in the Toronto region. Still, one seismic event could lead to many different foundation failures. Because not much research has been done on the topic of seismic building code calibration, this thesis should be a useful addition to the body of work, and hopefully will contribute to a safer design philosophy in general.

7

Recommendations for Further Research

Inaccuracies in this thesis mainly come from the lack of computational power and time. The finite element model had to be as simple as possible, so that a large enough number of realizations was feasible. For future research, it is recommended that a more complex model is used to simulate the soil behavior, while still maintaining a high number of performed realizations. For example, the use of a coupled model, or the use of a dynamic model instead of a pseudo-dynamic approach would greatly improve the accuracy of the solution.

Another problem worth looking into is the difference of target lifetime reliabilities between design return periods. In this thesis, all foundations were tested until the soil failed completely. This is not completely correct, since failure is defined differently for different design return periods in the CHBDC. For example, for a design return period of 475 years, failure can be defined as minimal damage to a Major-route bridge, whereas extensive damage is the minimum performance for a 2475 year design return period. The difference in damage means that different lifetime reliabilities are targeted for the different design return periods. It needs to be verified that all these performance level targets are satisfied for the targeted resistance factor.

References

Allen, T. M., Nowak, A. S., & Bathurst, R. J. (2005). *Calibration to Determine Load and Resistance Factors for Geotechnical and Structural Design*. Washington, D.C.: Transportation Research Board. Retrieved 2019-09-13, from http://www.nap.edu/catalog/21978 doi: 10.17226/21978

Bartlett, F. M., Hong, H. P., & Zhou, W. (2003, April). Load factor calibration for the proposed 2005 edition of the National Building Code of Canada: Statistics of loads and load effects. *Canadian Journal of Civil Engineering*, *30*(2), 429–439. Retrieved 2019-10-04, from http://www.nrcresearchpress.com/doi/10.1139/l02-087 doi: 10.1139/l02-087

Becker, D. E. (1996a). Eighteenth Canadian Geotechnical Colloquium: Limit States Design For Foundations. Part I. An overview of the foundation design process. *Canadian Geotechnical Journal*, *33*, 956–983.

Becker, D. E. (1996b). Eighteenth Canadian Geotechnical Colloquium: Limit States Design For Foundations. Part II. Development for the National Building Code of Canada. *Canadian Geotechnical Journal*, *33*, 984–1007.

Bond, A., & Harris, A. (2008). *Decoding Eurocode 7* (1st ed ed.). London ; New York: Taylor & Francis. (OCLC: ocn166383807)

Budhu, M., & Al-Karni, A. (1993, March). Seismic bearing capacity of soils. *Géotechnique*, *43*(1), 181–187. Retrieved 2019-03-29, from http://www.icevirtuallibrary.com/doi/10.1680/geot.1993.43.1.181 doi: 10.1680/geot.1993.43.1.181

Campbell, K. W. (1997, January). Empirical Near-Source Attenuation Relationships for Horizontal and Vertical Components of Peak Ground Acceleration, Peak Ground Velocity, and Pseudo-Absolute Acceleration Response Spectra. *Seismological Research Letters*, *68*(1), 154–179. Retrieved 2019-05-15, from https://pubs.geoscienceworld.org/srl/article/68/1/154-179/142166 doi: 10.1785/gssrl.68.1.154

Cascone, E., & Casablanca, O. (2016, May). Static and seismic bearing capacity of shallow strip footings. *Soil Dynamics and Earthquake Engineering*, *84*, 204–223. Retrieved 2019-03-29, from https://linkinghub.elsevier.com/retrieve/pii/S026772611600049X doi: 10.1016/j.soildyn.2016.02.010

*CEN. (2002). *Eurocode - Basis of structural design*.

CEN. (2005a). *Eurocode 7 - Geotechnical design Part 1 - General rules*.

*CEN. (2005b). *Eurocode 8 - Design of structures for earthquake resistance Part 1 - General rules, seismic actions and rules for buildings*.

CEN. (2005c). *Eurocode 8 - Design of structures for earthquake resistance Part 5 - Foundations, retaining structures and geotechnical aspects*.

Cimellaro, G. P., & Marasco, S. (2018). *Introduction to dynamics of structures and earthquake engineering* (Vol. 45). New York, NY: Springer Berlin Heidelberg.

*CSA. (2019a). *Canadian Highway Bridge Design Code - Section 1*.

CSA. (2019b). *Canadian Highway Bridge Design Code - Section 3*.

CSA. (2019c). *Canadian Highway Bridge Design Code - Section 4*.

CSA. (2019). *Canadian Highway Bridge Design Code - Section 6*.

Darendeli, M. B. (2001). *Development of a New Family of Normalized Modulus Reduction and Material Damping Curves* (Ph.D.). University of Texas, Austin, Texas.

Das, B. M. (2008). *Fundamentals of geotechnical engineering* (3rd ed.). Australia: Thomson. (OCLC: 769037404)

Das, B. M. (2011). *Principles of foundation engineering*. Australia: Thomson/Brooks/Cole. (OCLC: 879304445)

Elia, G., & Rouainia, M. (2014, August). Performance evaluation of a shallow foundation built on structured clays under seismic loading. *Bulletin of Earthquake Engineering*, *12*(4), 1537–1561. Retrieved 2019-03-29, from http://link.springer.com/10.1007/s10518-014-9591-3 doi: 10.1007/s10518-014-9591-3

Esposito, G., Fenton, G. A., & Naghibi, F. (2019). Seismic Reliability of Axially-Loaded Vertical Piles. *TO BE PUBLISHED*.

Fenton, G. A. (2013). Geotechnical Design Code Development in Canada. *Advances in Soil Mechanics and Geotechnical Engineering*, 277–294. doi: 10.3233/978-1-61499-163-2-277

Fenton, G. A., & Griffiths, D. V. (2000, July). Bearing Capacity of Spatially Random Soils. In *Proceedings of the Probabilistic Mechanics and Structural Reliability Conference* (p. 6). Notre Dame, Indiana.

Fenton, G. A., & Griffiths, D. V. (2003, February). Bearing Capacity Prediction of Spatially Random c-&phi Soils. *Canadian Geotechnical Journal*, *40*(1), 54–65.

Fenton, G. A., & Griffiths, D. V. (2008). *Risk Assessment in Geotechnical Engineering*. Hoboken, NJ, USA: John Wiley & Sons, Inc. doi: 10.1002/9780470284704

Fenton, G. A., Griffiths, D. V., & Cavers, W. (2005, October). Resistance factors for settlement design. *Canadian Geotechnical Journal*, *42*(5), 1422–1436. Retrieved 2019-03-28, from http://www.nrcresearchpress.com/doi/10.1139/t05-053 doi: 10.1139/t05-053

Fenton, G. A., Griffiths, D. V., & Zhang, X. (2008, November). Load and resistance factor design of shallow foundations against bearing failure. *Canadian Geotechnical Journal*, *45*(11), 1556–1571. Retrieved 2019-03-29, from http://www.nrcresearchpress.com/doi/10.1139/T08-061 doi: 10.1139/T08-061

Fenton, G. A., & Naghibi, F. (2017, October). Probabilistic Seismic Design of Geotechnical Systems. Ottawa.

Fenton, G. A., Naghibi, F., Dundas, D., Bathurst, R. J., & Griffiths, D. (2016, February). Reliability-based geotechnical design in 2014 Canadian Highway Bridge Design Code. *Canadian Geotechnical Journal*, *53*(2), 236–251. doi: 10.1139/cgj-2015-0158

Fenton, G. A., & Naghibi, M. (2011, November). Geotechnical resistance factors for ultimate limit state design of deep foundations in frictional soils. *Canadian Geotechnical Journal*, *48*(11), 1742–1756. Retrieved 2019-03-28, from http://www.nrcresearchpress.com/doi/10.1139/t11-068 doi: 10.1139/t11-068

Foye, K. C., Salgado, R., & Scott, B. (2006, September). Resistance Factors for Use in Shallow Foundation LRFD. *Journal of Geotechnical and Geoenvironmental Engineering*, *132*(9), 1208–1218. Retrieved 2019-03-28, from http://ascelibrary.org/doi/10.1061/%28ASCE%291090-0241%282006%29132%3A9%281208%29 doi: 10.1061/(ASCE)1090-0241(2006)132:9(1208)

Hamrouni, A., Sbartai, B., & Dias, D. (2018, August). Probabilistic analysis of ultimate seismic bearing capacity of strip foundations. *Journal of Rock Mechanics and Geotechnical Engineering*, *10*(4), 717–724. Retrieved 2019-06-13, from https://linkinghub.elsevier.com/retrieve/pii/S1674775517302974 doi: 10.1016/j.jrmge.2018.01.009

Hicks, M. A. (2013). An Explanation of Characteristic Values of Soil Properties in Eurocode 7. *Advances in Soil Mechanics and Geotechnical Engineering*, 36–45. doi: 10.3233/978-1-61499-163-2-36

Honjo, Y., & Amatya, S. (2004, May). Partial factors calibration based on reliability analyses for square footings on granular soils. *Géotechnique*, *55*(6), 479–491. Retrieved 2019-03-21, from https://www.icevirtuallibrary.com/toc/jgeot/55/6

Huang, C.-C. (2005, September). Seismic Displacements of Soil Retaining Walls Situated on Slope. *Journal of Geotechnical and Geoenvironmental Engineering*, *131*(9), 1108–1117. doi: 10.1061/(ASCE)1090-0241(2005)131:9(1108)

Idriss, I., & Boulanger, R. (2006, February). Semi-empirical procedures for evaluating liquefaction potential during earthquakes. *Soil Dynamics and Earthquake Engineering*, *26*(2-4), 115–130. Retrieved 2019-05-15, from https://linkinghub.elsevier.com/retrieve/pii/S0267726105000710 doi: 10.1016/j.soildyn.2004.11.023

Jakka, R. S. (2013, March). Earthquake Resistant Design of Shallow Foundations. Roorkee. doi: 10.13140/RG.2.1.3851.9849

Karamitros, D. K., Bouckovalas, G. D., & Chaloulos, Y. K. (2013, April). Insight into the Seismic Liquefaction Performance of Shallow Foundations. *Journal of Geotechnical and Geoenvironmental Engineering*, *139*(4), 599–607. Retrieved 2019-03-29, from http://ascelibrary.org/doi/10.1061/%28ASCE%29GT.1943-5606.0000797 doi: 10.1061/(ASCE)GT.1943-5606.0000797

Kishida, T., & Tsai, C.-C. (2014, March). Seismic Demand of the Liquefaction Potential with Equivalent Number of Cycles for Probabilistic Seismic Hazard Analysis. *Journal of Geotechnical and Geoenvironmental Engineering*, *140*(3), 04013023. Retrieved 2019-05-31, from http://ascelibrary.org/doi/10.1061/%28ASCE%29GT.1943-5606.0001033 doi: 10.1061/(ASCE)GT.1943-5606.0001033

Latha, G. M., & Garaga, A. (2010, November). Seismic Stability Analysis of a Himalayan Rock Slope. *Rock Mechanics and Rock Engineering*, *43*(6), 831–843. Retrieved 2019-06-13, from http://link.springer.com/10.1007/s00603-010-0088-3 doi: 10.1007/s00603-010-0088-3

Matasovic, N. (1993). *Seismic response of composite horizontally-layered soil deposits* (Unpublished doctoral dissertation). Los Angeles.

Melo, C., & Sharma, S. (2004, August). Seismic Coefficients for Pseudostatic Slope Analysis. In (p. 15). Vancouver, B.C..

Naghibi, F., & Fenton, G. A. (2018, October). Calibration of resistance factors for geotechnical seismic design. *Canadian Geotechnical Journal*, 1–8. doi: 10.1139/cgj-2018-0433

Nen-En. (2018). *Nationale bijlage bij NEN-EN 1997-1 Eurocode 7: Geotechnisch ontwerp - Deel 1: Algemene regels*.

Nouri, H., Fakher, A., & Jones, C. (2008, June). Evaluating the effects of the magnitude and amplification of pseudo-static acceleration on reinforced soil slopes and walls using the limit equilibrium Horizontal Slices Method. *Geotextiles and Geomembranes*, *26*(3), 263–278. Retrieved 2019-06-13, from https://linkinghub.elsevier.com/retrieve/pii/S0266114407000763 doi: 10.1016/j.geotexmem.2007.09.002

nrcan. (2015). *National Building Code of Canada seismic hazard values.* Retrieved 2019-05-14, from http://earthquakescanada.nrcan.gc.ca/hazard-alea/interpolat/calc-en.php

OpenStreetMap contributors. (2019). *Planet dump retrieved from https://planet.osm.org.* Retrieved 2019-09-07, from https://www.openstreetmap.org

Oudah, F., El Naggar, M. H., & Norlander, G. (2019, April). Unified system reliability approach for single and group pile foundations – Theory and resistance factor calibration. *Computers and Geotechnics*, *108*, 173–182. Retrieved 2019-03-28, from https://linkinghub.elsevier.com/retrieve/pii/S0266352X18303082 doi: 10.1016/j.compgeo.2018.12.003

Paolucci, R., & Pecker, A. (1997, August). Soil inertia effects on the bearing capacity of rectangular foundations on cohesive soils. *Engineering Structures*, *19*(8), 637–643. Retrieved 2019-03-29, from http://linkinghub.elsevier.com/retrieve/pii/S0141029696001411 doi: 10.1016/S0141-0296(96)00141-1

Park, J. H., Huh, J., Kim, K. J., Chung, M., Lee, J. H., Kim, D., & Kwak, K. (2013, July). Resistance factors calibration and its application using static load test data for driven steel pipe piles. *KSCE Journal of Civil Engineering*, *17*(5), 929–938. Retrieved 2019-03-28, from http://link.springer.com/10.1007/s12205-013-1038-x doi: 10.1007/s12205-013-1038-x

Pecker, A. (2004). Earthquake Resistant Design of Shallow Foundations. In A. Ansal (Ed.), *Recent Advances in Earthquake Geotechnical Engineering and Microzonation* (Vol. 1, pp. 285–301). Dordrecht: Kluwer Academic Publishers. Retrieved 2019-08-15, from http://link.springer.com/10.1007/1-4020-2528-9_11 doi: 10.1007/1-4020-2528-9_11

Phoon, K.-K., & Kulhawy, F. H. (1999). Characterization of geotechnical variability. *Canadian Geotechnical Journal*, *36*, 612–624.

Puri, V. K., & Prakash, S. (2013, April). Shallow Foundations for Seismic Loads: Design Considerations. In (p. 17). Missouri University of Science and Technology.

Rahman, M. S., Gabr, M. A., Sarica, R. Z., & Hossain, M. S. (2002, July). *Load and Resistance Factor Design (LRFD) for Analysis/Design of Piles Axial Capacity* (Tech. Rep. No. FHWA/NC/2005-08). Raleigh, North Carolina: North Carolina State University In Cooperation.

Sarma, S. K., & Iossifelis, I. S. (1990). Seismic bearing capacity factors of shallow strip footings. *Géotechnique*, *40*(2), 265–273.

Scott, B., Kim, B. J., & Salgado, R. (2003, April). Assessment of Current Load Factors for Use in Geotechnical Load and Resistance Factor Design. *Journal of Geotechnical and Geoenvironmental Engineering*, *129*(4), 287–295. doi: 10.1061/(ASCE)1090-0241(2003)129:4(287)

Smith, I. M., Griffiths, D. V., & Margetts, L. (2014). *Programming the Finite Element Method* (5th ed.). Chichester: Wiley.

Soubra, A.-H., Al-Bittar, T., Thajeel, J., & Ahmed, A. (2019, October). Probabilistic analysis of strip footings resting on spatially varying soils using kriging metamodeling and importance sampling. *Computers and Geotechnics*, *114*, 103107. Retrieved 2019-09-16, from https://linkinghub.elsevier.com/retrieve/pii/S0266352X19301636 doi: 10.1016/j.compgeo.2019.103107

Srbulov, M. (2008). *Geotechnical earthquake engineering: simplified analyses with case studies and examples* (No. 9). Dordrecht: Springer. (OCLC: 637134573)

Särndal, C.-E., Swensson, B., Wretman, J. H., & Särndal-Swensson-Wretman. (2003). *Model assisted survey sampling* (1. softcover print ed.). New York, NY: Springer. (OCLC: 249456962)

Sun, S. L., & Ruan, X. B. (2013, March). Seismic stability for landfills with a triangular berm using pseudo-static limit equilibrium method. *Environmental Earth Sciences*, *68*(5), 1465–1473. Retrieved 2019-06-13, from http://link.springer.com/10.1007/s12665-012-1843-4 doi: 10.1007/s12665-012-1843-4

Tsai, C.-C., Mejia, L. H., & Meymand, P. (2014, November). A strain-based procedure to estimate strength softening in saturated clays during earthquakes. *Soil Dynamics and Earthquake Engineering*, *66*, 191–198. Retrieved 2019-05-15, from https://linkinghub.elsevier.com/retrieve/pii/S0267726114001614 doi: 10.1016/j.soildyn.2014.07.003

Wang, Hicks, M. A., & Vardon, P. J. (2016, June). Slope failure analysis using the random material point method. *Géotechnique Letters*, *6*(2), 113–118. Retrieved 2019-09-16, from http://www.icevirtuallibrary.com/doi/10.1680/jgele.16.00019 doi: 10.1680/jgele.16.00019

Wang, & Xu. (2019, May). Traffic Load Simulation for Long-Span Suspension Bridges. *Journal of Bridge Engineering*, *24*(5), 05019005. Retrieved 2019-10-04, from http://ascelibrary.org/doi/10.1061/%28ASCE%29BE.1943-5592.0001381 doi: 10.1061/(ASCE)BE.1943-5592.0001381

Yu, H.-S. (2006). *Plasticity and geotechnics* (No. v. 13). New York, N.Y: Springer-Verlag. (OCLC: ocm73081989)

A

Result Graphs

A.1. Scenario 1

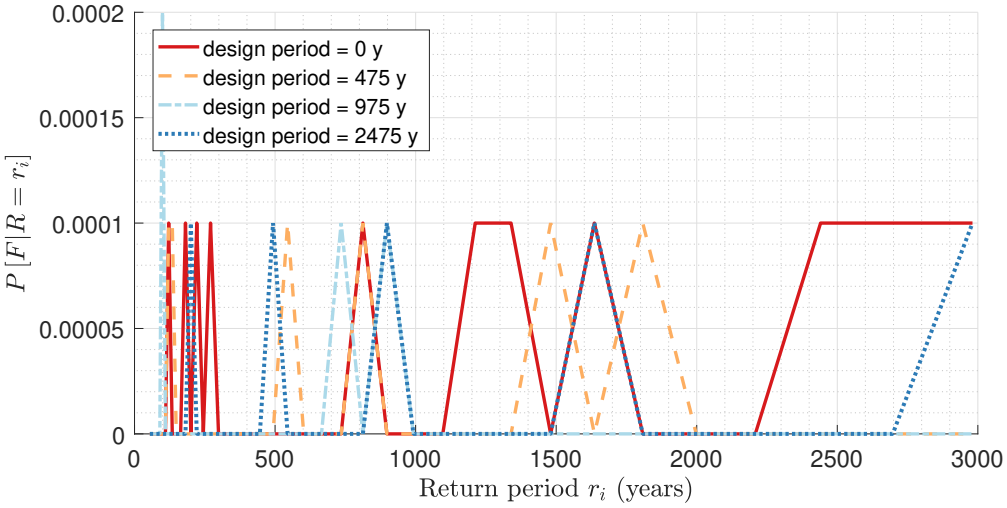

Figure A.1: Scenario 1 - A plot of the conditional probability of failure against the PGA values ($\varphi_{gu} = 0.4$)

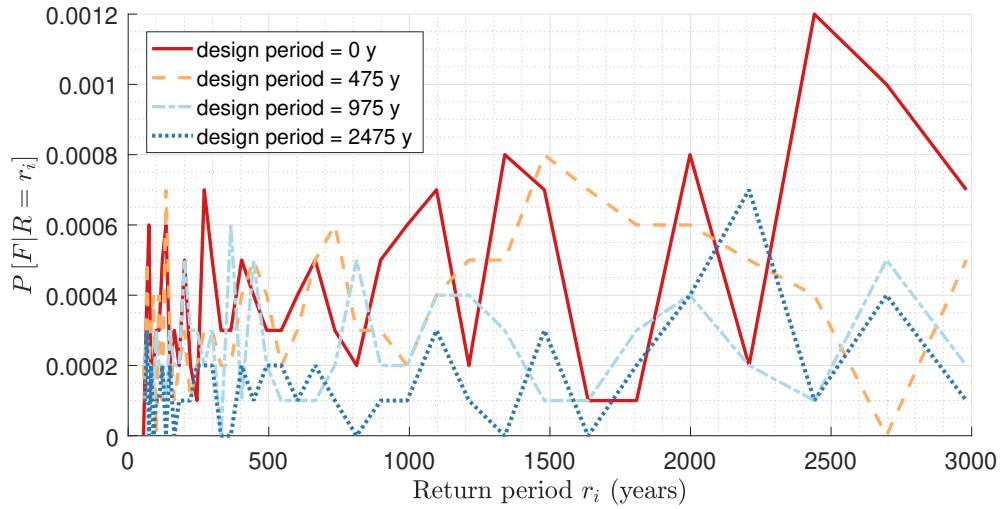

Figure A.2: Scenario 1 - A plot of the conditional probability of failure against the PGA values ($\varphi_{gu} = 0.5$)

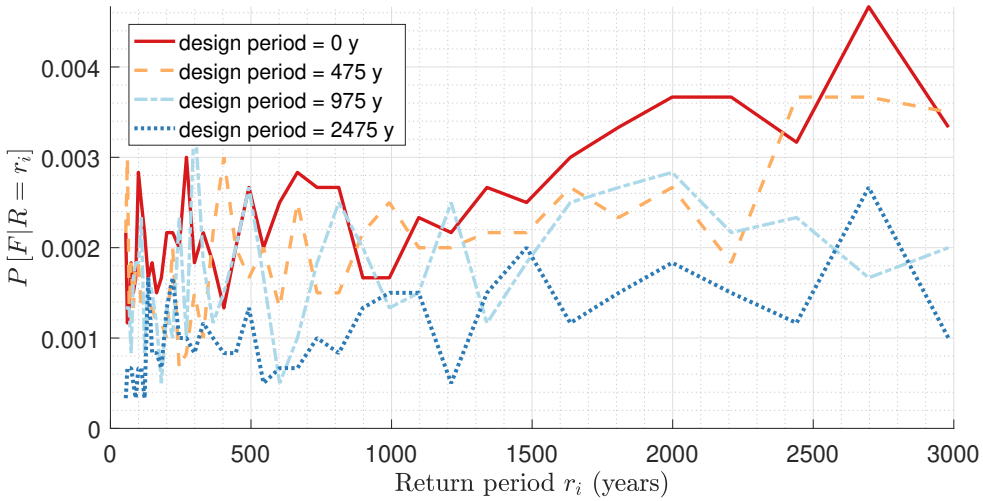

Figure A.3: Scenario 1 - A plot of the conditional probability of failure against the PGA values ($\varphi_{gu} = 0.6$)

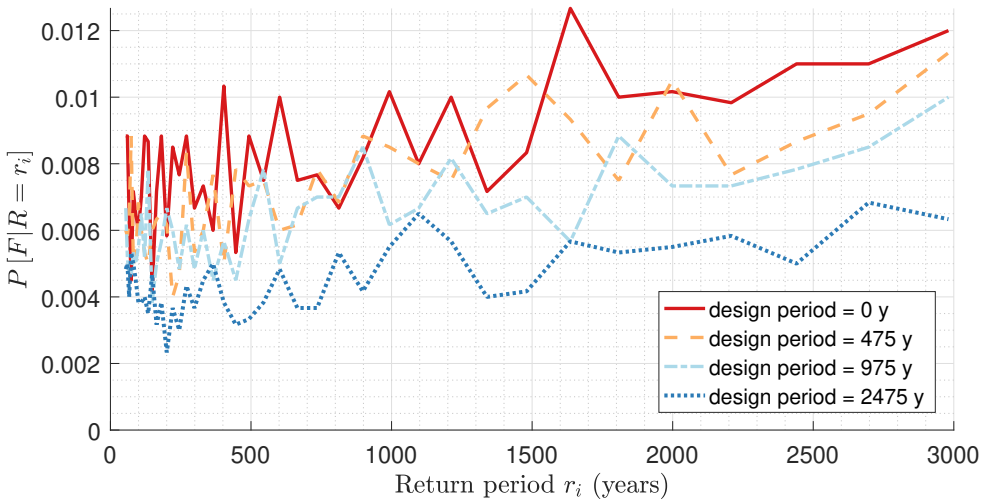

Figure A.4: Scenario 1 - A plot of the conditional probability of failure against the PGA values ($\varphi_{gu} = 0.7$)

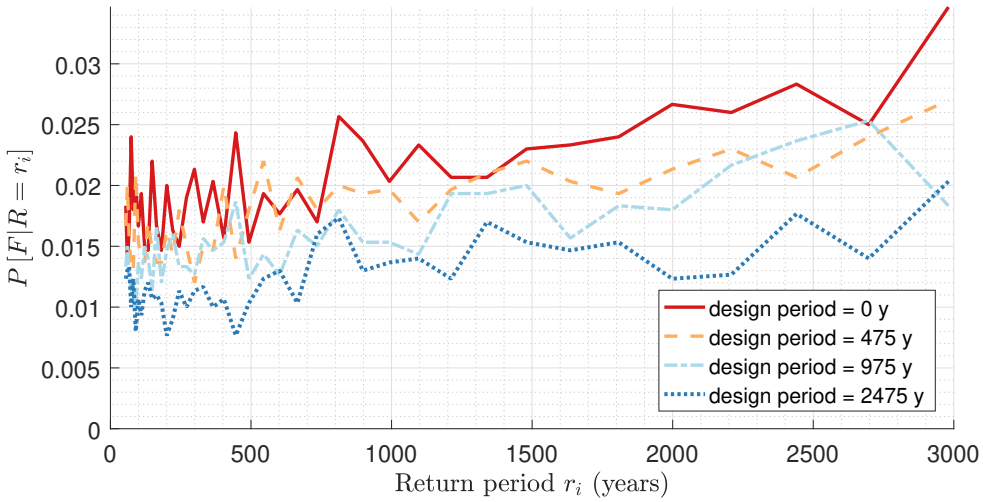

Figure A.5: Scenario 1 - A plot of the conditional probability of failure against the PGA values ($\varphi_{gu} = 0.8$)

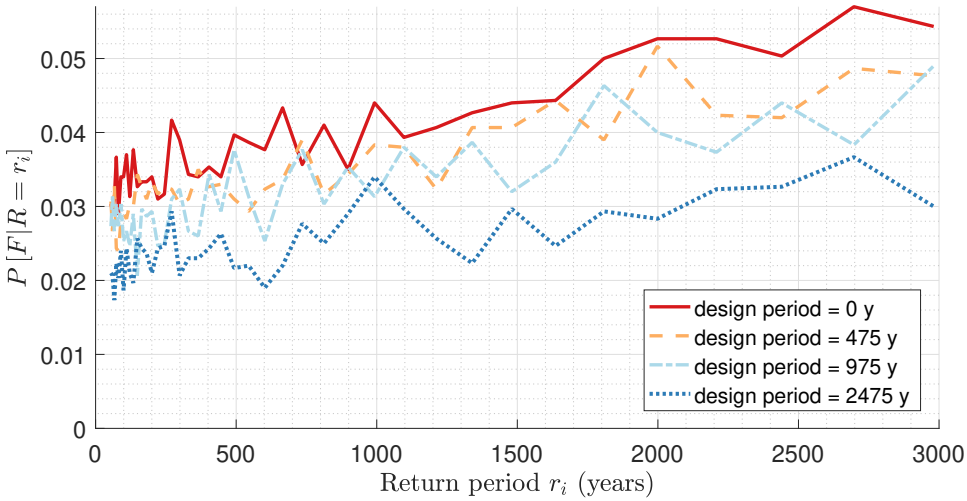

Figure A.6: Scenario 1 - A plot of the conditional probability of failure against the PGA values ($\varphi_{gu} = 0.9$)

Figure A.7: Scenario 1 - A plot of the conditional probability of failure against the PGA values ($\varphi_{gu} = 1.0$)

A.2. Scenario 2

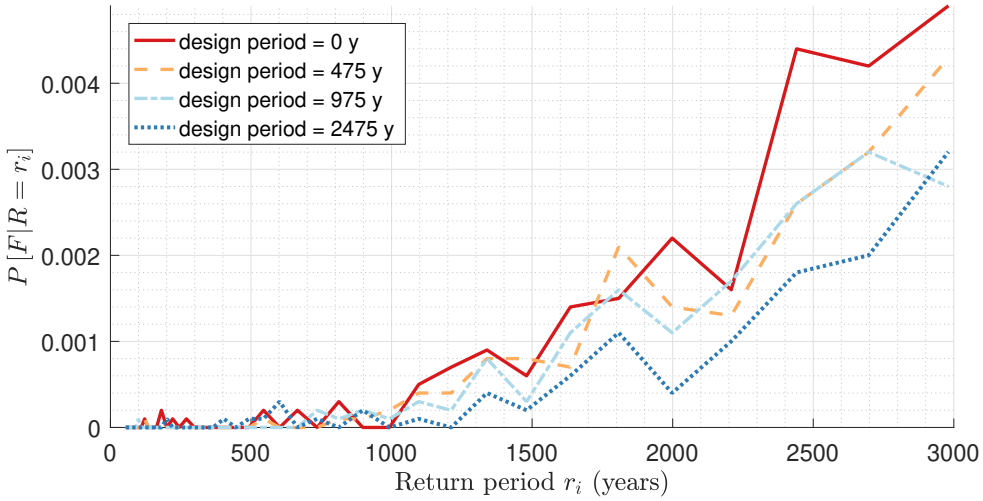

Figure A.8: Scenario 2 - A plot of the conditional probability of failure against the PGA values ($\varphi_{gu} = 0.4$)

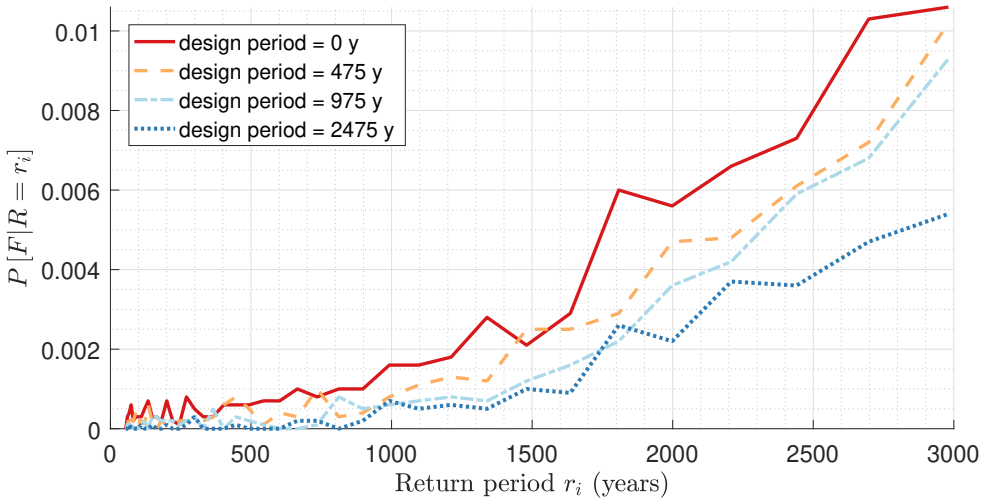

Figure A.9: Scenario 2 - A plot of the conditional probability of failure against the PGA values ($\varphi_{gu} = 0.5$)

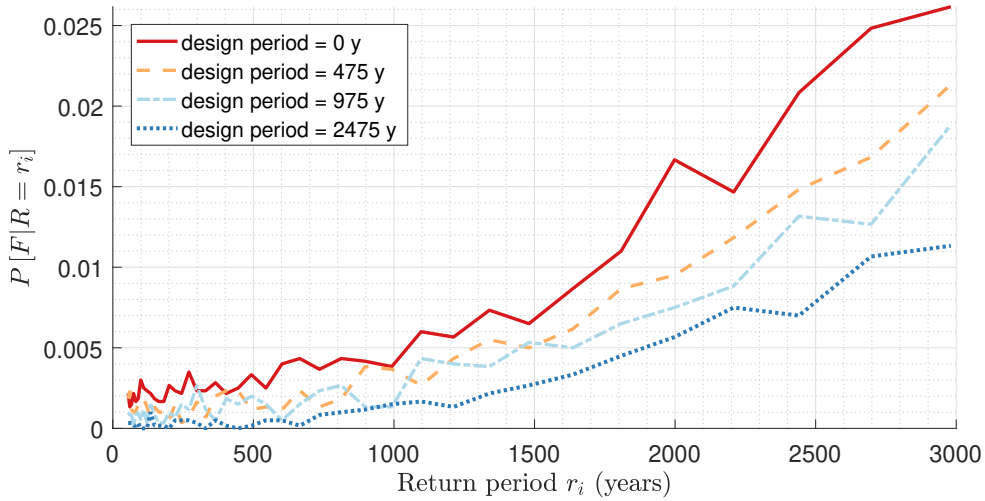

Figure A.10: Scenario 2 - A plot of the conditional probability of failure against the PGA values ($\varphi_{gu} = 0.6$)

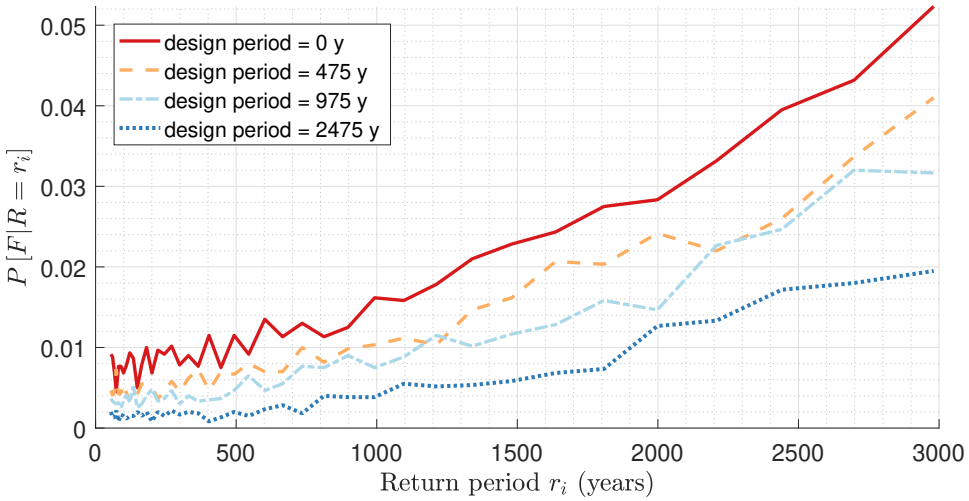

Figure A.11: Scenario 2 - A plot of the conditional probability of failure against the PGA values ($\varphi_{gu} = 0.7$)

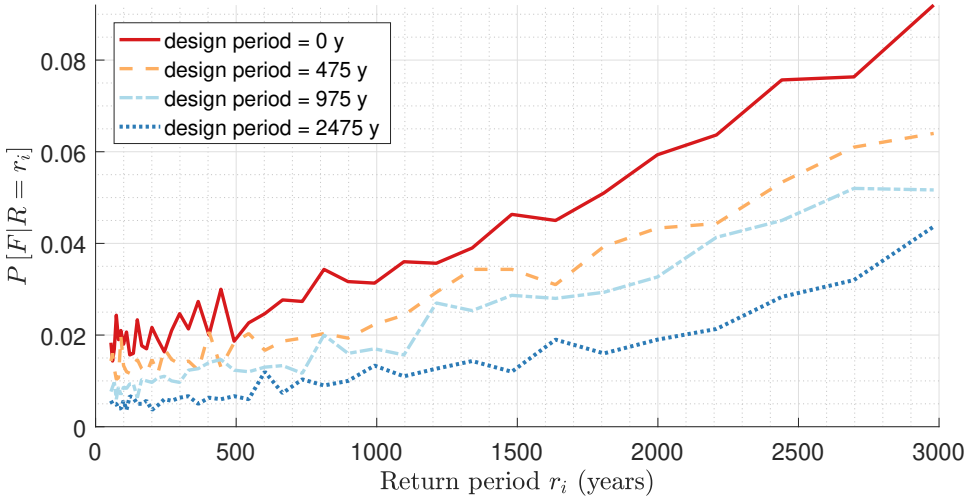

Figure A.12: Scenario 2 - A plot of the conditional probability of failure against the PGA values ($\varphi_{gu} = 0.8$)

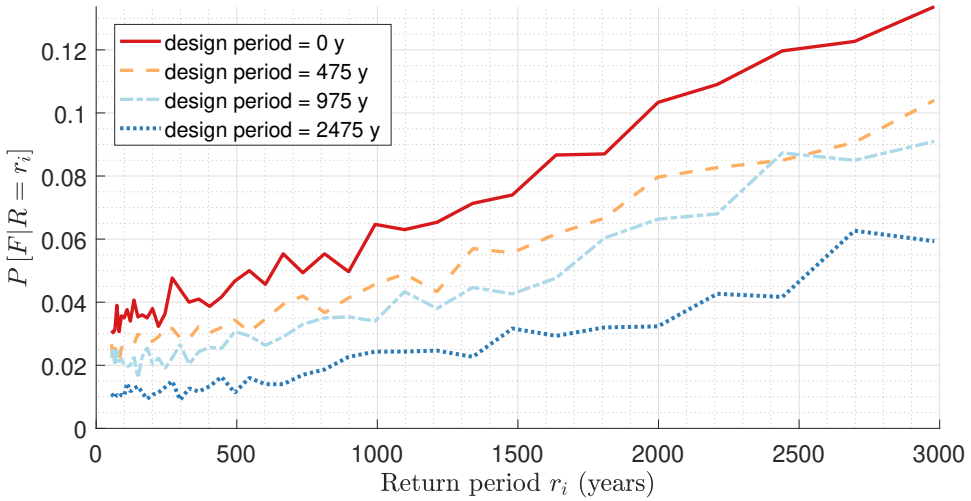

Figure A.13: Scenario 2 - A plot of the conditional probability of failure against the PGA values ($\varphi_{gu} = 0.9$)

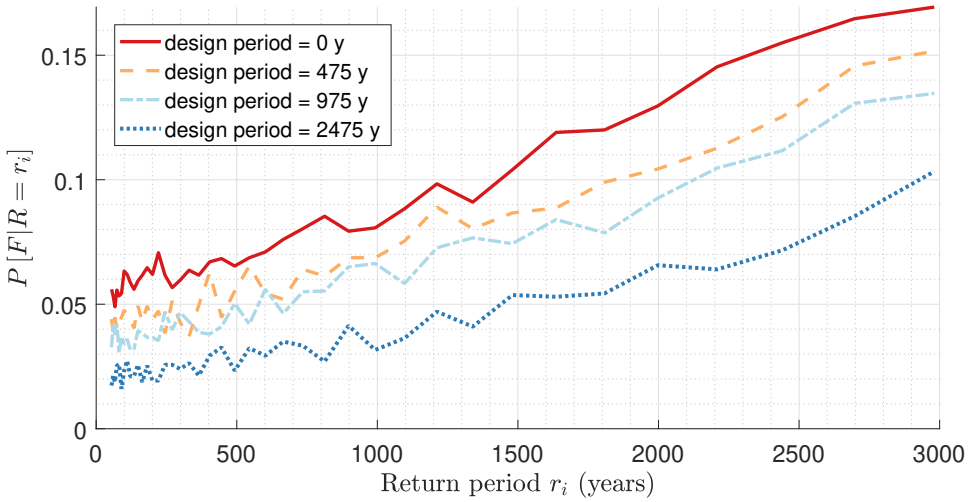

Figure A.14: Scenario 2 - A plot of the conditional probability of failure against the PGA values ($\varphi_{gu} = 1.0$)

A.3. Scenario 3

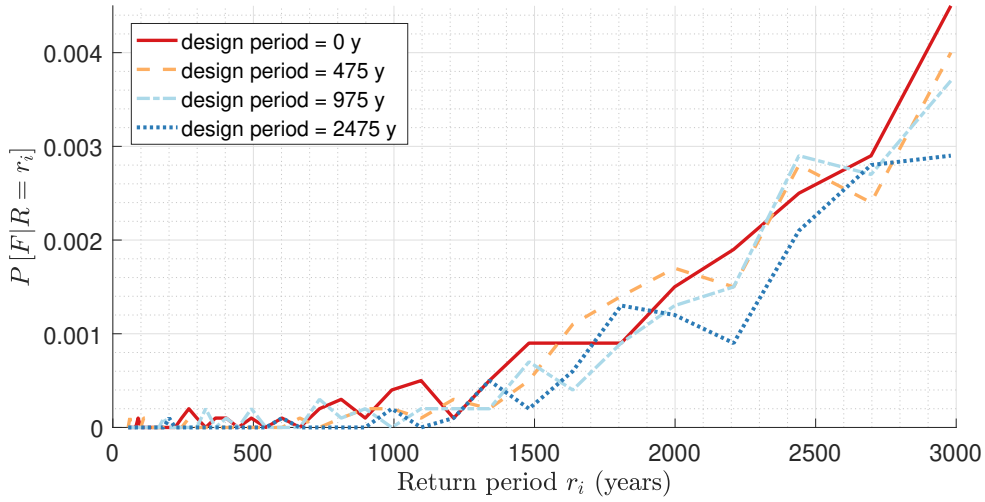

Figure A.15: Scenario 3 - A plot of the conditional probability of failure against the PGA values ($\varphi_{gu} = 0.4$)

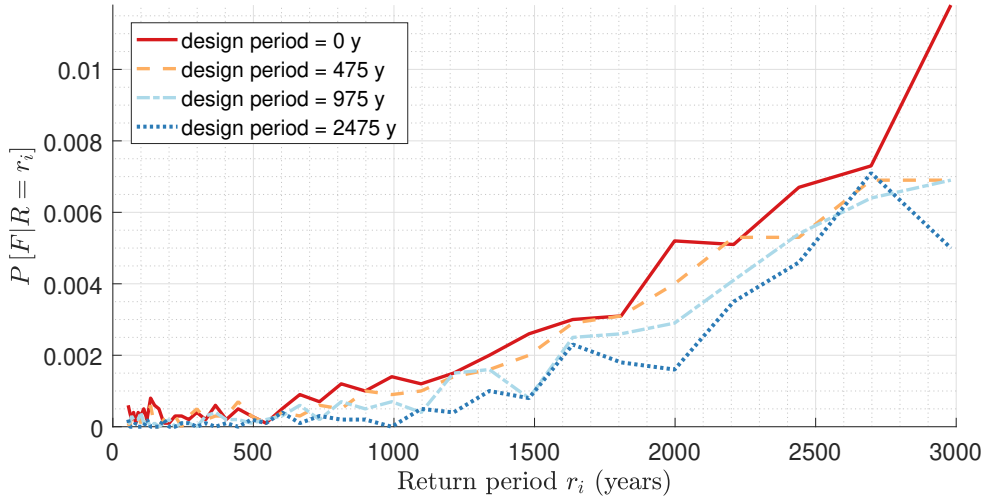

Figure A.16: Scenario 3 - A plot of the conditional probability of failure against the PGA values ($\varphi_{gu} = 0.5$)

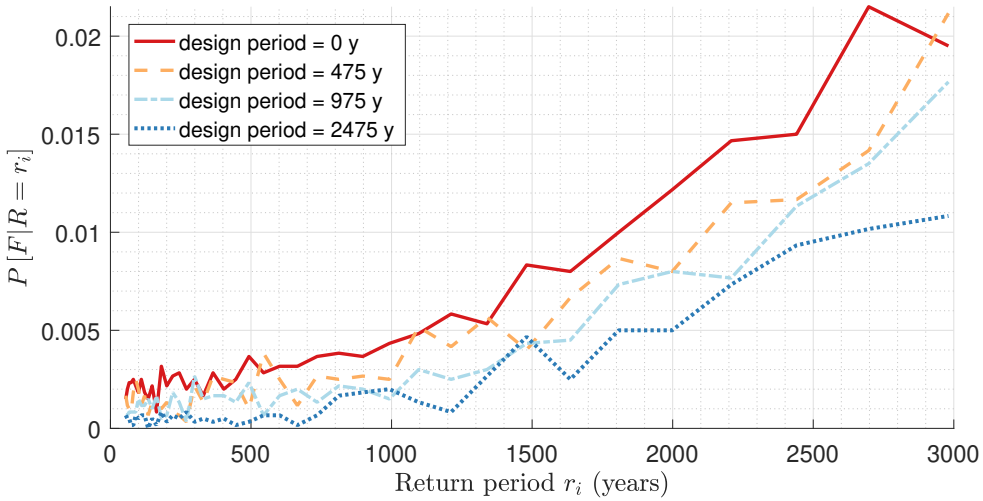

Figure A.17: Scenario 3 - A plot of the conditional probability of failure against the PGA values ($\varphi_{gu} = 0.6$)

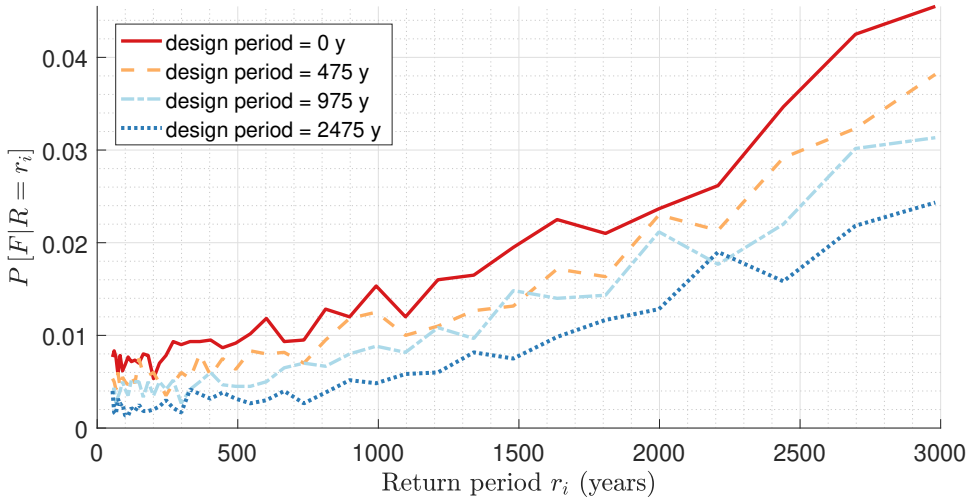

Figure A.18: Scenario 3 - A plot of the conditional probability of failure against the PGA values ($\varphi_{gu} = 0.7$)

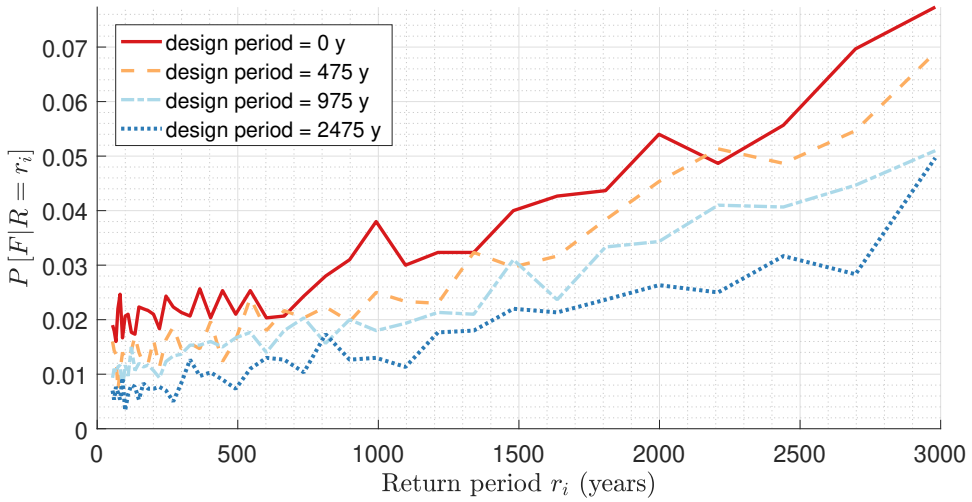

Figure A.19: Scenario 3 - A plot of the conditional probability of failure against the PGA values ($\varphi_{gu} = 0.8$)

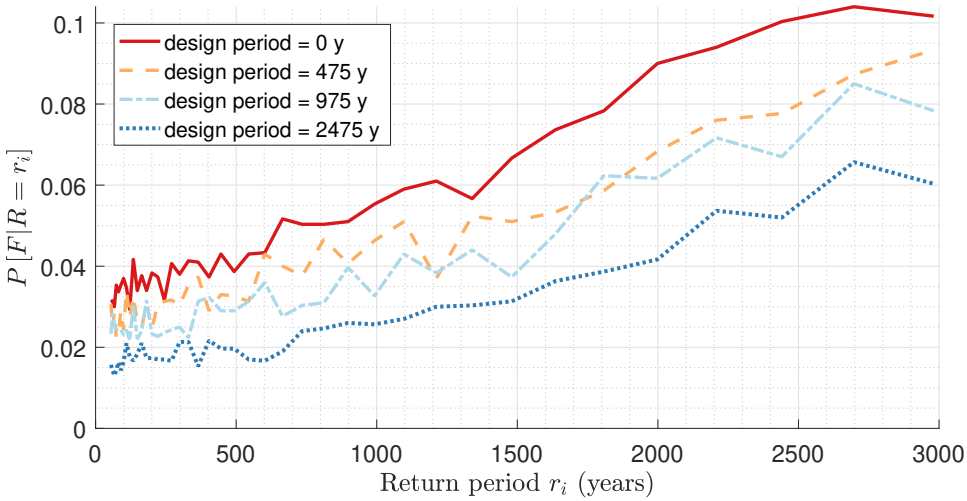

Figure A.20: Scenario 3 - A plot of the conditional probability of failure against the PGA values (φ_{gu} = 0.9)

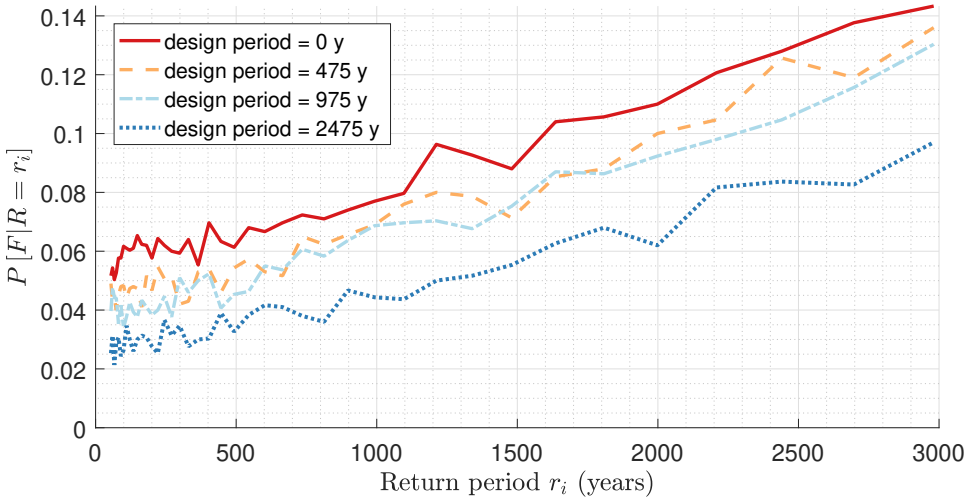

Figure A.21: Scenario 3 - A plot of the conditional probability of failure against the PGA values (φ_{gu} = 1.0)

A.4. Scenario 4

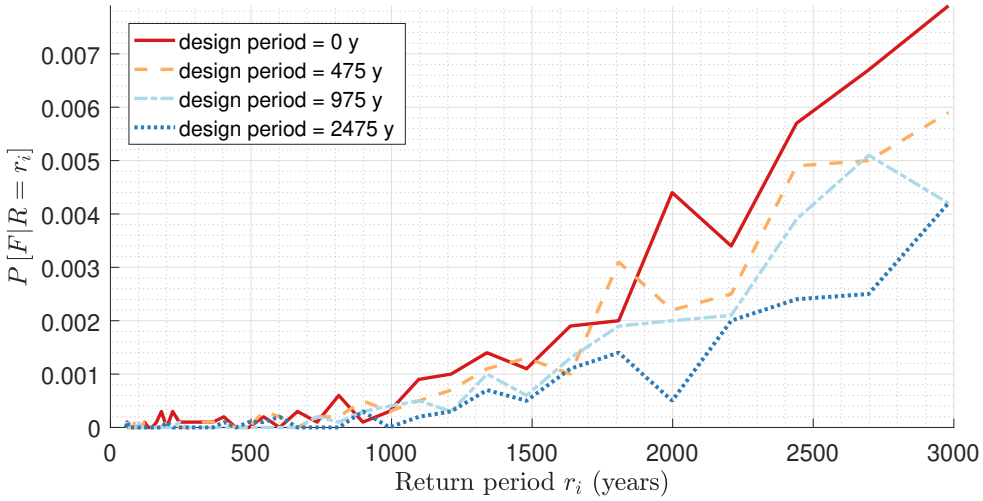

Figure A.22: Scenario 4 - A plot of the conditional probability of failure against the PGA values ($\varphi_{gu} = 0.4$)

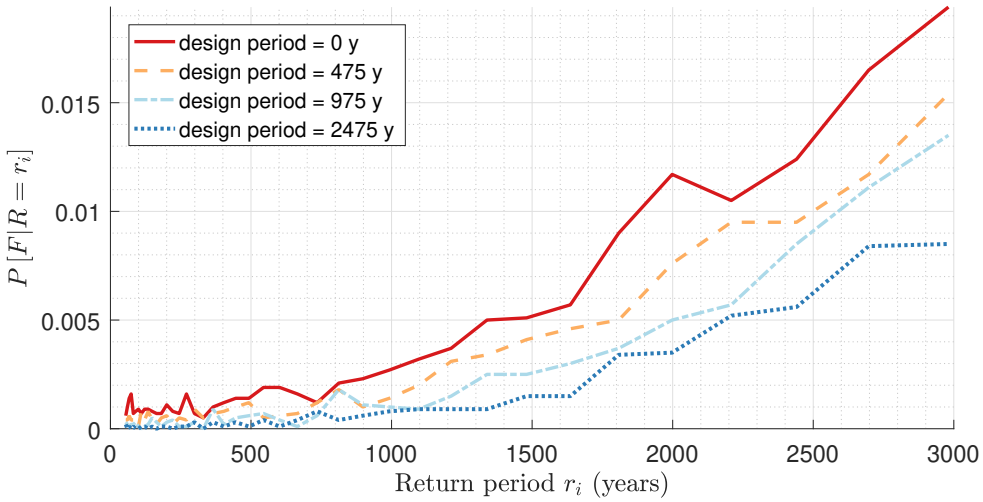

Figure A.23: Scenario 4 - A plot of the conditional probability of failure against the PGA values ($\varphi_{gu} = 0.5$)

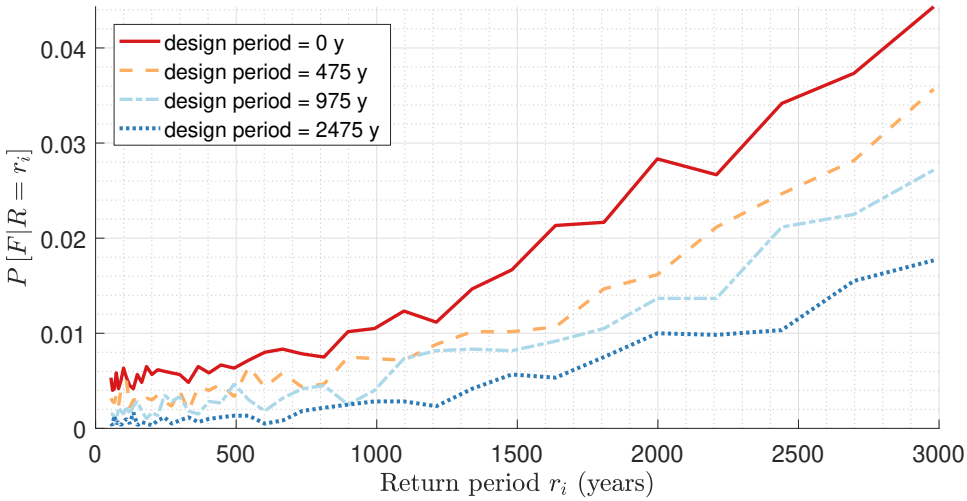

Figure A.24: Scenario 4 - A plot of the conditional probability of failure against the PGA values ($\varphi_{gu} = 0.6$)

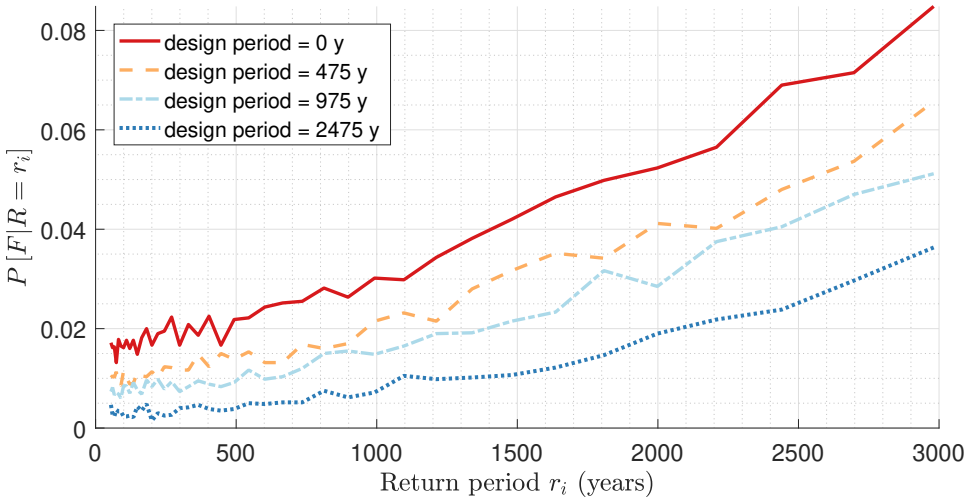

Figure A.25: Scenario 4 - A plot of the conditional probability of failure against the PGA values ($\varphi_{gu} = 0.7$)

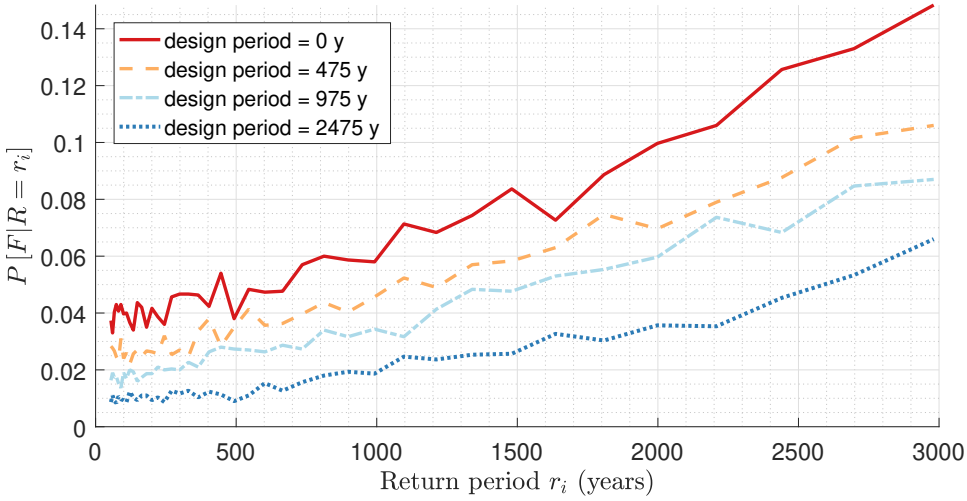

Figure A.26: Scenario 4 - A plot of the conditional probability of failure against the PGA values ($\varphi_{gu} = 0.8$)

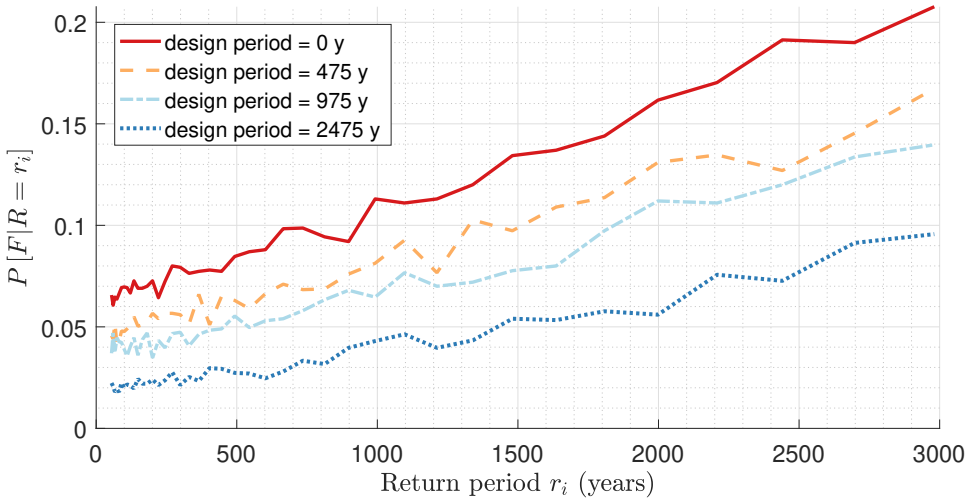

Figure A.27: Scenario 4 - A plot of the conditional probability of failure against the PGA values ($\varphi_{gu} = 0.9$)

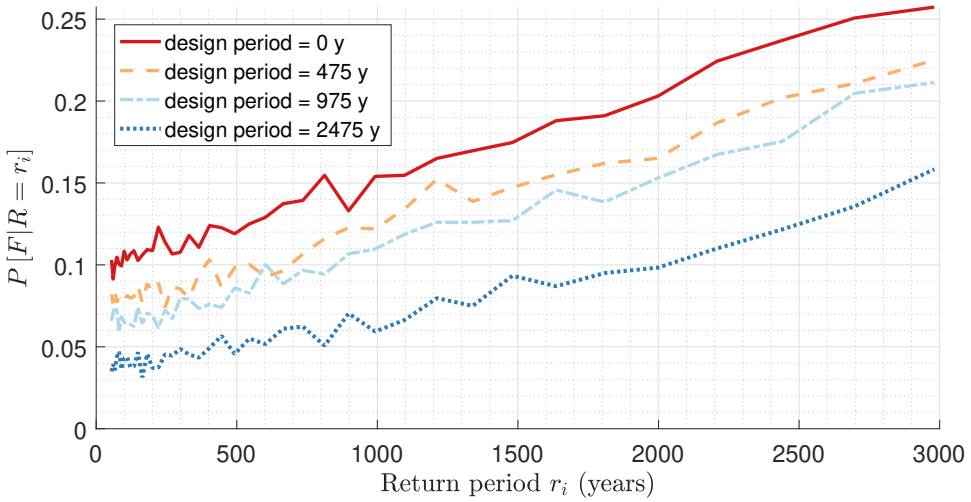

Figure A.28: Scenario 4 - A plot of the conditional probability of failure against the PGA values ($\varphi_{gu} = 1.0$)

A.5. Scenario 5

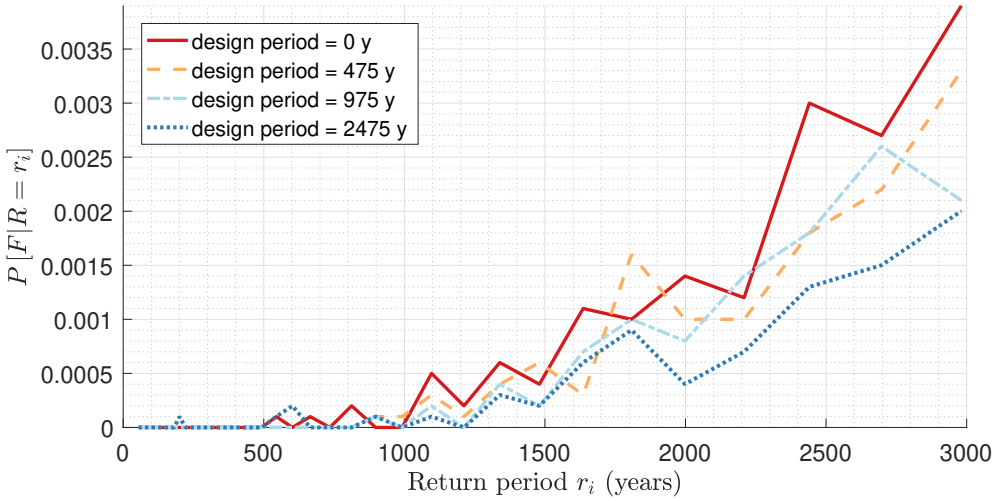

Figure A.29: Scenario 5 - A plot of the conditional probability of failure against the PGA values ($\varphi_{gu} = 0.4$)

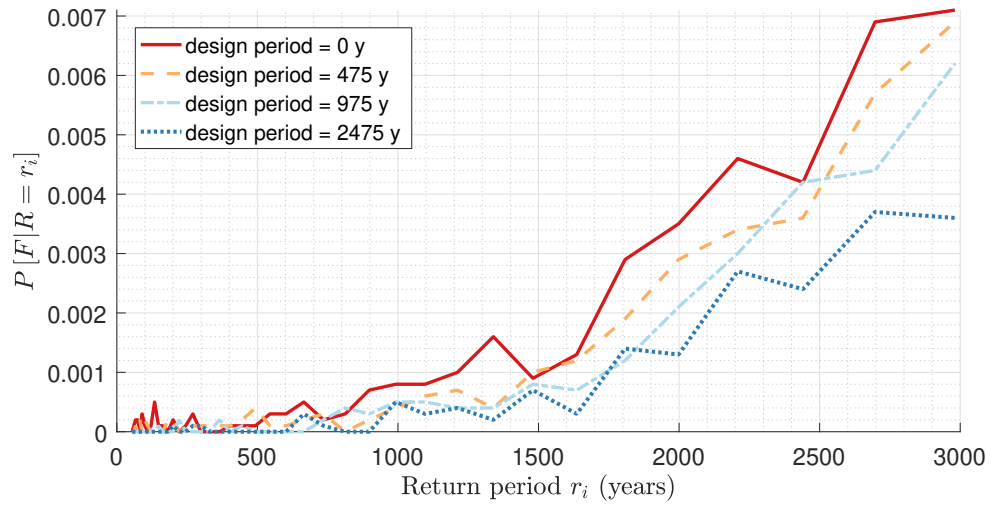

Figure A.30: Scenario 5 - A plot of the conditional probability of failure against the PGA values ($\varphi_{gu} = 0.5$)

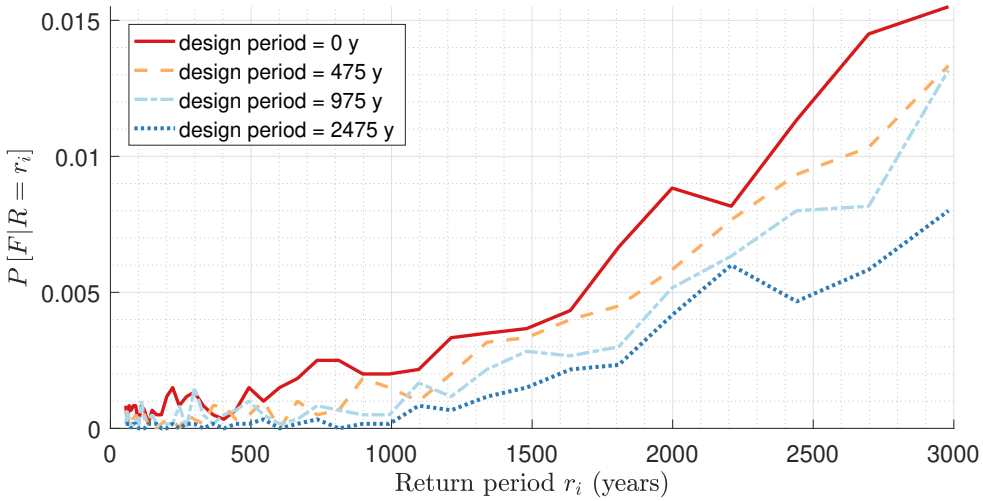

Figure A.31: Scenario 5 - A plot of the conditional probability of failure against the PGA values ($\varphi_{gu} = 0.6$)

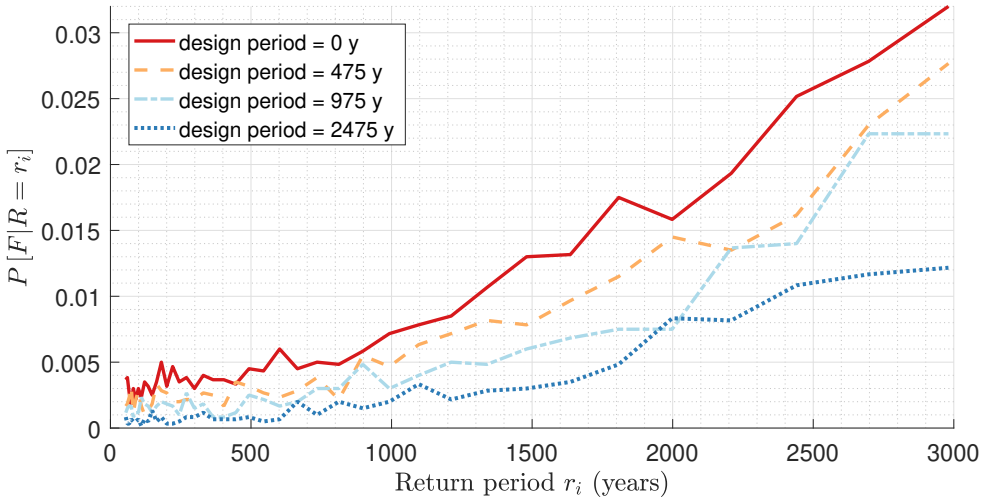

Figure A.32: Scenario 5 - A plot of the conditional probability of failure against the PGA values ($\varphi_{gu} = 0.7$)

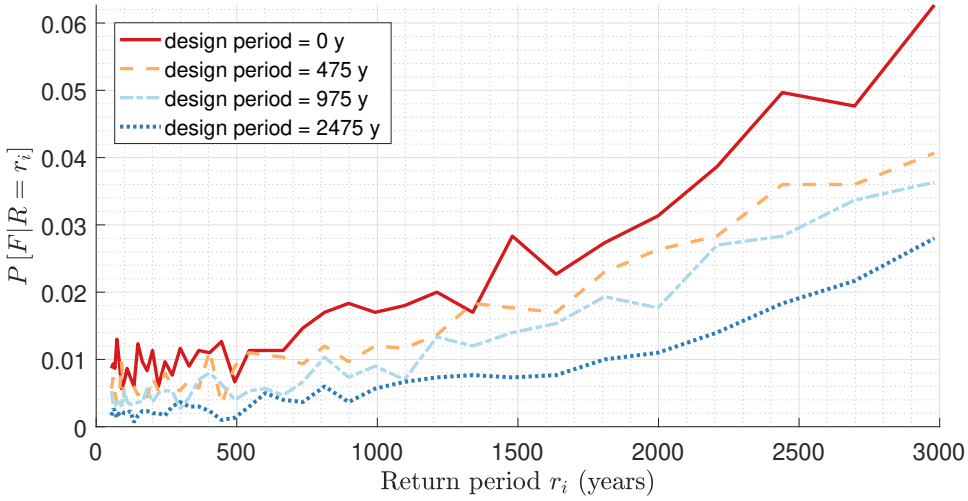

Figure A.33: Scenario 5 - A plot of the conditional probability of failure against the PGA values ($\varphi_{gu} = 0.8$)

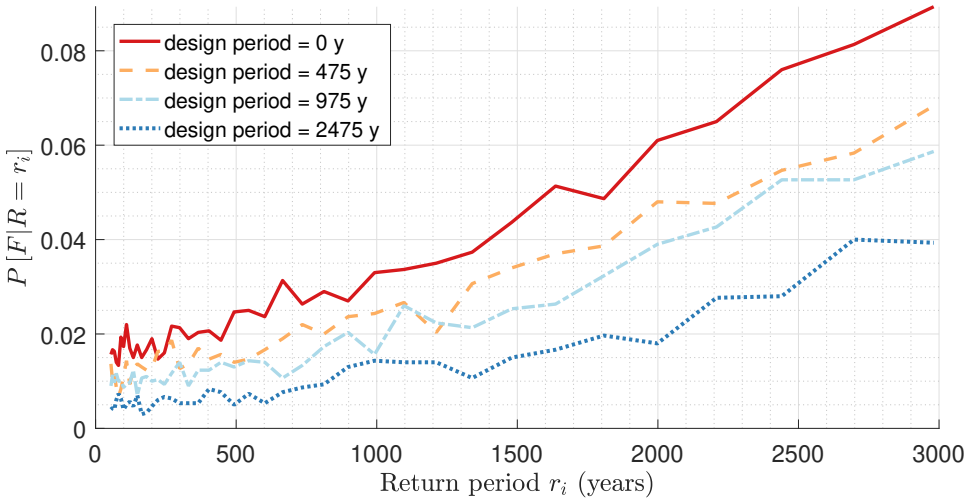

Figure A.34: Scenario 5 - A plot of the conditional probability of failure against the PGA values (φ_{gu} = 0.9)

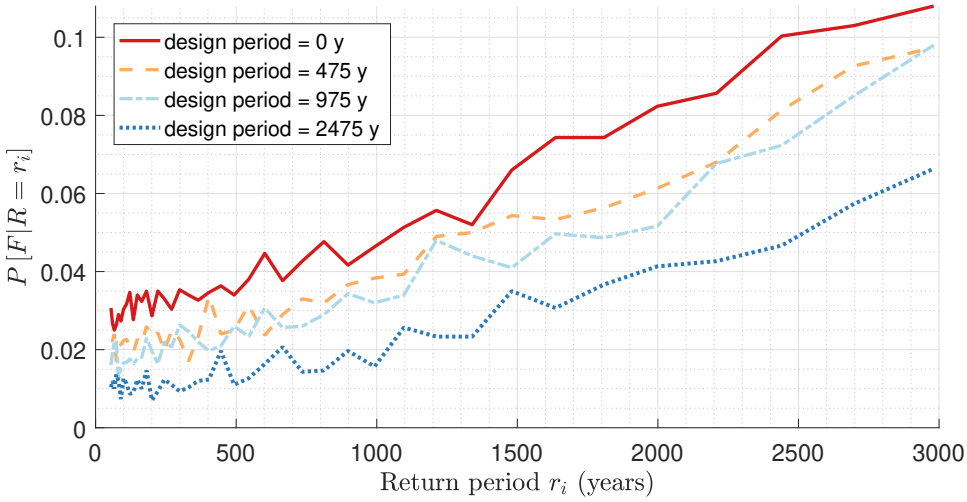

Figure A.35: Scenario 5 - A plot of the conditional probability of failure against the PGA values (φ_{gu} = 1.0)

A.6. Scenario 5

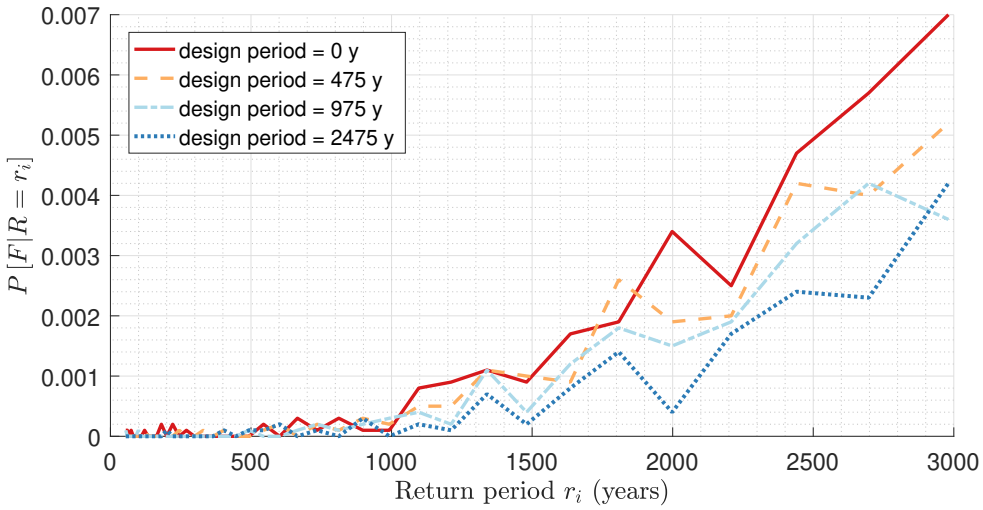

Figure A.36: Scenario 6 - A plot of the conditional probability of failure against the PGA values ($\varphi_{gu} = 0.4$)

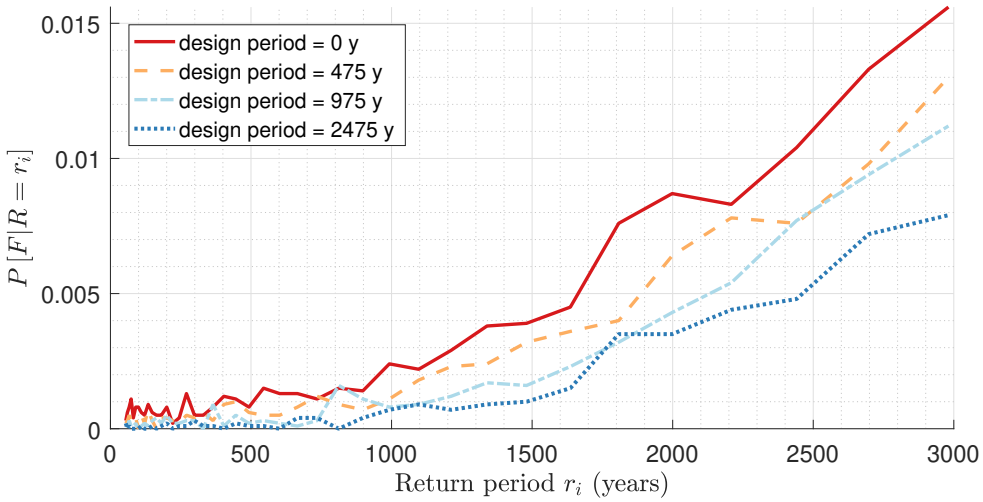

Figure A.37: Scenario 6 - A plot of the conditional probability of failure against the PGA values ($\varphi_{gu} = 0.5$)

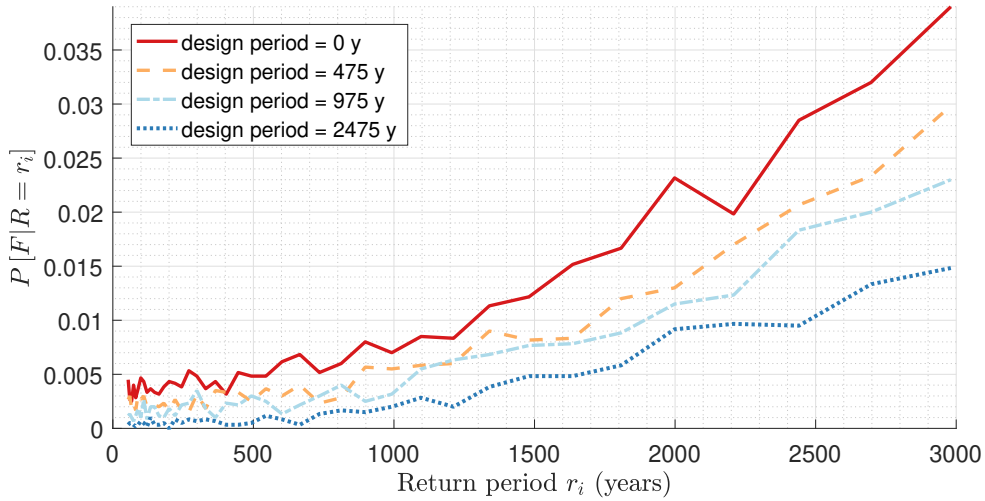

Figure A.38: Scenario 6 - A plot of the conditional probability of failure against the PGA values ($\varphi_{gu} = 0.6$)

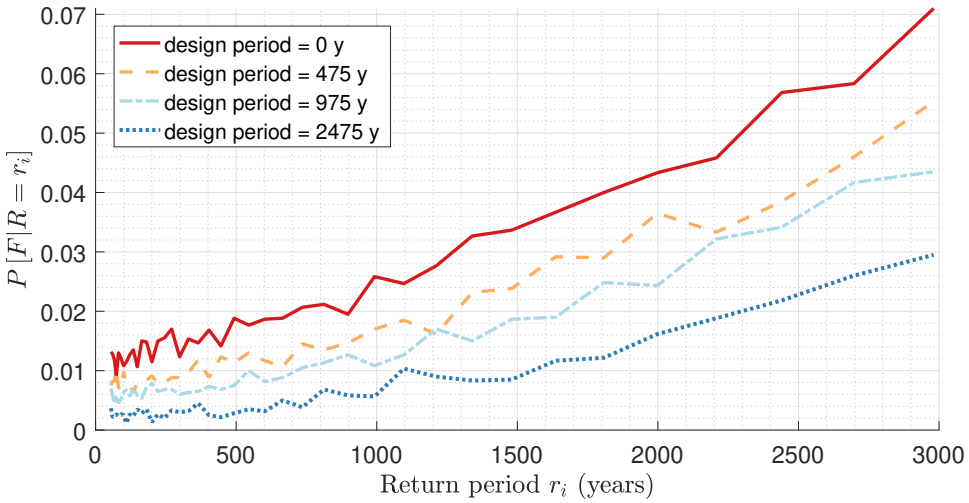

Figure A.39: Scenario 6 - A plot of the conditional probability of failure against the PGA values ($\varphi_{gu} = 0.7$)

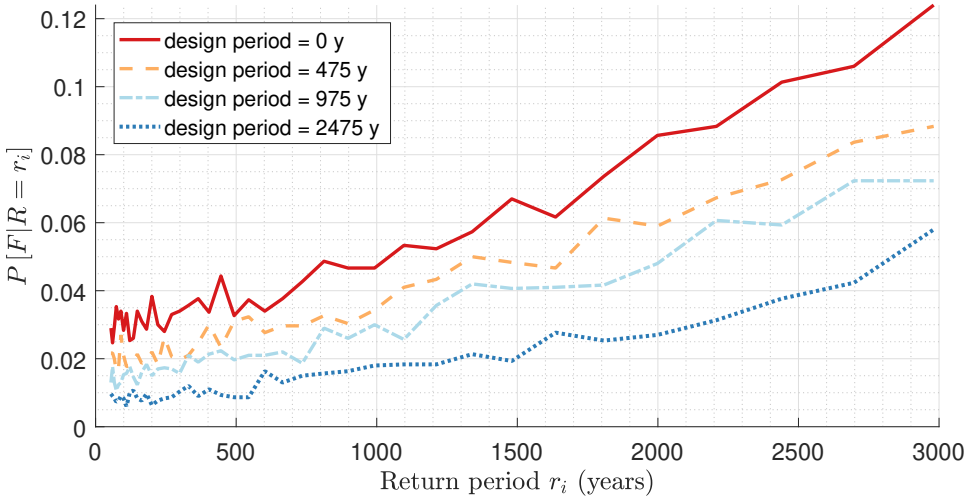

Figure A.40: Scenario 6 - A plot of the conditional probability of failure against the PGA values ($\varphi_{gu} = 0.8$)

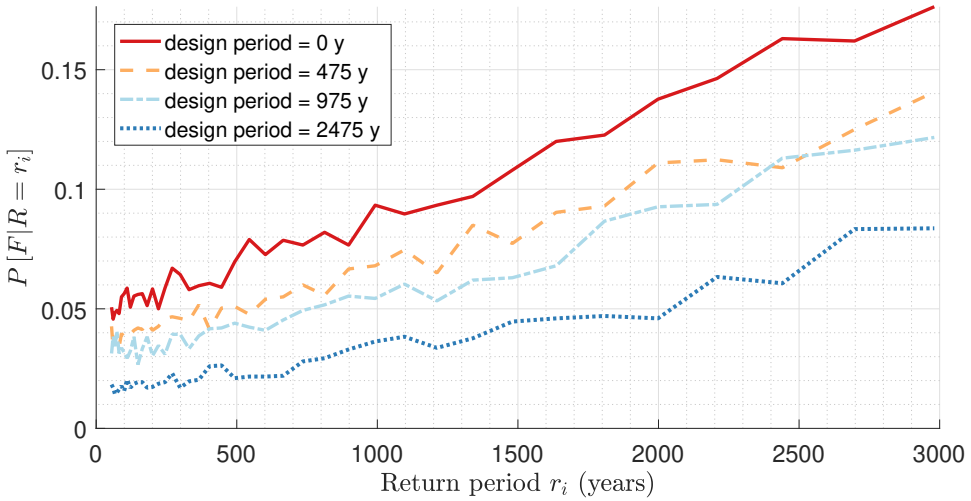

Figure A.41: Scenario 6 - A plot of the conditional probability of failure against the PGA values ($\varphi_{gu} = 0.9$)

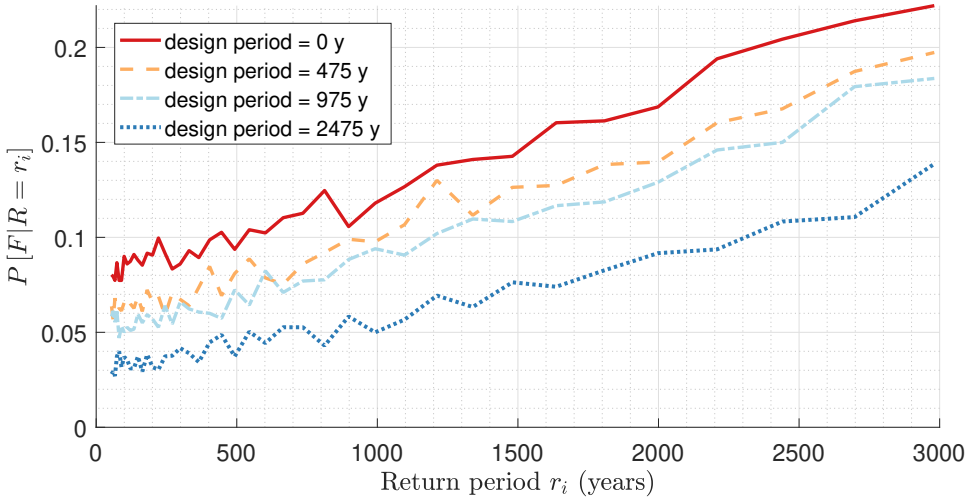

Figure A.42: Scenario 6 - A plot of the conditional probability of failure against the PGA values ($\varphi_{gu} = 1.0$)